Summer 8-18-2007

EFFECTS OF AGGREGATES ON PROPERTIES AND PERFORMANCE OF MASTICS AND SUPERPAVE HOT MIX ASPHALT MIXTURES

Francisco Aragão
University of Nebraska - Lincoln, fthiago@huskers.unl.edu

EFFECTS OF AGGREGATES ON PROPERTIES AND PERFORMANCE OF MASTICS AND SUPERPAVE HOT MIX ASPHALT MIXTURES

by

Francisco Thiago Sacramento Aragão

A THESIS

Presented to the Faculty of

The Graduate College at the University of Nebraska

In Partial Fulfillment of Requirements

For the Degree of Master of Science

Major: Civil Engineering

Under the Supervision of Professor Yong-Rak Kim

Lincoln, Nebraska

May, 2007

EFFECTS OF AGGREGATES ON PROPERTIES AND PERFORMANCE OF MASTICS AND SUPERPAVE HOT MIX ASPHALT MIXTURES

Francisco Thiago Sacramento Aragão, M.S.

University of Nebraska, 2007

Adviser: Yong-Rak Kim

Superpave, a set of advancements in testing devices and specifications for asphalt binders and mixtures, was limited to address the effects of aggregates. Because aggregates represent around 95% in mass of the asphalt mixtures, it is important to understand how these materials affect properties and performance of such mixtures. This research focus on how different types and contents of aggregates affect properties of mastics and asphalt mixtures, and their performance considering the viscoelastic nature of the asphalt material.

Five different types of aggregates and hydrated lime were used for sample fabrication together with two different binders. Several different tests were performed to the aggregates separately. Viscoelastic properties for both mastics and hot mix asphalt mixtures were characterized. In addition, the mixtures produced with those aggregates were also evaluated for rutting and fatigue performances using the APA and UTM-25kN machines.

Among the studies conducted in this research work are: restricted zone, a controversial concept and its redundancy; rutting potential of mixtures with different

coarse and fine angularities; the stiffening potential of binders provided by different fillers; the stiffening provided by different contents of hydrated lime to asphalt concrete mixtures and fatigue and rutting potential of mixtures with different contents of hydrated lime.

The results indicate that the restricted zone should not be a criterion for the selection of mixture gradations, that angularity somewhat affects the rutting potential of asphalt concrete mixtures, that fillers of different materials provide different gain in stiffness for binders and that this improvement is binder dependent. Also, hydrated lime was found to have higher stiffening potential than general mineral fillers used in this study. Hydrated lime was also proven to improve the stiffness of asphalt concrete mixtures. Even though stiffening the mixtures, hydrated lime was shown to improve the fatigue performance of the mixtures. Finally, this filler also improved the rutting resistance of mixtures.

Ao meu melhor amigo e fonte de força Jesus Cristo,

À minha esposa, amiga e companheira nas aventuras da vida, Gabriella Moreira,

À minha mãe e exemplo a ser seguido, Maria de Fátima Sacramento,

Aos meus amados irmãos Thiciano Sacramento Aragão e Layla Pereira,

À minha avó e maior fã, Francisca Pernambuco VB, e

Ao meu pai, Demountiez Aragão, que me amou e investiu em minha educação.

AGRADECIMENTOS

"*Se consegui enxergar mais longe foi porque me apoiei em ombros de gigantes*." É baseado nesta idéia de Isaac Newton que eu venho prestar meus agradecimentos aos gigantes das diversas áreas da minha vida, cujos ombros me permitiram enxergar mais longe e concluir esta desafiadora mas necessária fase da minha carreira profissional. Eu sinceramente divido esta vitória com vocês e lhes devo todo respeito e honra.

Meus primeiros e mais importantes agradecimentos são dedicados à minha fonte de força, razão para viver e exemplo a ser seguido: ao meu melhor amigo Jesus Cristo. Muito obrigado, ó Senhor, por verdadeiramente ter sido meu amigo em todas as horas em que a vida e as suas circunstâncias tentaram me oprimir.

Eu agradeço ao Dr. Yong-Rak Kim por seu apoio, pelas vezes em que ele disse "Vá em frente," pela sua paciência e pelas vezes em que ele me impeliu a buscar ao máximo o aperfeiçoamento das minhas abilidades profissionais. Eu também extendo a ele os meus agradecimentos pela preocupação com a minha vida pessoal e por frases como "Eu não quero ser somente o seu orientador. Eu me preocupo com a sua vida."

Eu agradeço ao Dr. David H. Allen pelo exemplo de profissional bem sucedido que se preocupa com o sucesso de estudantes mais novos e por me inspirar a buscar o mais alto nível em minha educação. Eu também o agradeço por constantemente dividir com o nosso grupo de pesquisa conselhos sábios como "Nunca copie uma idéia" ou "Aprenda a pensar por você mesmo."

Eu agradeço ao Dr. Jorge Barbosa Soares pelo exemplo de perseverança e por me inspirar a acreditar que tudo é possível quando estamos seriamente dispostos a pagar o

preço que a vida cobra pelo atingimento dos nossos objetivos. Assim como lhe disse três anos atrás: Eu acredito no seu sonho.

Eu agradeço à minha esposa, Gabriella Moreira, por sua paciência, devoção, amor e amizade; por seu cuidado com a minha vida cristã; pelas vezes nas quais ela segurou a minha mão e me acompanhou à universidade por dias e noites, semanas e finais de semana; por seus ouvidos atenciosos aos meus longos discursos sobre meus temas de pesquisa; e por ela não ter hesitado em deixar toda a sua vida para trás pelo simples propósito de se aliar a mim. Sem o seu suporte a dolorosa vida de estudante de mestrado certamente teria sido ainda mais sofrida.

Eu agradeço à minha querida mae, Fátima Sacramento, pelas vezes em que rimos e choramos juntos; por seu zelo para com a minha vida cristã; por sempre tentar me convencer de que sou bom no que faço; por ter me ensinado a ser honesto com os meus sentimentos e atitudes; e por ter me ensinado a nunca me acomodar e lutar pelo que sonho. Eu também a agradeço por insistentemente tentar acertar em sua vida pra que suas atitudes servissem de exemplo para mim e para meus irmãos.

Eu agradeço aos meus amados irmãos Thiciano Aragão e Layla Pereira por verdadeiramente serem meus amigos e por sempre escutarem meus conselhos e respeitarem a minha opinião de irmão mais velho. Eu também agradeço às minhas irmãs de coração Ana Dilza, Marjorie e Laísa Barroso por sempre estarem comigo e por darem suporte à minha mãe em minha ausência.

Eu agradeço à minha avó Francisca Pernambuco VB por seu amor e por sua clara admiração por mim.

Eu agradeço à minha mãe carioca Cirlei Barcellos por tudo que ela tem feito por mim e pela Gabriella, por suas orações e amor.

Eu agradeço às minhas amigas Kamilla Vasconcelos e Verônica Castelo Branco por se importarem com a minha vida e por serem verdadeiramente amigas próximas apesar da distância que nos separa. Eu também agradeço à minha querida amiga Verônica pelas horas preciosas que ela dispensou a leitura dos conteúdos deste trabalho de pesquisa e pelas gentis sugestões de melhoramentos.

Eu agradeço aos meus amigos brasileiros de Lincoln, Paulo Marchon e Roberto Soares, por sempre estarem comigo tanto em momentos felizes quanto nos difíceis. Eu também agradeço ao meu querido amigo Roberto Soares pelo tempo dedicado à leitura desta tese e pelas gentis sugestões de melhoramentos.

Eu agradeço Marilena Carvalho, Felipe Freitas e Dulce Freitas pelo suporte e pelos conselhos durante o primeiro ano de meus estudos de mestrado.

Eu agradeço aos meus companheiros de escritório Chad Cecrle, Derek Kowalski, Minki Hong, Gina Rust e Patrick Dening pela sua amizade. Agradecimentos especiais são extendidos aos amigos Chad e Minki pelo investimento diário em nossa amizade e por gestos que podem ter parecido simples, mas que significaram muito pra mim.

Eu agradeço aos meus ajudantes Daniel Carvalho e Paulo Enrico Siqueira pela sua essencial contribuição nas atividades laboratoriais que me permitiram concluir este trabalho. Agradecimentos especiais eu dedico ao Paulo por ter se tornado um amigo em um curto período de convivência. Neste grupo de ajudantes eu tambem incluo John Dageforde pelas vezes em que ele “esticou” o seu tempo para ser apto a me ajudar em minha pesquisa.

Finalmente, eu agradeço ao grupo de asfalto e agregados do NDOR por gentilmente me conceder materiais e informações. Agradecimentos especiais eu dedico aos senhores Larry Koves, Dale Byre e James Beason.

To my closest friend and source of strength Jesus Christ,

To my wife, friend, and partner of life adventures, Gabriella Moreira,

To my mom and example to be followed, Maria de Fátima Sacramento,

To my beloved brothers Thiciano Sacramento Aragão and Layla Pereira,

To my grandmother and biggest fan, Francisca Pernambuco VB, and

To my father, Demountiez Aragão, who loved me and invested in my education.

ACKNOWLEDGEMENTS

"I *was able to see further because I was standing on the shoulder of giants*." It is based on Isaac Newton's idea that I come to thank the giants in the diverse areas of my life whose shoulders allowed me to see further and to conclude this challenging but necessary phase of my professional career. I sincerely share this victory and owe you all my respect and honor.

My first and most special thanks are dedicated to my source of strength, reason to live, and example to be followed: my closest friend Jesus Christ. Thanks are for Thee for truly being with me every time life and its circumstances tried to push me down.

I thank Dr. Yong-Rak Kim for all his support, for the times he said "Keep on going," for his patience, and also for the times he pushed me to seek for a higher quality in my professional skills. I also want to thank him for the times he worried about my personal life, and for when he said "I don't want to be only your adviser. I care about your life."

I thank Dr. David H. Allen for the example of a successful professional who cares about the success of younger students and for inspiring me to seek for the highest quality of my education. I also thank him for continuously sharing with our group concepts such as "Never copy an idea" or "Learn how to think by yourself."

I thank Dr. Jorge Barbosa Soares for the example of perseverance and for inspiring me to believe that everything is possible if we are decided to seriously pay the price that life requires for the achievement of our goals. As I said three years ago: I believe in your dream.

I thank my wife, Gabriella Moreira, for her patience, devotion, love, friendship, and partnership; for her care about my Christian life; for all the times she held my hands and joined me at the University nights and days, weeks and weekends; for the times and times she listened to my long talks about my research subjects; and for her not having hesitated to leave all her life behind for the simple purpose to join me. Without her support, life would have been much harder during those painful times of graduate school.

I thank my dear mom, Fatima Sacramento, for the times she cried and laughed with me, for her care about my Christian life, for always trying to convince me that I was good, for having taught me to be honest with my feelings and attitudes, and for having taught me never to accommodate and to fight for what I dream about. I also thank her for continuously trying to make things right to serve as example to me and my brothers.

I thank my beloved brothers, Thiciano Aragao and Layla Pereira, for truly being my friends, and for always listening to my advice and respecting my opinions as an older brother. I also thank my sisters in heart Ana Dilza, Marjorie, and Laísa Barroso for being with me and for supporting my mom in my absence.

I thank my grandmother, Francisca Pernambuco VB, for her love and clear admiration for me.

I thank my "carioca" mom Cirlei Barcellos for all she has been doing for me and for Gabriella, for her prays and love.

I thank my friends Kamilla Vasconcelos and Veronica Castelo Branco for caring about my life and for being truly close friends in spite of the distance. I also thank my dear friend Veronica for having spent hours reading the contents of this research work and kindly suggesting improvements.

I thank my Brazilian friends in Lincoln, Paulo Marchon and Roberto Soares, for always being there for me, be it in moments to laugh or in the hard times. I also thank my dear friend Roberto for spending his time reading this thesis and kindly suggesting improvements.

I thank Marilena Carvalho, Felipe Freitas, and Dulce Freitas for their support, care, and pieces of advice in the first year of my Masters degree studies.

I thank my officemates and friends Chad Cecrle, Derek Kowalski, Minki Hong, Gina Rust, and Patrick Dening for their friendship. Special thanks are for Chad and Minki for investing daily in our friendship with attitudes that may seem small, but that meant a lot to me.

I thank my helpers Daniel Carvalho and Paulo Siqueira for their fundamental contribution on the lab activities that allowed me to finish this work. Special thanks are for Paulo for having become a friend even in a short period of time. In this group of helpers I could also include John Dageforde for all the times he stretched his time to be able to help me with my research.

Finally, I thank the NDOR asphalt and aggregates team for gently providing me with materials and information. Special thanks to Mr. Larry Koves, Mr. Dale Byre, and Mr. James Beason.

LIST OF TABLES

FIGURE INDEX

TABLE OF CONTENTS

CHAPTER 1

INTRODUCTION

Safe and comfortable transport of goods and people is the key for local and national development in any part of the world. The transportation business involves a number of professionals from diverse disciplines and with different expertise and receives a huge portion of the public investment. In 2005, the United States roadway network (including both rural and urban segments) encompassed 4,010,247 miles, of which 1,408,757 miles were unpaved and the majority of the paved roadway network used flexible pavements (FHWA, 2005).

According to the Nebraska Department of Roads (NDOR, 2003), the expenditures for roadways in the state of Nebraska occupy the second place, only next to Education and Health and Human Services. Thus, it is not surprising that during the fiscal year 2003, 9% of the state money was used for NDOR activities. In 2005, the state government invested $621 million to move people and goods across and throughout the state. From the money reserved for construction, $5,440,666 (2%) was spent on railroad viaducts, $61,571,715 (19%) on bridges, and $259,187,316 (79%) on roadways (NDOR, 2005).

Whereas during the fiscal year 2006, $356,075,000 was spent for construction in the Nebraska's Highway System, out of which $191,481,000 was spent for the construction of smaller roadways within the eight Nebraska districts, $99,937,000 was

spent on expressways, and $64,657,000 on interstate services (Bettenhausen, 2006). Again in 2006, approximately 1.6 million of tons of asphalt concrete were laid in Nebraska at a total cost of $60,660,213.33 (Miller, 2006).

The numbers mentioned above provide an idea of the importance and robustness of the transportation business. The increase in traffic volume over the past decades required the laying down of higher quality roadways. Researchers worldwide try to develop better composites, both affordable and more resistant, and a lot of money is invested on the development of new performance tests that better simulate field conditions. The quality level of highways is directly associated with the proper selection of materials (aggregates, binder, and additives), mix design, proper construction procedures, and adequate structural design of the pavement layers. If these factors are optimized, the distresses on the structure will be reduced, thereby significantly affecting the costs associated with rehabilitation and replacement of the structures.

This thesis presents a study of the effects of aggregates on the properties and performance of mastics and hot mix asphalt (HMA). The viscoelastic nature of the asphalt binder as well as several other aspects of the HMA are considered. First, a study as to how different mixtures behave relative to the restricted zone criterion was conducted. This zone lies on the maximum-density line of the mixture gradations, and researchers of the strategic highway research program (SHRP) suggested that it should be avoided to create stronger mixtures against permanent deformations. The performances of five different mix gradations (one above, two through, and two below the restricted zone) with respect to permanent deformation were characterized using the asphalt pavement analyzer (APA). The results obtained from APA testing were also used to

compare the rutting potential of mixtures with different fine aggregate angularity (FAA) and coarse aggregate angularity (CAA).

Furthermore, this study also investigated as to how the type and amount of fillers changed the viscoelastic property $|G^*|$, the dynamic shear modulus of each mastic. A similar investigation was conducted to assess how different contents of hydrated lime changed the viscoelastic property, the dynamic modulus ($|E^*|$) of each HMA sample.

The viscoelastic properties $|G^*|$ and $|E^*|$ were then translated into master curves, a representation of the properties over a wider range of frequencies. From the $|G^*|$ and $|E^*|$ properties, relaxation shear modulus, (G(t)), and relaxation modulus, (E(t)), functions were obtained, respectively. This was performed by curve-fitting Prony series on the experimental data with the aid of the collocation method.

The next step was to evaluate the fatigue life of HMA mixtures by varying the contents of hydrated lime. For this case, curves that represent applied stress and the number of cycles to failure (so-called S-N curves) were created for a controlled-force testing mode.

Finally, rutting performances of similar HMA mixtures were indirectly evaluated by considering the vertical permanent-deformation from creep and recovery tests as a comparison parameter. Also, constant loads that are high enough to cause damage were applied to samples at a temperature close to the highest temperature in the performance grade (PG) of the binders used. The beginning of the tertiary flow was monitored to compare the rutting potentials of mixtures.

This research is divided into five chapters as follows.

Chapter 2 is a review of topics related to the research. The main issues addressed are the definition and characterization of asphalt, its compositional model, the effects of chemical composition on performance, the viscoelastic nature of the material, definitions of the viscoelastic properties, the importance of their characterization and the mechanical analogs used to represent those properties accurately, the energy-dissipation concept used to relate the viscoelastic properties of mastics to rutting and fatigue distresses, the concept of linear viscoelasticity, the time-temperature superposition principle, and curve-fitting procedures available to fit expressions of the viscoelastic properties to the experimental data. For the aggregates, definitions and classifications are provided, along with their effect on the performance of asphalt mixtures. Superpave and its innovations including the control points and the controversial restricted-zone concept are also discussed. A short description of the major distresses in asphalt pavements is also found in that section. Finally, there is a discussion related to the derivations of solutions for the viscoelastic properties of HMA when tested in indirect tension (IDT) mode.

Chapter 3 discusses methods, loading shapes and levels, frequencies, temperatures, and equipments chosen to characterize the properties and performance of mastics and asphalt concrete mixtures. Curve-fitting procedures are also described. Finally, this chapter discusses how testing results are interpreted and related to the potential of the mixtures to the fatigue and rutting distresses.

Chapter 4 presents the testing results and relates APA and UTM-25 results with fatigue- and rutting-performance potential of mixtures.

Chapter 5 summarizes the conclusions and recommendations with regard to this research work.

CHAPTER 2

LITERATURE REVIEW

2.1. Asphalt

2.1.1. Definition

Asphalt is a complex material composed of hydrocarbons and has high viscosity, is black in color, and is present chiefly in crude petroleum and in some natural deposits. There are some disagreements among chemists regarding the structure of asphalt, but it is most commonly modeled as a colloid, with asphaltene as the dispersed phase and maltene as the continuous phase. Asphalt can also be defined as "a brown or black, tar-like, bituminous substance that mainly consists of hydrocarbons, found in large flat beds or made by refining petroleum." Bitumen can be defined as "1) asphalt found in natural state, 2) any of various black, combustible, solid to semisolid mixtures of hydrocarbons that are usually obtained from the distillation of petroleum, used to make roofing materials, sealants, paints, etc (Webster's dictionary, 2005)." Krishnan and Rajagopal (2003) suggested that bitumen and asphalt could be interchangeable terms.

2.1.2. Applications

Asphalt cement is one of the oldest engineering materials. There are records of the use of asphalt in the ancient times as mortar between bricks and stones, as waterproofing agent, and as a material to embalm mummies (Egypt, B.C. 2600) etc. According to Roberts et al. (1996), a Sumerian who thrived on shipbuilding industry used the material in B.C. 6000. The Sumerians also used the black material for inlaying shells, precious stones, and pearls (WSDOT, 2006). Around 1500 A.D., there were records of the use of a material similar to the modern bituminous macadam to pave the Incas' highway system in Peru. In modern times, the first roadway in the U.S. to be paved using asphalt was Pennsylvania Avenue in Washington D.C., in 1876 (Roberts et al., 1996).

Krishnan and Rajagopal (2003) referred to the Shell Bitumen Handbook to summarize more than 250 known current uses of bitumen in agriculture, construction, hydraulics, erosion control, automobile industry, electrical industry, railways, paving industry, etc. According to the authors, however, the most widespread use of asphalt is in the construction of roadways and runways.

2.1.3. Chemistry Involved

Roberts et al. (1996) referred to a study conducted by Peterson (1984) about the chemical composition of asphalt. The author related this composition to the durability of

the material. In the study, the author published the composition of different asphalts shown in Table 2.1.

Table 2.1 - Elemental analysis of representative petroleum asphalts

Element	Asphalt type			
	Mexican Blend	**Arkansas Louisiana**	**Boscan**	**California**
Carbon (%)	83.77	85.78	82.90	86.77
Hydrogen (%)	9.91	10.19	10.45	10.93
Nitrogen (%)	0.28	0.26	0.78	1.10
Sulfur (%)	5.25	3.41	5.43	0.99
Oxygen (%)	0.77	0.36	0.29	0.20
Vanadium (ppm)	180	7	1380	4
Nickel (ppm)	22.00	0.40	109.00	6.00

It is clear from Table 2.1 that carbon and hydrogen together represent approximately 95% of the asphalt composition. The next most abundant element is sulfur. There are also some small amounts of nitrogen and oxygen and heavy metals such as vanadium and nickel. The polar part of the asphalt (sulfur, nitrogen, and oxygen) defines how the asphalt molecules interact with each other and with other materials.

The elements are linked together in the form of long chains that can be arranged in three different ways: 1) straight chains: “aliphatic;” 2) simple or complex saturated rings: “naphtenic;” and 3) one or more stable six-carbon condensed, unsaturated ring structures: “aromatic.”

There are disagreements on the conceptual composition of the asphalts. Researchers have proposed different conceptual models. Petersen et al. (1994) discussed the history of these models. The main ones are as follows:

Asphalt as a Colloidal System: Petersen et al. (1994) used the “McGraw-Hill Encyclopedia of Science and Technology” to define a *colloidal system* as the phase made

up of particles having dimensions of 1-1000 nm that are dispersed in another phase. The authors claimed that Nellensteyn (1924) was the first to recognize the colloidal nature of asphalts. After Nellesteyn, Mack (1932) also concluded that asphalts are colloidal materials. Labout (1950) suggested that the amounts and characteristics of the asphaltene and maltene can be defined if the asphalt acts as "*sol*" (the asphaltenes are highly dispersed in the oily phase), "*gel*" (the resins are not as effective for dispersing the asphaltenes in the oily phase), or "*sol-gel*" (there is an intermediate dispersion).

Strategic Highway Research Program (SHRP) Microstructural Model: Jones and Kennedy (1991) mentioned other denominations given to the model. According to them, the SHRP model is also named as "polar dispersed fluid," "spaghetti and sauce," or "spider" model. There are two distinguishable phases: *associated* or *polar molecules*, which form the network and are responsible for the elastic behavior of the asphalt, and *solvent* or *nonpolar molecules*, which form the body of the network and are responsible for the viscous properties. Excessive amounts of the associated phase result in brittle asphalts and problems associated with cracking. Very low association results in problems associated with damage caused by moisture and in permanent deformation. SHRP also identified a type of molecule known as "amphoterics," which constituted only 10-15% of the asphalt composition, but are largely responsible for their viscoelastic properties. Figure 2.1 has been used by Jones and Kennedy (1991) as a scheme of the model. According to the authors, the SHRP study gave a clearer relationship between the chemistry and performance of asphalts.

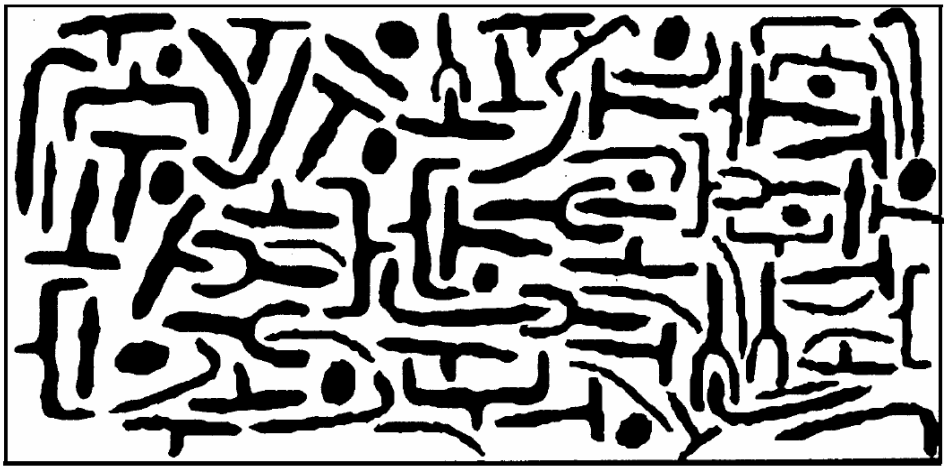

Figure 2.1 - SHRP microstructural model (Jones and Kennedy, 1991)

WSDOT (2006) summarized the failure mechanisms of the asphalt concrete and related them to the basic molecular or intermolecular chemistry of the asphalt. In case of the rutting distress, it is suggested that if the molecular network is relatively simple and not interconnected, asphalt will tend to deform inelastically when a load is applied (e.g., not all the deformation is recoverable). In addition, asphalt with a higher percentage of nonpolar dispersing molecules possesses better flow and plastic-deformation capabilities. The various fragments of network-forming polar molecules can move more easily relative to one another because of the higher percentage of nonpolar molecules in the fluid. In case of fatigue cracking, it is suggested that if the molecular network becomes very organized and rigid, asphalt will fracture rather than deform elastically under stress. Therefore, asphalt with a higher percentage of polar, network-forming molecules may be more susceptible to fatigue cracking. Details about aging, thermal cracking, stripping, and damage caused by moisture can be found in the references.

2.1.4. Viscoelastic Nature

According to Elseifi et al. (2006), the use of elastic theory to describe HMA behavior often results in an underestimation of the pavement responses for intermediate and high temperatures, where there is a flow and energy dissipation by frictional losses. The pavement response under high temperatures or loading in low frequencies results in distresses such as permanent deformation (rutting). The authors stated that HMA has only an elastic behavior at low temperatures or at highloading frequencies, when the rigidity of the HMA confers characteristics of an elastic solid to the material. This low-temperature elastic behavior causes nonload-associated low-temperature cracking. Fatigue occurs at intermediate temperatures and is a load-associated type of distress.

Stresses are a single-valued function of the strains in elastic materials, which are inappropriate for asphalt concretes, since stresses of asphalt concretes are functions of the entire history of the strains due to the viscoelastic characteristics. Findley et al. (1976) stated that viscoelasticity characterizes materials that exhibit strain-rate effects in response to applied stresses. In addition, Kim et al. (2002) stated that the responses of such types of materials are not only functions of the current input but also of the entire input history. The authors used the hereditary integral to relate the input (stress or strain) to the response (strain or stress) of linear viscoelastic materials.

Marasteanu and Anderson (2000) suggested that viscoelastic materials will be in their linear region when the magnitude of the deformation is sufficiently small or when the rate of deformation is sufficiently low relative to the relaxation time of the material. According to homogeneity concept, the strain output due to a stress input is equal to a

scalar multiplied by the strain output due to a stress input that was multiplied by that scalar. This means that if the input is doubled, the output should also be so. The superposition principle states that the strain output due to the combination of two arbitrary but different stress inputs applied at different times is equal to the sum of the strain outputs due to the stress inputs acting separately. Equations 2.1 and 2.2 provide an explanation for those concepts.

$$R\{cI\} = cR\{I\} \tag{2.1}$$

$$R\{Ia\} + R\{Ib\} = R\{Ia + Ib\} \tag{2.2}$$

where R = response (stress for strain input or strain for stress input);

I = input (either stress or strain);

a, b, c = scalar constants.

Kim et al. (2002) also distinguished aging from nonaging systems. For the aging systems, the response at any time is a function of the current time of loading (t) and the initial time of loading application (τ). For the nonaging system, the response at any time is a function of only the history of loading application time, or (t-τ). According to the researchers, the nonaging system is commonly used. Assuming that the system is nonaging, that the input starts at time $t = 0$, and that both input and response are zero for "t" < 0, the hereditary integral becomes

$$R = \int_0^t R_H(t-\tau)\frac{dI}{d\tau}d\tau \tag{2.3}$$

where R = response (stress if the strain is the input or strain if the stress is the input);

R_H = unit response function: creep compliance (D(t)) for stress input or relaxation modulus (E(t)) for strain input due to $H(t-\tau)$;

$H(t-\tau)$ = Heaviside Unit Step Function;

I = input (either stress or strain).

The Heaviside step function can be defined as follows:

$$H(n) = \begin{cases} 0, n < 0 \\ 1, n \geq 0 \end{cases} \tag{2.4}$$

For $n = (t - \tau)$,

$$H(\mathrm{t} - \tau) = \begin{cases} 0, \mathrm{t} < \tau \\ 1, \mathrm{t} \geq \tau \end{cases} \tag{2.5}$$

On the basis of Schapery's studies, Kim et al. (2002) also showed that there is a correspondence principle relating the constitutive equations of elastic and certain viscoelastic media. This principle is suitable for both linear and nonlinear materials. It states that stresses and strains are not necessarily physical quantities in the viscoelastic body, but pseudo variables in the form of convolution integrals. The uniaxial pseudo strain (ε^R) can be represented by:

$$\varepsilon^R = \frac{1}{E_R}\int_0^t E(t-\tau)\frac{\partial \varepsilon}{\partial \tau}d\tau \tag{2.6}$$

Where ε^R = uniaxial pseudo strain;

E_R = reference modulus that is an arbitrary constant and has the same unit as the relaxation modulus (E(t)). The authors use 1.0 in their research;

$E(t-\tau)$ = uniaxial relaxation modulus.

For the linear viscoelastic materials, a uniaxial stress-strain relationship is given as

$$\sigma(t) = \int_0^t E(t-\tau)\frac{d\varepsilon}{d\tau}d\tau \tag{2.7}$$

Using the pseudo strain, the stress equation mentioned above can be rewritten as

$$\sigma = E_R \varepsilon^R \tag{2.8}$$

Or, considering the Laplace domain and operations

$$L\left[\int f(t-\tau)g(\tau)d\tau\right] = \bar{f}\,\bar{g} \tag{2.9}$$

$$L\left[\frac{dh(t)}{dt}\right] = s\bar{h}, \tag{2.10}$$

Equation 2.7 becomes

$$\bar{\sigma} = \bar{E}\left(s\bar{\varepsilon}\right) \tag{2.11}$$

where f, g, and h = arbitrary functions;

s = Laplace transform variable;

$s\bar{E}$ = Carson transform of E.

Equation 2.11 is equivalent to Hooke's Law (linear elastic stress-strain relationship), except that stress and strain are in the Laplace transform domain and the Young's Modulus in the Carson transform domain. If the material is not tested beyond its linear viscoelastic range, no damage will be induced and the accumulated strain will be due exclusively to the viscoelasticity of that material. This argument indicates that the elastic-viscoelastic correspondence principle is a powerful tool to define the limits between the cases in which damage is induced and those in which damage is not induced.

Kim et al. (2004) suggested that the pseudo-strain concept based on Schapery's elastic-viscoelastic correspondence principle can represent nonlinear behavior of the viscoelastic material due to damage. Using this concept, material nonlinearity can be identified by characterizing the pseudo-variable history.

Figure 2.2 and Figure 2.3 were used by Lee and Kim (1998) to illustrate the linear nature of the relationship between stress and pseudo strain for cyclic loading tests when damage is not induced on the asphalt concrete specimen. The authors also defined how to obtain the pseudo strains, but this is out of the scope of this thesis and will be one of the targets of future works using data from this research. This research effort, however, has characterized the relaxation curves of mastics and HMA mixtures as a function of time, which are the fundamental quantities necessary for obtaining the pseudo strains for further stress-strain analyses.

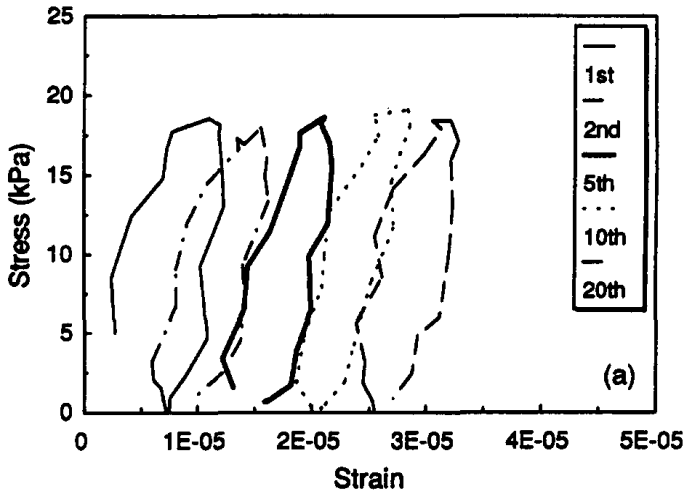

Figure 2.2 - Stress vs. strain (Lee and Kim, 1998)

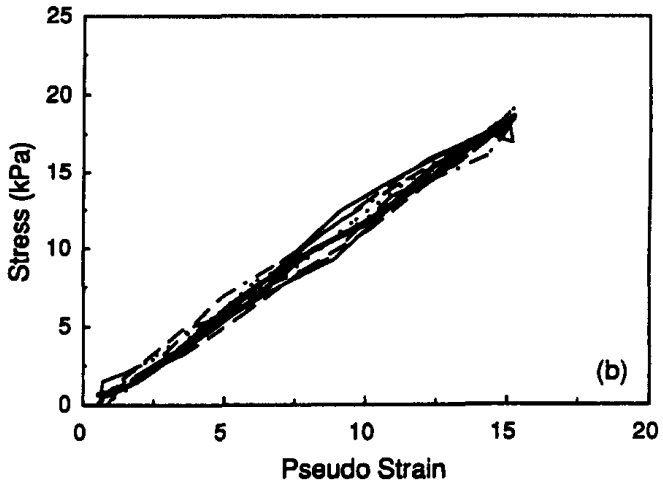

Figure 2.3 - Stress vs. pseudostrain (Lee and Kim, 1998)

AASHTO T315 recommends a procedure to define whether the material is within the viscoelastic range using Dynamic Shear Rheometer (DSR) tests. According to the recommendation, strain sweep tests should be conducted, and the linear region will then be defined as the range of strains where the $|G^*|$ is 95% or more of the initial value.

Marasteanu and Anderson (2000) presented a general approach for checking both homogeneity and superposition principles in oscillatory (by DSR), creep (by bending beam rheometer (BBR)), and monotonic constant strain-rate (by direct tension (DT)) tests. According to the authors, there are no documented studies for checking the superposition principle using DSR tests. They suggested that a multiwave experiment in which the applied stress (or strain) is composed of many stress (or strain) signals should be conducted simultaneously. For the linear range, the material response due to the multiwave signal should be equal to the sum of the responses due to the individual signals.

Smith (2004) defined viscoelastic material as "one that can both store and dissipate mechanical energy in response to deformation by a mechanical stress. The storage ability is referred to as elasticity and the dissipative losses are due to viscous effects." According to the author, an elastic material is the one that responds instantaneously to the solicitations, whereas viscous effects act to delay the response to a time-varying stress or strain. This delay is called "phase angle" (ϕ) or "time lag." A phase angle (ϕ) of 90° represents a perfect viscous behavior, whereas the 0° time lag characterizes an elastic material. Viscoelastic materials have phase angle between 0° and 90°. This means that when they are loaded, parts of the deformation are recoverable or elastic and the remaining parts are nonrecoverable or viscous.

According to Kim et al. (2002), the viscoelastic properties that should be obtained when modeling asphalt concrete are creep compliance, relaxation modulus, or complex modulus (from which phase angle and dynamic modulus are determined). The authors stated that the creep compliance and the complex modulus can be easily obtained from testing, whereas the relaxation modulus, which is essential for the calculation of the pseudo strains (Haifang, 2001), cannot be easily obtained from testing because of the high initial load caused by a step displacement input. However, the authors suggested that these three material properties are related and showed procedures to obtain the relaxation modulus from either the creep compliance or the complex modulus.

The asphalt resistance to deformation when subjected to a repeated sinusoidal load is represented by the so-called complex modulus (E^*). This modulus is expressed by a complex number composed of a real and an imaginary part. The real part is related to the so-called storage or elastic modulus (E'), whereas the imaginary part represents the

loss or viscous modulus (*E"*). The dynamic modulus can be obtained from the storage and loss modulus by using equation 2.12.

$$|E^*| = \sqrt{(E')^2 + (E'')^2} \tag{2.12}$$

Whereas *E'* and *E"* can be obtained from $|E^*|$ and ϕ by using the following relationships:

$$E' = |E^*| \cos\phi \tag{2.13}$$

$$E'' = |E^*| \sin\phi \tag{2.14}$$

Dougan et al. (2003) suggested that for the case where $\phi = 0°$ (pure elastic material), *E** confounds to its absolute value $|E^*|$.

The characterization of such a property of the binder is performed by applying a pure shear loading, using a DSR to produce the complex shear modulus (*G**). Figure 2.4 shows schematic illustrations relating *G**, *G'*, *G"*, and ϕ for two different binders.

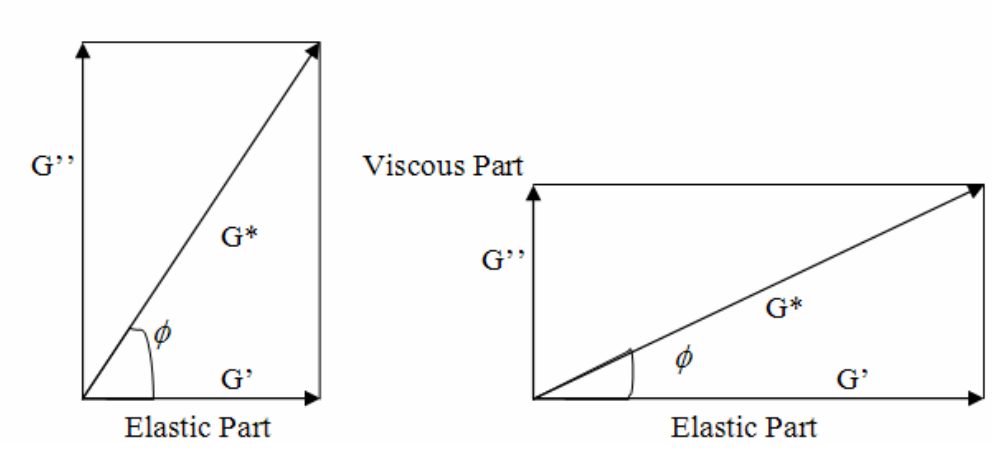

(a) **(b)**

Figure 2.4 - Dynamic shear modulus as a complex number for two different binders (Roberts et al., 1996)

Roberts et al. (1996) used Figure 2.4 to show that the complex modulus is not enough to characterize binders. The phase angle is also required. In Figure 2.4, both the first and second binders have the same dynamic shear modulus, represented by the length of the G* arrow. However, the binder in Figure 2.4a has a viscous portion that is larger than the second one. This means that this binder will display less recoverable and more nonrecoverable deformation when loaded than the binder shown in Figure 2.4b.

Roberts et al. (1996) also related G* and ϕ with rutting and fatigue performances, respectively. They stated that for any damage phenomena that occur in asphalt, the lower the amount of energy dissipated per cycle, the less is the distress that will occur. The authors used the work-dissipation concept to explain that, for improving rutting performance, the binder should exhibit a larger $|G^*|$ and a lower ϕ. The $|G^*|$ guarantees more resistance to permanent deformation because it represents a stiffer binder. Whereas the low ϕ produces a more elastic binder, which also increases the resistance to permanent or plastic deformation. For the enhancement of fatigue performance (strain-controlled phenomenon for thin HMA pavement layers), however, a binder with lower $|G^*|$ and lower ϕ should be used. The low $|G^*|$ allows the binder to deform without building up large stresses. The low ϕ allows the binder to regain its original condition after loading without dissipating work. Equations 2.15 and 2.16 are used to address the relationship between dissipated work and complex shear modulus and phase angle for rutting and fatigue, respectively.

$$W_c = (\pi)(\sigma_o)^2\left[\frac{1}{|G^*|/\sin\phi}\right] \tag{2.15}$$

$$W_c = (\pi)(\varepsilon_o)^2\left[|G^*|\sin\phi\right] \tag{2.16}$$

where W_c = work dissipated per load cycle;

σ_o = stress applied during the load cycle;

$|G^*|$ = dynamic shear modulus;

ϕ = phase angle;

ε_o = strain applied during the load cycle;

The total dissipated work after N cycles in either Equation 2.15 or 2.16 is then defined as:

$$W_{tot} = \sum_{i=1}^{N} W_c \tag{2.17}$$

Dougan et al. (2003) mentioned that the E^* of the mixtures is related to the G^* of the binders through the following equation:

$$E^* = 2(1+\upsilon)G^* \tag{2.18}$$

where υ = Poisson's ratio.

Note that Equation 2.18 is valid for the elastic case. For viscoelastic materials, the change in υ as a function of time should be taken into account.

The other two viscoelastic characteristics, stress relaxation and creep, are defined by Smith (2004) as follows: stress relaxation is the phenomenon of decay occurring over the time of induced stresses in a body when a strain is applied and then maintained constant (step function). Whereas creep is the increase in the strain deformation over time when stresses are applied as a step function to a body and may be defined as the time-dependent part of strain due to an applied stress. Creep compliance is the time-dependent strain divided by the applied stress (AASHTO T322). Relaxation modulus is the stress per unit of applied strain (Findley et al., 1976). Since the stiffness of asphalt is time

dependent, Anderson et al. (1994) suggested that such material should be classified as rheological material. The word is derived from the Greek "*rheo,*" which translates literally as "to flow." In addition, asphalt is also temperature dependent. Therefore, loading rate and temperature variations should be taken into account when characterizing the flow properties of asphaltic materials.

The time-temperature dependency in materials such as asphalt can be classified as thermorheologically simple because they exhibit similar behavior at fast loading rates and cold temperatures and at slow loading rates and high temperatures. This time-temperature dependency can be represented by a single parameter called reduced time, ξ, through the time-temperature superposition principle. This principle is a powerful tool to predict material behavior over a range of loading times that are much wider than the range of testing times. Lundström and Isacsson (2004) and Kim et al. (2002) expressed the reduced time as shown in Equation 2.19.

$$\xi = \frac{t}{a_T} \tag{2.19}$$

where t = physical time, i.e., time during the test;

a_T = time-temperature shift factor.

Kim et al. (2002) also suggested that, since the complex modulus is described as a function of frequency (f), a new parameter called reduced frequency, γ, should be used. Equation 2.20 represents the reduced frequency as a function of a_T.

$$\gamma = f \times a_T \tag{2.20}$$

The shift factor can be determined from any of the linear viscoelastic tests and should be the same for all the viscoelastic material properties, i.e., creep compliance,

relaxation modulus, and complex modulus. A more detailed discussion will appear later in the section Methodology.

The characterization of the viscoelastic materials is conducted based on simplistic models with arrangements of a number of Hookean springs representing the elastic behavior of the material and Newtonian dashpots representing the viscous part. For the springs, force is proportional to the applied deformation by a factor k (spring constant), such as $F = kx$. For the Newtonian dashpots, force is now proportional to the velocity of the deformation by a factor η (viscosity) such as $F = \eta \frac{dx}{dt}$. A combination of springs and dashpots is then used to characterize the viscoelastic models.

The creep and recovery of viscoelastic materials follow the pattern shown in Figure 2.5. The figure shows six distinct regions that explain the creep evolution. The material first deforms instantaneously and elastically because of the instantaneous change of load (Region 1). Then, there is a deceleration of the creep and this is the so-called primary or transient creep (Region 2). Furthermore, the primary region blends asymptotically into the secondary or steady-state creep (Region 3). When the load is removed, there is an instantaneous or elastic recovery (Region 4). Findley et al. (1976) suggested that this region is large for plastics and small for metals. At this point, it is important to state that, if the load is not removed, the secondary creep region will eventually change its slope, when the creep starts to accelerate and material begins to fracture. This is the so-called tertiary creep and is not shown in Figure 2.5. More details about the tertiary creep can be found in Gittus (1975). The next creep stage is the delayed recovery (Region 5). Finally, the material does not recover all of the deformation, and the irrecoverable or plastic portion appears (Region 6).

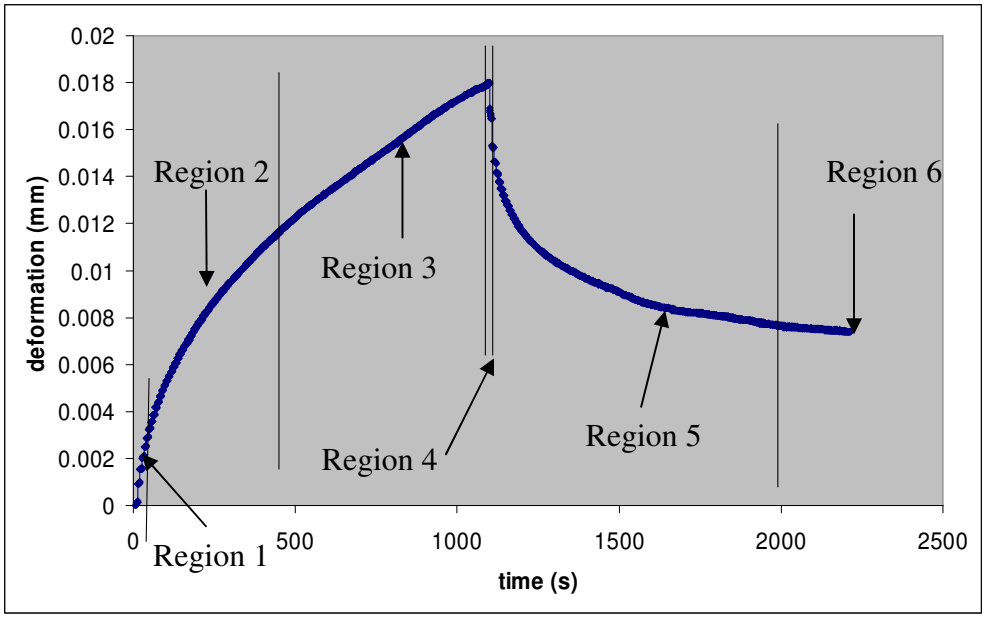

Figure 2.5 - Creep behavior of viscoelastic materials

The relaxation behavior is less complex than the creep. The stress of a viscoelastic material subjected to a constant strain will relax as shown in Figure 2.6.

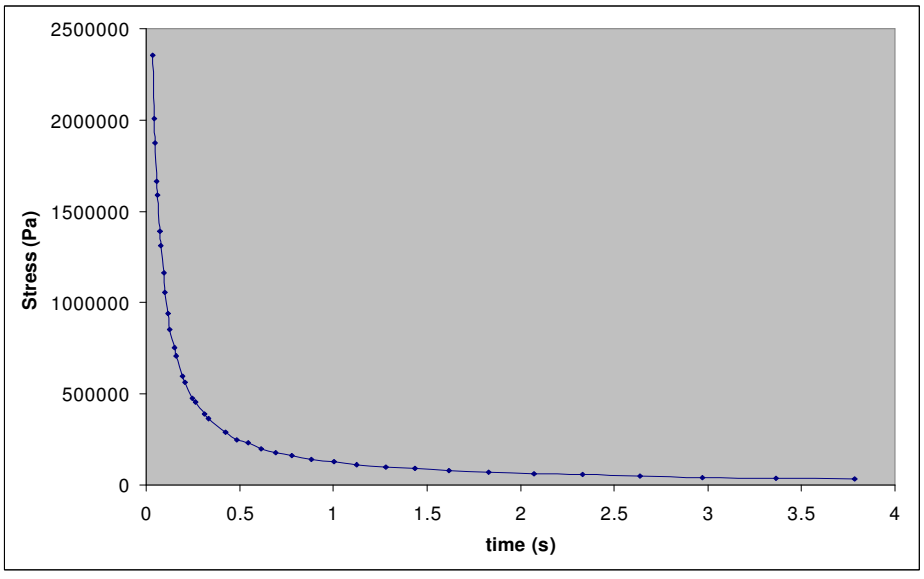

Figure 2.6 - Stress relaxation behavior of viscoelastic materials

There are several mechanical analogs available for viscoelastic analyses. The simplest ones are the Maxwell's (James Clerk Maxwell, 1831-1879) and the Voigt's (Woldemar Voigt, 1850-1919) models. In the Maxwell's model, one spring and one dashpot are combined in series. The resulting relaxation modulus (E_{MAX}) and creep compliance (D_{MAX}) as a function of time are:

$$E_{MAX}(t) = E_M e^{-\frac{E_M}{\eta_M}t} \tag{2.21}$$

$$D_{MAX}(t) = \frac{1}{E_M} + \frac{1}{\eta_M}t \tag{2.22}$$

where E_M = Young's modulus of the Maxwell's spring;

η_M = viscosity of the Maxwell's dashpot.

The corresponding graphs are shown in Figure 2.7 and Figure 2.8.

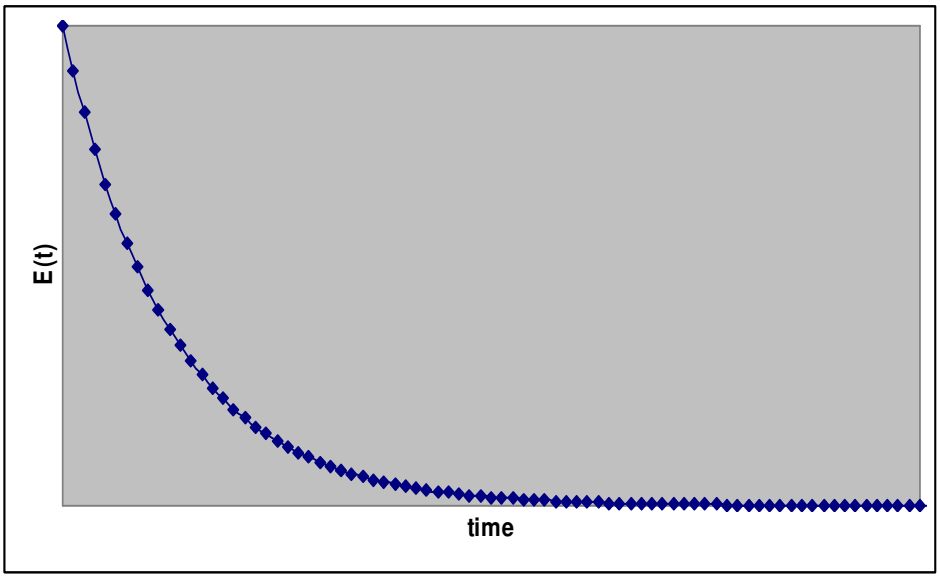

Figure 2.7 - Maxwell's model - relaxation modulus

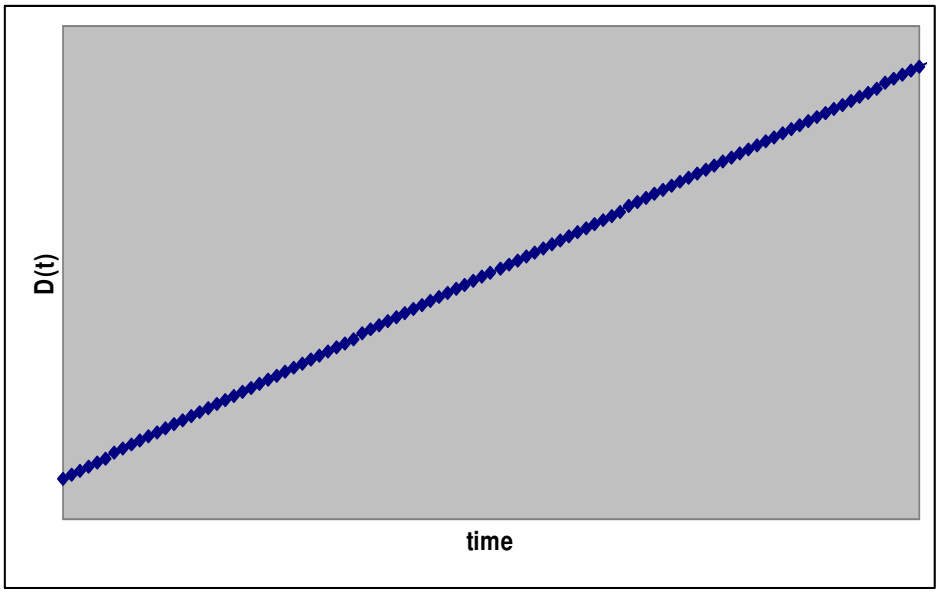

Figure 2.8 - Maxwell's model - creep compliance

Figure 2.8 shows that Maxwell model does not represent the reality, since the creep compliance in reality typically converges to an asymptotic value.

Voigt's model combines one spring with one dashpot in parallel. The corresponding relaxation modulus (E_{VOI}) and creep compliance (D_{VOI}) as a function of time are:

$$E_{VOI}(t) = E_V \tag{2.23}$$

$$D_{VOI}(t) = \frac{1}{E_V}(1 - e^{-\frac{E_V}{\eta_V}t}) \tag{2.24}$$

where E_V = Young's modulus of the Voigt's spring;

η_V = viscosity of the Voigt's dashpot.

The corresponding graphs are shown in Figure 2.9 and Figure 2.10.

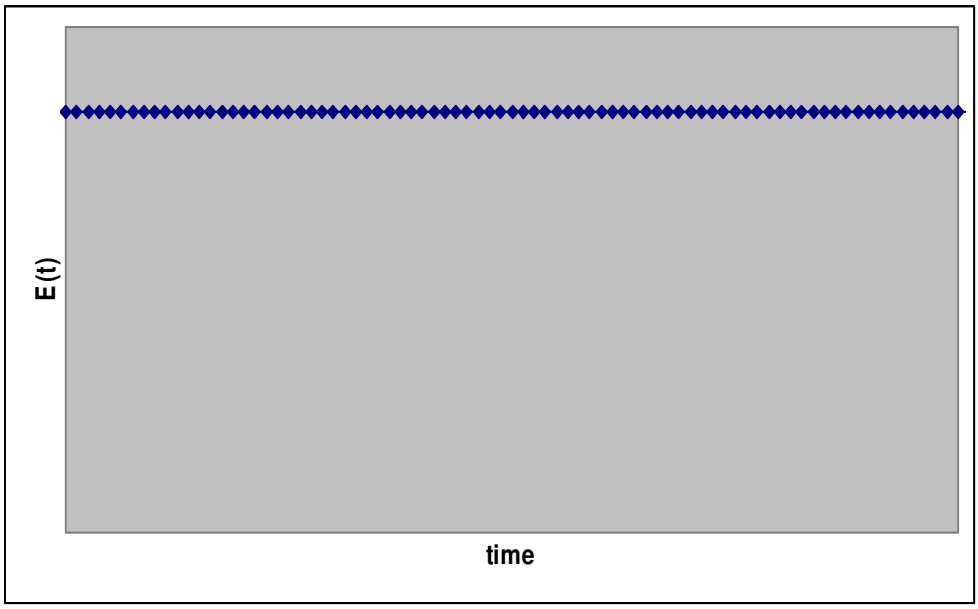

Figure 2.9 - Voigt's model - relaxation modulus

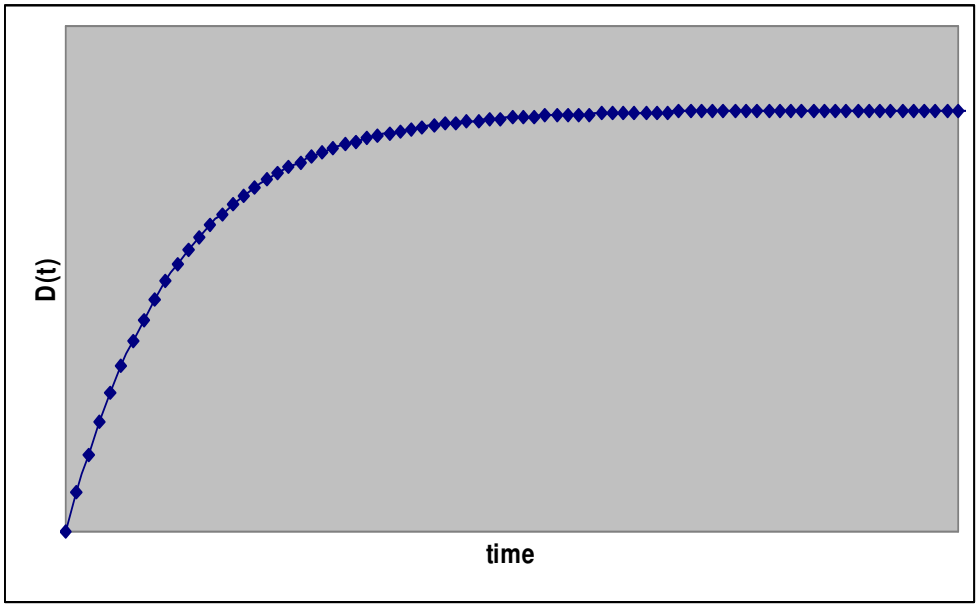

Figure 2.10 - Voigt's model - creep compliance

The limitation of the Voigt's model is evident due to the constant nature of its relaxation modulus. Another limitation is that its creep does not exhibit the instantaneous initial behavior as shown in Figure 2.5.

More elaborated arrangements are the standard linear solid (SLS) and the Burgers' (Johannes Martinus Burgers, 1895-1981) models. The SLS combines a Maxwell's element with a spring in series. The corresponding creep and relaxation behavior differ from the ones shown in Figure 2.5 and Figure 2.6. The stress of the SLS model relaxes in a manner similar to that shown in Figure 2.6, but does not tend to be zero or infinity, and the creep compliance has also a similar behavior to the one shown in Figure 2.5, but Region 6 is not present.

For the Burgers' model, there is an association in series of a Maxwell's and a Voigt's element. The presence of the Maxwell's dashpot creates the permanent strain (Region 6) shown in Figure 2.5. The Burgers' relaxation curve is also similar to the one shown in Figure 2.6.

To obtain more accurate viscoelastic representations, it is common to use a generalized Voigt (or Kelvin's - William Thomson, 1st Baron Kelvin, 1824-1907) or a generalized Maxwell (or Wiechert's - Dieter Weichert, 1948 to present date) model. Kelvin's model is an association in series of "*n*" Voigt's elements with one Maxwell's element. The Wiechert's model is an association in parallel between a spring and "*n*" Maxwell's elements. The analytical Prony-series expressions representing the relaxation modulus of the Wiechert's model and the creep compliance of the Kelvin's model are presented in the next section.

2.1.5. Analytical Representation of Linear Viscoelastic Properties

Kim et al. (2002) and Chehab and Kim (2007) summarized the primary ways of analytically representing the linear viscoelastic response functions: dynamic modulus, creep compliance, and relaxation modulus, and how to obtain one as a function of any of the other two.

The first task is to obtain one of the properties through experimental tests. To obtain the dynamic modulus, tests should be conducted at different temperatures and loading frequencies. The time-temperature superposition principle is then applied for the construction of master curves for $|E^*|$ and ϕ as a function of reduced frequencies. At this point, a mathematical function should be fitted to the master curve and this procedure will generate a representative analytical expression for the response over a broad frequency (or loading time) range.

The main analytical representations are: power laws, namely, pure power law (PPL), generalized power law (GPL), and modified power law (MPL), and the Prony series.

2.1.5.1. Power Laws

Chehab and Kim (2007) mentioned that the power-law expressions, though approximate and simplistic, yields fits that are globally smooth and stable. The first common power law is the so-called pure power law (PPL). This is the simplest one and can be represented by the following expression for creep compliance:

$$D(t) = D_1 t^n \tag{2.25}$$

where D_1 = creep compliance at t = 1 sec;

n = representative slope of the experimental data over the transient region plotted on a log-log scale.

The authors suggested that this power law has a limitation of poor representation to the regions other than the transient zone.

SHRP simple performance-test procedure for the creep testing (Appendix E) suggests the use of a PPL to fit the testing data. The next common power law is the generalized power law (GPL). The expression representing the creep compliance in a GPL form is given by:

$$D(t) = D_g + D_1 t^n \tag{2.26}$$

where D_g = glassy compliance or $D_g = \lim_{t \to 0} D(t)$.

The GPL fits the response more accurately than the PPL for the short-time behavior due to the D_g factor. However, it is not good for long-time data simulation.

The modified power law (MPL) for $D(t)$ can be represented as follows:

$$D(t) = D_g + \frac{D_e - D_g}{\left(1 + \frac{\tau}{t}\right)^n} \tag{2.27}$$

where D_e = long-time equilibrium or rubbery compliance or $D_e = \lim_{t \to \infty} D(t)$;

τ = characteristic retardation time;

n = slope of the linear portion of the creep-compliance master curve in log-log scale.

D_g and D_e can be determined by a simple inspection of the experimental data. This power law fits data in a much better way than the PPL and GPL. It creates a characteristic, broad-band, S-shaped curve. The MPL limitation lies in the representation of the top and bottom asymptotes of the S-shaped curve, where the curvatures are maximum. An improvement of this power law is the power law series (PLS) as represented below:

$$D(t) = D_g + \sum_{i=1}^{M} \frac{\hat{D}_i}{\left(1 + \frac{\hat{\tau}_i}{t}\right)^n} \tag{2.28}$$

where $\hat{D}_i$, $\hat{\tau}_i$ (for i = 1 to M), n and M being constants.

$\hat{\tau}_i$ values are to be assigned a priori, and the glassy compliance and n are determined from the measured data. To solve for the $\hat{D}_i$ values, one should solve the system of M equations by using the collocation method. Huang (2004) defines the collocation method as "an approximate method to collocate the computed and actual responses at predetermined number of time durations." The author also explained the determination of the coefficients of the Prony series using the collocation method. In general, the PLS fits data better as the number of "i" terms increases. However, Kim et al. (2002) and Chehab and Kim (2007) suggested that five terms (M=5) are enough for an accurate representation.

2.1.5.2. Prony Series

Chehab and Kim (2007) stated that the Prony series method is popular because of its ability to describe a wide range of viscoelastic response. In addition, it is computationally efficient because it is represented by exponential functions. Furthermore, it has also a basis in the theory of mechanical models represented by linear springs and dashpots, as mentioned previously.

The Prony series representing the creep compliance of the Kelvin's model and the relaxation modulus of the Wiechert's model are represented:

$$D(t) = D_0 + \sum_{j=1}^{n} D_j \left[1 - e^{-\frac{t}{\tau_j}} \right] \tag{2.29}$$

$$E(t) = E_\infty + \sum_{i=1}^{m} E_i e^{-\frac{t}{\rho_i}} \tag{2.30}$$

where D_o = glassy compliance related to the short-time creep behavior or $D_0 = \lim_{t \to 0} D(t)$;

E_∞ = long-time equilibrium modulus or $E_\infty = \lim_{t \to \infty} E(t)$;

D_j, E_i = Prony-series regression coefficients related to the retardation and relaxation;

τ_j = retardation time;

ρ_i = relaxation time.

2.1.6. Conversions Among the Viscoelastic Properties

Relaxation modulus, $E(t)$, is an essential parameter that is used to characterize pseudo strains. It was mentioned previously that it is a hard task to obtain *E(t)* directly from tests due to the high initial stress caused by the strain-step function input. However, the theory of linear viscoelasticity states that the viscoelastic material properties E(t), D(t), and $|E^*|$ are related and can be interconverted.

Before discussing the interconversions among the properties, it is appropriate to introduce the reader to a short mathematical overview of the problem. For an elastic material, the Young's modulus relates to the material compliance by:

$$E = \frac{1}{D} \tag{2.31}$$

However, this is not true if time dependency is introduced, as in a viscoelastic material. In that case, Equation 2.31 is not valid, and the relationship becomes:

$$\int_0^t E(t-\tau)\frac{dD(\tau)}{d\tau}d\tau = 1 \tag{2.32}$$

or

$$\int_0^t E(t-\tau)D(\tau)d\tau = t \tag{2.33}$$

These expressions are derived from the following constitutive equations:

$$\sigma(t) = \int_0^t E(t-\tau)\frac{d\varepsilon}{d\tau}d\tau \tag{2.34}$$

$$\varepsilon(t) = \int_0^t D(t-\tau)\frac{d\sigma}{d\tau}d\tau \tag{2.35}$$

Taking Laplace transform of Equations 2.34 and 2.35 and combining them, yields:

$$\overline{E}\,\overline{D} = \frac{1}{s^2} \tag{2.36}$$

or taking Carson transform, Equation 2.36 becomes:

$$\tilde{E}(s)\tilde{D}(s) = 1 \tag{2.37}$$

Taking the inverse Laplace transform of Equation 2.36, one obtains Equation 2.32 and/or Equation 2.33. Finally, Equation 2.37 is similar to Equation 2.31; however, Equation 2.37 is Carson transformed. Equations 2.38 and 2.39 show the Carson-transform expressions for the relaxation modulus and creep- compliance functions, respectively.

$$\tilde{E}(s) \equiv s\int_0^\infty E(t)e^{-st}dt \tag{2.38}$$

$$\tilde{D}(s) \equiv s\int_0^\infty D(t)e^{-st}dt \tag{2.39}$$

Equations 2.38 and 2.39 are defined by Park and Schapery (1999) as the operational modulus and compliance, respectively. The operational functions are in the Laplace domain. The authors also relate the operational functions to the functions of the complex material as follows:

$$E^*(w) = \tilde{E}(s)\Big|_{s\to i\omega} \tag{2.40}$$

$$D^*(w) = \tilde{D}(s)\Big|_{s\to i\omega} \tag{2.41}$$

From Equations 2.37, 2.40, and 2.41, the following relationship between the complex functions can be drawn:

$$E^*(\omega)D^*(\omega) = 1 \tag{2.42}$$

Finally, considering the Prony series representations of the creep compliance and of the relaxation modulus functions described previously in Equations 2.29 and 2.30, Park and Schapery (1999) presented the operational and the complex material functions as follows:

$$\tilde{E}(s) = E_\infty + \sum_{i=1}^{m} \frac{s\rho_i E_i}{s\rho_i + 1} \tag{2.43}$$

$$\tilde{D}(s) = D_0 + \frac{1}{\eta_0 s} + \sum_{j=1}^{n} \frac{D_j}{s\tau_j + 1} \tag{2.44}$$

$$E'(\omega) = E_\infty + \sum_{i=1}^{m} \frac{\omega^2 \rho_i^2 E_i}{\omega^2 \rho_i^2 + 1} \tag{2.45}$$

$$E''(\omega) = \sum_{i=1}^{m} \frac{\omega \rho_i^2 E_i}{\omega^2 \rho_i^2 + 1} \tag{2.46}$$

$$D'(\omega) = D_0 + \sum_{j=1}^{n} \frac{D_j}{\omega^2 \tau_j^2 + 1} \tag{2.47}$$

$$D''(\omega) = \frac{1}{\eta_0 \omega} + \sum_{j=1}^{n} \frac{\omega \tau_i D_i}{\omega^2 \tau_j^2 + 1} \tag{2.48}$$

where: s = Laplace variable;

ω = angular frequency;

η_0 = zero shear or long - time viscosity. For viscoelastic solids, $\eta_0 = 0$.

As can be seen from Equations 2.30, 2.43, 2.45, and 2.46, the coefficients to be determined in any expression of the complex modulus or of the operational modulus are the same as the ones presented in the expression for the relaxation modulus. Thus, one can define the relaxation function in Equation 2.30 by using the same coefficients

obtained from the fitting of Prony series to the experimental data of E'(ω), E"(ω), or $\tilde{E}(s)$. Note that both expressions 2.45 and 2.46 have the angular frequency.

There are other documented approaches to obtain E(t) from E'(ω), such as the one described by Kim et al. (2002). The authors used the following approximation:

$$E(t) \approx \frac{1}{\lambda'} E'(\omega)\Big|_{\omega=\left(\frac{1}{t}\right)} \tag{2.49}$$

$$\lambda' \approx \Gamma(1-n)\cos\left(\frac{n\pi}{2}\right) \tag{2.50}$$

$$n \equiv \frac{d\log E'(\omega)}{d\log \omega} \tag{2.51}$$

where $E(t)$ = relaxation modulus;

$E'(\omega)$ = storage modulus;

ω = angular frequency $= 2\pi f$;

Γ = gamma function.

The storage modulus is obtained from Equation 2.13. The value "*n*" is used for calculating each relaxation modulus point. Finally, after predicting the relaxation moduli over the desired time range, Equation 2.30 is fitted to this data and the coefficients, E_i and ρ_i, of the Prony series are determined.

Finally, Daniel and Kim (1998) use another approximated method proposed by Christensen (1982). According to the researchers, time and frequency are inversely proportional, but the relationship between time obtained from creep compliance and frequencies from dynamic modulus is not clearly defined. According to the authors, a common approximation used is:

$$f = \frac{0.1}{t} \tag{2.52}$$

They stated that this approximation comes from a relationship between *E(t)* and *E'(ω)* proposed by Christensen (1982) as follows:

$$E(t) \approx E'(\omega)\Big|_{\omega=\frac{2}{\pi t}} \tag{2.53}$$

where $\omega =$ angular frequency or $\omega = 2\pi$ f

Park and Schapery (1999) showed different ways to interconvert the viscoelastic functions. They discussed the relationships involving transient functions, operational functions, and complex functions. They suggested that when a set of constants, either $\{\rho_i, E_i (i = 1,..., m)$ and $E_\infty\}$ or $\{\tau_j, D_j (j = 1,..., n)$ and $D_0\}$, is known and the target-time constants (τ_j or ρ_i) are specified, the other set of constants can be determined by solving the resulting system of linear equations. For more details, the reader is referred to Park and Schapery (1999).

2.2. Aggregates

2.2.1. Definition

Aggregates are the broad category of basic materials used in construction, including sand, gravel, crushed stone, slag, and recycled concrete. Aggregates are a basic resource, necessary for any kind of modern construction. They are input materials to

concrete and asphalt mixtures. In addition, aggregates are used as base materials for foundations and roads. They are also defined as the components of a composite material used to resist compressive stresses.

2.2.2. Types

2.2.2.1. By Origin

According to Roberts et al. (1996), aggregates are largely obtained from local supplies of natural rock. Among the natural rocks, three main types have been identified by geologists. They are as follows:

Igneous rocks: formed by the cooling of molten rock magma; the classification is done based on the composition.

Sedimentary rocks: formed either by deposition of insoluble residue formed from the disintegration of existing rocks or from deposition of the inorganic remains of marine animals; the predominant mineral present is used for classification purposes (calcareous for predominance of limestone and siliceous for predominance of sandstone and argillaceous).

Metamorphic rocks: igneous or sedimentary rocks that have been subjected to heat and/or pressure sufficient to change their mineral structure.

Some materials such as lightweight aggregate produced by heating clay and slag from the steel production are mentioned as artificial aggregates used for HMA mixtures.

Gravels and sands are formed from the breakdown of any natural rock and the most resistant final residue formed by the deterioration of natural rocks, respectively.

Castelo Branco (2004) studied the effects of the heterogeneous steel-slag material on the performance of Marshall mixtures. She first characterized the expansible behavior of the material. The mechanical behavior of the asphalt mixtures with steel slag was characterized through tests such as the split tensile-strength test, resilient modulus test, fatigue test in controlled stress mode, and tests with moisture-induced damage. The author concluded that the steel slag is a potential material for asphalt surfacing layers. However, due to the high expansibility observed, a better control in the steel-slag production facilities should be made.

Roberts et al. (1996) summarized the quality of engineering properties of HMA mixtures using igneous, sedimentary, and metamorphic aggregates. They also stated that the most important effect of aggregate mineralogy is its influence on adhesion and damage caused by moisture. Asphalt cement normally tends to bond better to some aggregates such as limestone than to siliceous ones such as gravels. Prowell et al. (2005) stated that clay-like fine particles in the presence of water tend to produce mixtures prone to damage caused by moisture because they coat the fine aggregates and prevent the adherence of the asphalt to the aggregate surface.

Druta (2006) studied a possible link between G^* of binders with the ones of mastics and asphalt mixtures using the "master curve" technique and modified Hirsch and Shenoy models based on volumetric composition of asphalt mastics and mixtures. This model was used for estimating the asphalt concrete E* from binder modulus, voids in the mineral aggregate (VMA), and voids filled with asphalt (VFA). These volumetric

parameters will be discussed later in this thesis. Repeated shear creep and recovery tests were conducted to be used as a possible means to estimate the rate of accumulation of permanent strain in the mastics. Druta used a binder PG 64-22 and three types of filler (donna fill, limestone, and granite) in five varying amounts by volume (5, 10, 15, 20, and 30%) for the DSR characterization. From the analyses, he concluded that granite produced mastics with higher G* and rutting parameter $G^*/\sin\phi$, and this was due to its higher elastic modulus. These parameters were also higher for the highest amount of filler in volume (30%), which means that larger amounts of filler result in higher stiffness for mastics at the same temperature. Another conclusion was that shear phase-angles of mastics and asphalt concrete mixtures experienced the same trend at different testing temperatures (increasing the temperature leads to increase in the shear phase angles), whereas different loading frequencies of mastics and asphalt concrete mixtures showed opposing trends. For the mastics, the higher the loading frequency, the lower is the shear phase-angle. Whereas for the mixtures, the higher the loading frequency, the higher is the shear phase-angle. The author stated that this is due to the effect of mineral aggregate on the asphalt binder, which makes the binder behave more elastically.

2.2.2.2. By Gradation

Gradation is defined as the distribution of particle sizes expressed as a percent of the total weight. If the specific gravities of the aggregates used are similar, the gradation in volume will be similar to the gradation in weight. Roberts et al. (1996) suggested that "gradation is perhaps the most important property of an aggregate. It affects almost all

the important properties of a HMA, including stiffness, stability, durability, permeability, workability, fatigue resistance, frictional resistance, and resistance to moisture damage."

To determine the aggregate gradation, a sieve analysis shall be conducted. This is done by simply stacking a series of sieves with increasing openings from bottom to top and by weighing the material retained on each sieve. The typical sieves used are: 2", 1 ½", 1", ¾", ½", 3/8", No. 4, No. 8, No. 16, No. 30, No. 50, No. 100, and No. 200. A ½" sieve has openings equal to ½". A No. 4 sieve has four openings per inch. The sieves are stacked in such a way that the next sieve's openings are generally twice as large as the previous one (from bottom to top).

The gradation of aggregates can be classified as follows:

Dense-, well-, or continuous-graded: There is a continuous proportion of the various aggregate sizes, from fillers to coarse aggregates. This gradation provides high stability to the HMAs due to the increased particle contacts and the reduced VMA. However, the continuous gradations will result in mixtures more sensitive to slight changes in asphalt content.

Very dense gradations can generate problems with low air voids that do not allow a coating of enough film thickness of asphalt cement and produce nondurable mixtures. Many transportation agencies have suggested the use of gradations approximately parallel to the maximum density line (MDL) with some points above and below this line. Roberts et al. (1996) say that many researchers have proposed ideal gradations for maximum density. In the 1960s, FHWA introduced the 0.45-sieve size powered gradation. Using this type of chart, the MDL is easily drawn by connecting the origin to the percent

passing point of the nominal maximum aggregate size (NMAS) (defined later in the thesis).

Open-graded: It is the type of gradation that is typically used in the open-graded friction courses (OGFC). In a technical advisory, FHWA attributes the following advantages to the use of OGFC: it provides and maintains high speed and improved frictional qualities; reduces the potential for hydroplaning; reduces the amount of splash and spray; generally produces less noise, often providing a 3-5 decibel reduction in tire noise; improves night visibility of painted pavement markings; and helps in the preservation of high quality, polish-resistant aggregates, which may be scarce in some areas, because they are coated only as a surface layer, up to 3/4 inch thick. The limitations described in the same technical advisory are: it increases the potential for stripping of the surface and underlying pavement (it does not seal the underlying pavement against moisture intrusion); requires special snow- and ice-control methods and generally remains icy longer; requires special patching and rehabilitation techniques; does not add structural value to the pavement (its performance is governed by the condition of the underlying pavement); and may ravel and shove when used at intersections, locations with heavy turning movements, ramp terminals, curbed sections, and other adverse geometric locations.

Kandhal and Mallick (1998) asked numerous questions about OGFC to different agencies nationwide and concluded that significant improvements have been observed in the performance of OGFC since their introduction in the U.S. in the 1950s. Fifty percentage of the states indicated good experience with this type of mixture. A service life of eight years or more was reported by 70% of the states. The majority of the states

have good experience with the use of polymer-modified binders in the OGFC. Also, the gradations currently used tend to be coarser than the ones used in the past.

Mallick et al. (2000) evaluated the performance of OGFC with different gradations and types of additives and recommended a new mix-design system, so-called new-generation OGFC. The performance analysis was conducted based on drain-down potential, permeability, abrasion resistance, aging potential, and rutting. From their study, they concluded that coarser gradations produce better-performing OGFC mixtures. They also concluded that the use of modifiers (polymers and/or fibers) enhances the performance of OGFC.

Gap-graded: This is the type of gradation used for stone matrix asphalt (SMA) mixtures, a kind of asphaltic mixture developed in Germany in the 1960s and used in the U.S. since 1991 (Brown et al., 1997). SMA serves as a deformation-resistant and durable surfacing material and is suitable for roads with heavy traffic. SMA includes a high proportion of coarse aggregates that interlock to form a stone skeleton that resist permanent deformation. The stone skeleton is filled with a mastic composed of bitumen and filler, and fibers are added to provide stability to bitumen and to prevent drainage of binder during transport and placement. Typical SMA consists of 70-80% of coarse aggregate, 8.0-12.0% filler, 6.0-7.0% binder, and 0.3% fiber.

The advantages of using SMA are: the surface-texture characteristics of SMA are similar to those of OGFC so that the noise generated by traffic is lower than that from dense gradations, but equal to or slightly higher than OGFC; it can be produced and compacted using the same plant and equipment available for normal HMA mixtures; it may be used at intersections where OGFC is unsuitable; SMA surfacing may reduce

reflection cracking resulting from underlying cracked pavements due to the flexible mastic; and its durability is equal or greater than dense gradations and significantly greater than OGFC.

The disadvantages of SMA are: its high material costs; considerably longer mixing time and longer time taken for the addition of fillers; the possible delay in opening the traffic since SMA should be cooled to 40℃ to prevent flushing of the binder to the surface (bleeding); and its initial skid resistance may be insufficient until the thick binder is worn off from the top of the surface by traffic.

Brown et al. (1997) summarized mix design and performance data from 86 SMA projects nationwide. They concluded that more than 90% of the SMA projects had rutting measurements of less than 4 mm and approximately 25% did not even experience any rutting. Also, cracking (thermal and reflective) was not a significant problem. The authors stated that SMA appears to be more resistant to cracking than dense-graded mixtures. There was also no evidence of raveling. Finally, the authors believed that the extra cost for construction should be more than offset by the increased performance.

The gradations of all HMA mixtures used in this thesis were dense gradations and are in accordance with Superpave requirements.

2.2.2.3. By Size

Aggregates can be classified into coarse, fine, and filler based on their size. They can be defined as follows:

- Coarse aggregates are those retained on the sieve No. 4 (4.75 mm) (ASTM D692);
- Fine aggregates are those passing through the sieve No. 4 (4.75 mm) (ASTM 1073);
- Fillers are those materials of which at least 70% pass through the sieve No. 200 (0.075 mm) (ASTM D242). Pulverized limestone is the most commonly manufactured mineral filler, although other fillers such as stone dust, silica, hydrated lime, Portland cement, and certain natural deposits of finely divided mineral material are also used.

2.2.3. Properties

Several physical properties are necessary to characterize aggregates. Roberts et al. (1996) listed the physical properties as follows:

- Size and gradation
- Cleanliness/deleterious materials - resistance to weathering and effects of water
- Toughness/hardness - resistance to abrasion and degradation
- Durability - resistance to weather and aging effects
- Soundness - resistance to freezing and thawing
- Particle shape/surface texture - skid resistance
- Absorption

- Affinity to asphalt - related to the surface chemical characteristics of the aggregate.

Superpave defines the so-called consensus and the source properties. The former is uniformly adopted by all state agencies. Their criteria vary by traffic level and by properties related to rut depth in the pavement structure (Prowell et al., 2005). The consensus properties are:

Coarse aggregate angularity (CAA): It is specified at ASTM D5821. It is a subjective test that measures the number of one or more and two or more fractured faces in the coarse aggregates. The limit values depend on the traffic level and on the depth of the layer in the pavement structure. Rounded aggregates tend to contribute to shear failure of the pavement.

Fine aggregate angularity (FAA): It is specified at AASHTO T304-96 and represents a measurement of the amount of voids when a fine aggregate sample is poured into a cylinder. The amount of voids is proportional to the angularity of the fine aggregates. Limits also depend on traffic and on the depth of the layer in the pavement structure.

Flat and elongated particles (F&E): It is specified at ASTM D4791 and defines the ratio between the length and thickness of an aggregate. If the ratio is greater than five, the aggregate is said to be flat and elongated. Flat and elongated particles should be limited in the mixtures because they break easily, possibly leading to stripping of the asphalt film in the presence of water. This variation in the shape of aggregates also affects the volumetric parameters of the asphalt mixture. The amount of flat and elongated particles allowed is based on the traffic level.

Sand equivalent (SE) or clay content: It is specified at AASHTO T176 and is a measurement of the amount of fine dust or clay-like materials in soils or fine aggregates. The increased amount of dust reduces the binder adhesion to the aggregate particles. The outcome of the ASTM T176 test is related to the amount of sand and thus it is a minimum value in the specification. The limits for clay content are based on the traffic level.

Buchanan (2000) evaluated the effect of F&E on the volumetric properties of the mix design, rutting susceptibility, aggregate breakdown, and fatigue cracking of HMA mixtures. They used two types of aggregates: Alabama limestone and North Carolina granite. Both materials were evaluated by varying the 3:1 F&E percentages. Three different percentages were used. The rutting performance was evaluated by the APA test and the fatigue performance by the four-point beam fatigue test. The authors observed that increased amounts of 3:1 F&E led to increased breakdown of particles. More than 30% 3:1 F&E particles significantly affected the volumetric properties of the HMA mixtures. They also concluded that the amount of 3:1 F&E did not significantly affect the rutting results of mixtures using limestone during APA testing. For the HMA mixtures using granite, the rut depths increased with the increase of 3:1 F&E. However, for low percentages, this difference was not observed.

Pan et al. (2006) studied as to how the F&E, angularity index (AI), and surface texture (ST) affect the rutting performance of Superpave mixtures. The authors tested mixtures with above restricted zone (ARZ), through restricted zone (TRZ), and below restricted zone (BRZ) (to be defined later in the section "Superpave") gradations. They used a repeated load permanent deformation test with confinement to simulate more realistically the dynamic loading of highway traffic in the laboratory. From the tests, the

researchers characterized the slopes of the three permanent-deformation accumulation phases and the flow number (FN), which is the number of load repetitions at which the slope of the secondary phase increases and starts the tertiary phase. As defined previously in the thesis, this tertiary phase will lead to the eventual collapse of the asphalt concrete. Figure 2.11 illustrates these parameters. According to their study, F&E ratios had no measurable effects on the permanent deformations. FN tended to increase as the AI increased. This means that more angular coarse aggregates can improve the stability of the HMA. However, this relationship was with respect to only BRZ mixtures, whereas no measurable relationship between FN and AI was found for ARZ and TRZ mixtures. The researchers also concluded that mixtures with rougher textured aggregates have stronger aggregate structures, higher stability, longer lives, and better resistance to rutting. They finally concluded that the higher coefficient of determination (R^2) between FN and ST than the one between FN and AI infers a greater effect of surface texture than that of angularity on the rutting performances.

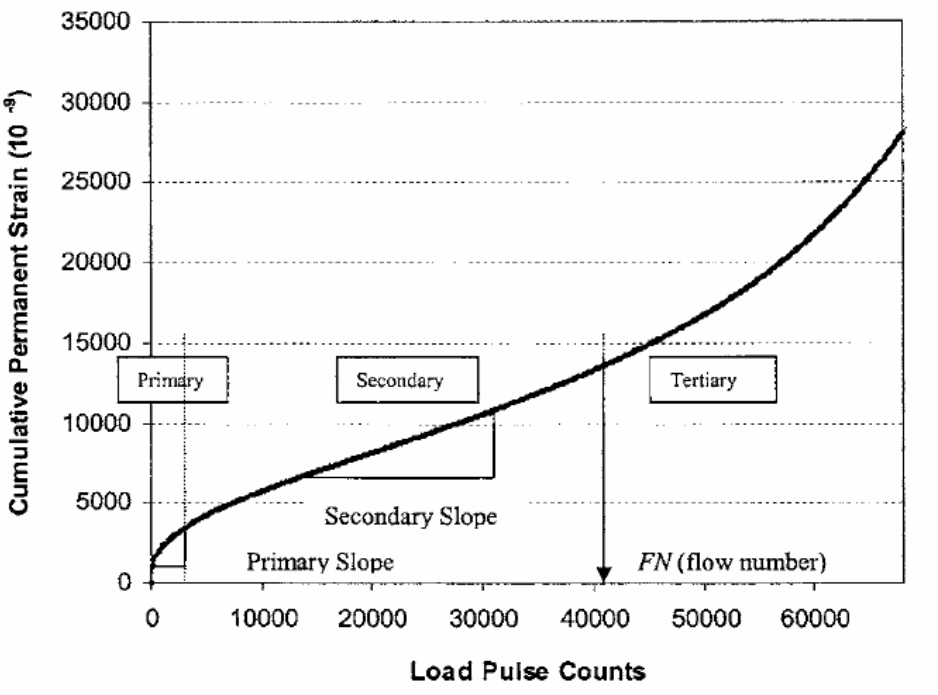

Figure 2.11 - Schematic of permanent strain accumulation in repeated load triaxial test (Pan et al., 2006)

Prowell et al. (2005) reviewed technical literature and ongoing research to analyze how consensus, source, or other aggregate properties significantly impacted the performance of HMA. For the consensus properties, they concluded that higher CAA produces more rutting-resistant mixtures. The researchers also suggested that there are several studies showing the proportionality between CAA and rutting performance, but there is little research to support the need for two fractured faces of at least 95%. Some agencies have lowered the fractured-face requirements, since it is nearly impossible to achieve 100%. For the FAA, several studies suggested 45% uncompacted voids for resistance to high traffic volume. However, there are some evidences demonstrating that mixtures with good performance can be obtained with the FAA between 43% and 45%. For F&E property, the authors suggested that only a limited number of studies have been conducted to relate the percentage of flat and elongated particles to performance since the

implementation of the Superpave program. According to them, none of those studies has addressed the relationship between the F&E and HMA performance at approximately the level of 10% particles exceeding the 5:1 ratio. The authors also concluded that no recent research has been able to show the relationship between clay-like particles and damage of HMA mixtures due to moisture.

White et al. (2006) used accelerated pavement testing techniques and ranked the aggregate tests depending on how well they relate to HMA performance. Full-scale accelerated loading conditions were used to relate aggregate properties to performance. The authors stated that the content of uncompacted voids of coarse aggregate (AASHTO TP56) was the best predictor of rutting performance of coarse-graded mixtures. This importance diminishes for lower traffic levels. At least 40% of the content of uncompacted voids is suggested for traffic level lower than 100,000 ESALs and at least 45% for traffic level over 100,000 ESALs. For the F&E analysis, they used a 2:1 (FOE21) ratio and concluded that rutting increases with increasing percentages of FOE21 particles. The resistance of HMAs to fatigue was also proportional to the amount of FOE21 particles. The content of uncompacted voids of fine aggregates was also related to the rutting performance of the HMA. However, similar to the coarse aggregates, the relationship between traffic level and the uncompacted voids in fine aggregates seemed to be less sensitive for lower traffic levels. At least 40% of the content of uncompacted voids was suggested for traffic levels below 500,000 ESALs and at least 45% for more than 500,000 ESALs. The resistance to fatigue cracking also tends to increase with the increase of the content of fine aggregate uncompacted voids.

Figure 2.12 and Figure 2.13 were used by the researchers to illustrate the difference in performance for two of the built sections during the study. Figure 2.12 shows a loading of 40 kN on dual wheels with a tire pressure of 690 kPa. This section failed after only 1,000 passes. The aggregate used for this section was uncrushed gravel. Figure 2.13 shows a pavement built with limestone. For this, a loading of 26.7 kN was applied to the dual wheels and the tire pressure was reduced to 620 kPa. Since this loading level caused no damage to the section, the load and pressure were gradually increased to 40 kN and 690 kPa, respectively. Only minor cracking appeared on the section, and the test was terminated after 80,000 passes. The subgrade, however, had to be repaired due to its failure.

Figure 2.12 - Weak asphalt section built with uncrushed gravel (White et al., 2006)

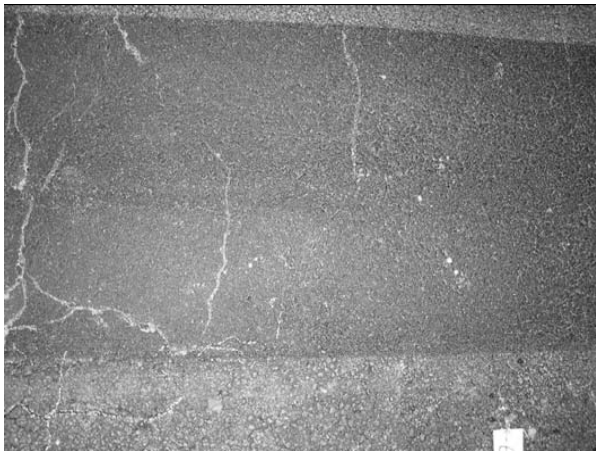

Figure 2.13 - Strong asphalt section built with limestone (White et al., 2006)

NDOR uses the following limits for the consensus properties of its different mixtures:

Table 2.2 - NDOR's consensus properties limits

Mix Type	FAA (min)	CAA (min)		F&E (%, max)	Sand Equivalent (min)
		> 1 fractured face (%)	> 2 fractured faces (%)		
SPS	N/R	35		25	30
SPL	43	83		N/R	N/R
SP-1	40	55		10	40
SP-2	43	65		10	40
SP-3	43	75		10	45
SP-4	45	85	80	10	45
SP-4 Special	45	85	80	10	45
SP-5	45	95	90	10	45
SP-6	45	95	90	10	45
RLC	45	85	80	10	45
LC	45	85	80	10	45

The source properties are optional, and their criteria are set from each state agency to account for the regional differences in geology. The source properties are:

Toughness: It is based on the Los Angeles abrasion test specified in AASHTO T96. According to Wu et al. (1998), aggregates must be tough and abrasion resistant to

prevent problems resulting from crushing, degradation, and disintegration during construction and under traffic loads. According to the authors, special care must be taken for OGFC, where coarse aggregates are subjected to high contact stress.

Soundness: AASHTO T104 uses sodium and magnesium sulfate to measure the soundness of aggregates. AASHTO T103 measures this material characteristic by subjecting the samples to freezing and thawing. These tests are used to measure the resistance to breakdown or disintegration of aggregates when subjected to wetting and drying and/or freezing and thawing conditions. Weak particles that break during compaction create stripping of the HMA, followed by problems associated with damage caused by moisture.

Deleterious materials: ASTM C142 is used to account for the presence of organics or other unsuitable materials (sulfate, alkalis, expansive silicates, etc.), which can contribute to pop-outs, raveling, and cracking in pavements.

2.3. Additives

Several different types of additives are available to improve performance of binders and HMA mixtures. Roberts et al. (1996) summarize additives as follows:

- Fillers
- Extenders
- Rubbers
- Plastics

- Combinations
- Fibers
- Oxidants
- Antioxidants
- Hydrocarbons
- Antistripping agents

Kandhal et al. (1998) conducted a study to determine the P200 (material passing through No. 200 sieve) characterization tests that are most related to the performance of HMA mixtures. In that attempt, the authors used a PG 64-22 binder and six P200 materials (natural sand, limestone, dolomite, granite, blast-furnace slag, and limerock) in two different filler/asphalt ratios by mass, 0.8 and 1.5. To characterize the six P200 materials, several different tests were conducted. The HMA mixtures were designed for intermediate traffic level (107 ESALs) and were tested using the Superpave shear tester and indirect tensile tester for evaluating HMA resistance to rutting and fatigue. Furthermore, the Hamburg wheel test and modified Lottman (AASHTO T283) test to characterize combined effects of rutting and moisture damage were also performed. From the testing data analyses, they concluded that the Superpave $G^*/\sin\phi$ is directly related to the fineness of the P200 materials. The finer the P200 materials, the more it modifies binder and HMA stiffness. No correlation was found between the Superpave shear-tester fatigue data and the P200 material properties. The stripping potential of the mixtures was also related to the fineness of the P200 materials in such a way that the finer the P200, the better is the stripping resistance of the mixtures.

2.3.1. Hydrated Lime: A Special Additive

Hydrated lime has been used as a mineral filler or an antistripping agent in HMA mixtures by many agencies across North America, including the NDOR. However, besides working as an antistripping agent, hydrated lime has also been recognized to improve properties and performance of asphalt mixtures.

The mechanisms and reactions occurring in the hydrated-lime-modified HMA mixtures are not fully understood (Bari and Witczak, 2005). Nevertheless, it has been known that hydrated lime forms insoluble salts with the highly polar molecules of the asphalt, which could decrease reactions with other mixture constituents to form water-soluble soaps that might promote stripping. Hydrated lime also improves the aggregate-asphalt bonding. The long-term oxidative aging potential of HMA can also be reduced by the addition of hydrated lime, from which it can be inferred that hydrated lime can reduce the viscosity-building polar components in the binder. Mixture segregation can be reduced by the use of hydrated lime because the finer particles of this material increase the binder film thickness and improve the binder cohesion, leading to the increased adhesion between aggregates and binder.

Bari and Witczak (2005) also reported that hydrated lime increases the indirect tensile strength and resilient modulus of mixtures. Moreover, the slope of HMA fatigue curves increases with the addition of hydrated lime, meaning that these mixtures support more loading cycles before failure. Rutting performance also improved because of the use of hydrated lime.

The National Lime Association (2006) has justified the improvement in fatigue performance of asphalt mixtures by the addition of hydrated lime with the following argument: "The greater improvement in fatigue life due to the addition of hydrated lime is a result of the reaction between hydrated lime and the polar molecules in the asphalt cement, which increases the effective volume of the lime particles by surrounding them with large organic chains. Consequently, the lime particles are better able to intercept and deflect microcracks, preventing them from coalescing into large cracks that can cause pavement failure."

Sebaaly (2006) updated a work from Little and Epps (2001), where the advantages of hydrated lime in HMA mixtures were analyzed. They suggested that the ability of hydrated lime to improve the resistance of HMA mixtures to damage caused by moisture, oxidative aging, mechanical properties, and fatigue and rutting performances results in approximate savings of $20/ton of HMA. They also analyzed field data and concluded that hydrated lime increases the average pavement lives in approximately 38%.

Kim et al. (2003) investigated the effect of fillers and binders on the fatigue performance of asphalt mixes. For this purpose, the researchers used two binders (AAD-1 and AAM-1) and two fillers (hydrated lime and limestone) in three different volume fractions (5, 10, and 25% filler/asphalt ratio). To analyze the effects of fillers, the authors used the theory of viscoelasticity, a continuum damage fatigue model, and a rheological particulate composite model. They concluded that filler type affected the fatigue behavior of asphalt binders and mastics. Fillers also stiffened the binders, and hydrated lime was more effective in stiffening binders than limestone-type filler. One of the conclusions

made by authors is that even if fillers stiffened the binders, they act in such a way that they provide better resistance to microcracking and thus increase fatigue life. The better performance observed in case of hydrated-lime-mixed mastics was interpreted by the authors as an indicator that a mechanism that goes beyond the volume-filling effect occurs. This can be supported by Sebaaly et al. (2006). Finally, the researchers concluded that the physicochemical interaction between the binder and the filler is material specific, since the improvement in fatigue life due to hydrated lime was much greater for the AAD-1 mix than for the AAM-1 mix.

Little and Petersen (2005) conducted a study to identify the unique effects of hydrated lime on the performance-related properties of asphalt cements. They concluded that if hydrated lime reacts as active filler with a binder, as shown by Kim et al. (2003) to occur for AAD-1 type but not for AAM-1-type binders, the hydrated lime provides a high-temperature filler effect that is greater than it would be predicted by models that do no account for physical interactions between the materials. However, it was shown that the effect of hydrated lime decreased as temperature is lowered. For very low temperatures, such as -20°C, the authors suggested that the stiffening provided by the use of hydrated lime is similar to the one provided by any other filler. They also concluded that the addition of hydrated lime toughens the mastics, which accounts for a higher resistance to fracture and crack propagation. Another finding was that hydrated lime is much more effective in extending fatigue life and in improving low-temperature cracking than is the limestone-type filler. Finally, they concluded that hydrated lime is more effective than limestone and that this effectiveness is bitumen dependent.

Bari and Witczak (2005) stated that the effects of hydrated lime on the dynamic modulus of HMA mixtures have rarely been evaluated. The authors mentioned that this evaluation is important since the dynamic modulus is the design-stiffness parameter at all three levels of hierarchical input for the HMA characterization of the new Mechanistic-Empirical Pavement Design Guide (MEPDG). In their studies, the authors used four different binders with different hydrated-lime contents and HMA mixtures from different locations, such as from Two Guns, Maryland Department of Transportation, WesTrack, Bidahouchi, and Salt River base mixtures. The general trend observed was the increase of stiffness as more amount of hydrated lime was added. However, for the Two Guns mixtures, an addition level of 2% of hydrated lime produced less stiff mixtures than the 1% addition case. On average, the rank of mixtures in the order of stiffness (low to high) was: 2%, 1% and 1.5%, 3%, and 2.5%. Finally, the authors quantified the amount of hydrated lime that interacts with the binder to increase stiffness. For 1% addition, the percentage interacting with the binder was approximately 2.8%. For the 2% case, this number increased to 3.3%. They concluded that the variation in these values reflects the complex interaction of hydrated lime with binder type and characteristics of aggregates.

2.4. Superpave

In an attempt to improve the performance, durability, safety, and efficiency of the HMA pavements, the U.S. Congress proposed the formation of the Strategic Highway Research Program (SHRP) in 1987. During five years of work (October 1987 - March 1993), $150 million was spent, of which $50 million was used for the development of

performance-based asphalt specifications to directly relate laboratory analysis to field performance (http://www.fhwa.dot.gov/ctdiv/whatsnew.htm, 2007). The SHRP researchers created the Superior Performing Asphalt Pavements (Superpave), a set of advancements in testing devices, protocols, and specifications for HMA materials and mixtures. Among these advancements are the novel method of grading binders and the novel mix design procedures.

The Superpave binder grading system in comparison to the traditional penetration and viscosity methods has the following advancements: It is not empirical. It relates physical and mechanical properties to the testing performances, considers various climates, includes the entire range of temperatures, controls the major pavement distresses (discussed later in the thesis), and includes specification for both modified and unmodified binders. For this grading system, performance parameters are fixed and a range of service temperatures within which the pavement exhibits satisfactory performance is determined. The extremes of this range represent the maximum pavement-temperature averaged from 7-day measurements at 20 mm deep and 1-day minimum temperature at pavement surface and are addressed by the so-called performance grade (PG). For example, a pavement with good performance with pavement temperatures ranging from -22 to 64°C is classified as PG 64-22.

2.4.1. Material Properties

The appropriate material selection, i.e. aggregates, binder, and additives is a key issue in the production of a high-quality HMA mixture. As mentioned previously, Superpave requires the characterization of the consensus aggregate properties.

The properties of binders to be addressed are related to their performance under high-, intermediate-, and low-temperature conditions. Superpave defines the following properties to characterize the binders: kinematic viscosity (in Pa.s) at 135°C, $G^*/\sin\phi$ (in kPa) with original and short-term aged conditions, $G^*\sin\phi$ (in kPa) with long-term aged conditions, creep stiffness (in MPa), and *m*-value with long-term aged conditions.

2.4.2. Binder Characterization Equipment

The binder properties are acquired from four equipments: the rotational viscometer (RV), the dynamic shear rheometer (DSR), the bending beam rheometer (BBR), and direct tension tester (DTT). The properties are evaluated under three different aging conditions: original (no aging), short-, and long-term aging. Aging of binders is simulated by performing the rolling thin film oven test (RTFOT) for the short-term aging and the pressure aging vessel (PAV) test to produce the long-term aged materials.

2.4.2.1. Rolling Thin Film Oven Test (RTFOT)

It is used to age the asphalt binders simulating short-term in-field aging conditions occurring during construction of HMA. Approximately 35 g of the binder is poured into each bottle, and this is placed in a rack inside the oven at 163°C. The rack is rotated for 75 minutes and the open orifice on the top of the bottle encounters an air jet during each rotation. The standard procedure for this test is shown in ASTM D2872.

2.4.2.2. Pressure Aging Vessel (PAV)

It simulates the aging of asphalt after 5 to 10 years of service life. This is achieved by exposing a 50 g RTFOT residue sample to a high air pressure (2,070 kPa) and temperature (90, 100, or 110°C) for 20 hours. The standards are ASTM D454 and ASTM D572.

2.4.2.3. Rotational Viscometer (RV)

It is used to determine the viscosity of asphalt binders at high construction temperatures (135°C for specification purposes) to ensure enough fluidity of the binder during the pumping and mixing activities. The equipment consists of a Bookfield viscometer and a stainless steel sample chamber, called Thermosel. The rotational viscosity is measured based on the torque necessary to maintain a constant rotational

speed (20 rpm) of a cylindrical spindle submerged in a binder at constant temperature. More details can be found from AASHTO TP48 and ASTM D4402.

2.4.2.4. Dynamic Shear Rheometer (DSR)

The DSR is used to characterize both elastic and viscous behaviors of binders. The test applies torque to the asphalt sample "sandwiched" between a fixed and an oscillating plate. The shape of loading wave is sinusoidal and is cyclic with no rest period. The loading frequency used for grading purposes is 10 rad/sec. The sample dimensions vary depending on the testing temperature: 8 mm diameter and 2 mm thick for testing temperatures between 4℃ and 40℃ and 25 mm diameter and 1 mm thick for higher testing temperatures.

The material properties directly obtained from the DSR test are G^* and ϕ. G^* is the ratio of the maximum shear stress (τ_{max}) to the maximum shear strain (γ_{max}) and ϕ is the phase angle between the shear stress and shear-strain sinusoidal wave peaks. Brown et al. (2001) suggested that this phase angle is generally obtained by the simple multiplication of the time lag (Δt) by the angular frequency applied (ω). These properties are used to evaluate the rutting and fatigue potentials of the binders using Equations 2.15 and 2.16, respectively. The goal for a better performance is achieved by minimizing the energy dissipation during the loading cycles to the lowest level. This is controlled by the minimum limit of 1 kPa and 2 kPa established by Superpave for $G^*/\sin\phi$ of unaged and RTFOT aged binders, respectively, and by the maximum limit of

5,000 kPa for $G^*\sin\phi$ of PAV aged binders. AASHTO TP5 is used as a standard for this test.

2.4.2.5. Bending Beam Rheometer (BBR)

This test is used to characterize the binder potential to thermal (or low temperature) cracking. This type of cracking occurs when the temperature drops resulting in a contraction in the pavement as the level of stress created exceeds the stress-relaxation ability of the HMA. Cracks are then produced to relieve this stress. A creep test is conducted by applying a constant load to a beam-shaped PAV aged specimen (125 mm long, 6.25 mm wide, and 12.5 mm high) at a constant low temperature. The deflection after 60 seconds of test is recorded and used to calculate the creep stiffness (*S(t)*). The rate of change in the stiffness is also characterized and expressed by the parameter "*m*-value," which represents the slope of the log *S(t)* versus log-time curve at any time. High *S(t)* is a sign that indicates that the thermal stresses that will occur in the pavement will be high and thus thermal cracking will become more likely. The reduction in the *m*-value represents a lower ability of the HMA to relieve the thermal stresses by flow, which increases the thermal-cracking-associated problems. Superpave requires maximum *S(t)* of 300 MPa and minimum *m*-value of 0.3. ASTM D790 is the specification associated with the BBR test.

2.4.2.6. Direct Tension Tester (DTT)

DTT is an optional test used to overcome the inability of BBR to characterize the low-temperature behavior of some modified binders, which may show very high creep stiffness (greater than 300 MPa but less than 600 MPa) but do not crack because of their good toughening mechanisms. The test is conducted by loading in small PAV aged "dog-bone"-shaped specimens under tension at a constant rate of 1 mm/min. The parameter recorded is the failure strain, which represents the deformation wherein the load on the specimen attains its maximum value. Superpave requires a minimum failure strain of 1%. AASHTO TP3 specifies testing procedures of the DTT.

2.5. Mix Design

The novel Superpave mix-design procedures are advanced compared with the traditional methods (Marshall and Hveem) because the Superpave mix-design methods simulate the field densification, the level of traffic, the different climates, and also provide a measurement of mixture compactability. The Superpave mix-design procedures will be explained in Section 3.5.

2.6. The Restricted Zone

Even though Superpave has raised innumerous advancements in comparison to the traditional methods, it has a limitation with regard to the study of aggregates. The only study of aggregates conducted by SHRP researchers was related to some issues on the asphalt-aggregate adhesion and the effects on it due to damage caused by moisture (Kandhal and Cooley Jr., 2001).

According to Khosla et al. (2001), the aggregates occupy approximately 85% of the volume of HMA. Prowell et al. (2005) stated that, considering mass, this number increased to 94-95%. On the basis of this fact, SHRP formed a group of 14 aggregate experts (aggregate Expert Task Group - ETG) that used the Modified Delphi method to develop recommendations and/or refinements of aggregate properties and gradations that should be used in the HMA mixtures and pavements. This method uses a series of questionnaires to collect experts' opinions and, in contrast to the traditional Delphi method, it allows the experts to meet face to face. The final recommended aggregate criteria included the control points and the restricted zone (RZ). Cooley Jr. et al. (2002) suggested that RZ was not a new concept. SHRP simply named a zone in gradations that had been for a long time recognized as a region in which, if gradations passed through, mixtures are susceptible to tenderness and rutting in field. Kandhal and Mallick (2001) mentioned that, prior to Superpave, most of the states in the U.S. have designed mixtures with above restricted zone (ARZ) or through restricted zone (TRZ) gradations.

The RZ lies along the maximum density line between the 0.3-mm sieve size (No. 50) and either the 2.36-mm (No. 8) or the 4.75-mm (No. 4) sieve size, depending on the

nominal maximum aggregate size (NMAS) of the mixture. The NMAS represents the sieve that is one sieve size larger than the first one through which more than 10% of the aggregates is retained. Figure 2.14 shows the RZ with a No. 8 sieve end and the maximum density line. According to the researchers, the RZ should not be violated because this would produce tender mixes during rolling and compaction. Another argument is that because mixes with gradations violating the RZ are denser than others, the voids in mineral aggregate (VMA) would be reduced and thus the mix would not have sufficient effective binder content and air voids. This scenario would result in mixes that are not resistant to surface flushing and rutting under the high summer temperatures. However, many research efforts showed that TRZ mixes perform similar or better than mixes not violating it. The general consensus is that mixes whose gradations undergo the restricted zone (i.e., below restricted zone (BRZ)) shows poor performance than the finer ones (i.e., ARZ and TRZ).

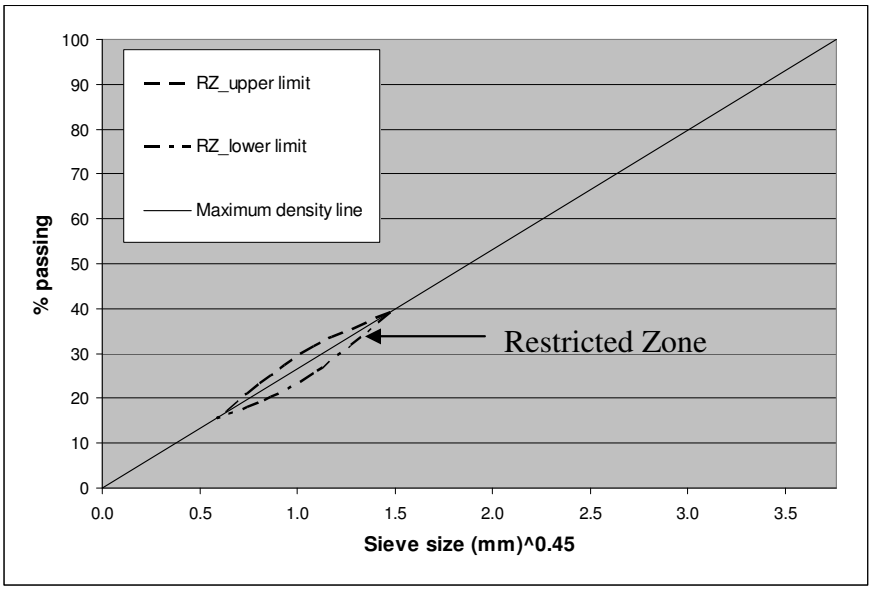

Figure 2.14 - Restricted zone and maximum density line in the 0.45 powered chart

Kim et al. (2006) analyzed the rutting performance of five different 12.5-mm (NMAS) Superpave dense-graded mixtures, of which one was ARZ, two TRZs violating the RZ concept (in the crossover style), and two BRZs. Confirming recent evidence from other research, the authors concluded that TRZ mixtures performed similar or better than others. The trend was that the finer gradation shows a better performance than coarser graded mixtures.

Nukunya et al. (2002) evaluated the Superpave RZ as a guideline for mixture design using either angular or nonangular aggregates and concluded that BRZ mixes are not rutting resistant because of the higher amount of asphalt cement necessary to achieve the high value of minimum specified VMA. The authors suggested that the VMA criteria for Superpave BRZ mixtures should be revised with caution to avoid the production of low-quality mixtures.

In 2001, Kandhal and Cooley performed intensive investigation of the Superpave RZ requirements by evaluating performances of ARZ, BRZ, and TRZs in three subcategories of gradations (humped through the restricted zone (Hump), all-the-way through the restricted zone (TRZ), and crossover through the restricted zone (Crossover)). Both 9.5- and 19-mm NMAS mixtures were analyzed. Figure 2.15 shows the gradations that were used. The researchers concluded that, if the volumetrics and FAA parameters meet the specification limits, the RZ is a redundant criterion. They also recommended that the RZ requirement should be deleted from AASHTO specifications and practice for Superpave volumetric design of HMA, regardless of NMAS or traffic level.

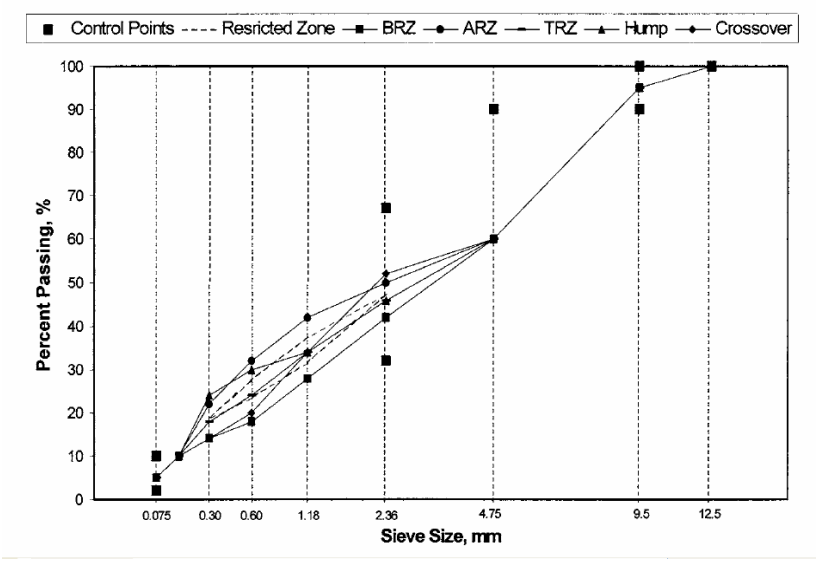

Figure 2.15 - Gradation types considering the restricted zone (Kandhal and Cooley Jr., 2001)

Cooley Jr. et al. (2002) reviewed 14 published research studies about RZ to determine its significance within Superpave gradation specifications. The vast majority of the research analyzed studied the effect of RZ on rutting performance of HMA. The relationships between RZ and fatigue and between RZ and low-temperature cracking were evaluated based on work of a single research project. They concluded that the literature indicates no relationships between RZ and rutting and fatigue performances.

Zhang et al. (2004) reported the effect of RZ on the HMA rutting performance of coarse-graded mixtures for high traffic levels specified by Alabama Department of Transportation (ALDOT). On the basis of the results of 12.5-, 19.0-, and 25.0-mm NMAS mixtures, these researchers again concluded that TRZ showed a similar or better performance than the others. They also suggested that the rutting performance of BRZ mixtures is more sensitive to aggregate properties than that of ARZ and TRZ mixtures.

Kandhal and Mallick (2001) evaluated the rutting potential of ARZ, TRZ, and BRZ Superpave dense-graded mixtures. The specimens were tested in the APA and Superpave shear tester (SST) machines. A PG 64-22 binder and three types of aggregates (limestone, gravel, and granite) were used. From the APA data, they found that, for granite and limestone, the ranking from worse to best rutting performance for gradations was of the order: BRZ, ARZ, and TRZ. For gravel mixtures, the trend was: ARZ, TRZ, and BRZ. From the SST test data for mixtures with granite, no significant differences were observed on the rutting potential between ARZ, TRZ, and BRZ. From the data on limestone mixtures, the researchers pointed the BRZ gradation as the most susceptible to rutting. Finally, for the mixtures with gravel, TRZ was the least susceptible to rutting and ARZ, the most susceptible to rutting.

Hand et al. (2001) evaluated the impact of gradation and NMAS on the rutting performance of HMA. A total of twenty-one mixes were evaluated. They found that NMAS did not significantly affect HMA performance. The laboratory test results for ARZ and TRZ gradations had a better permanent-deformation resistance than BRZ gradations.

Hand and Epps (2001) made a synopsis of recent research related to the impact of gradation with respect to the Superpave RZ on HMA performance. They reviewed thirteen journal papers and research reports that investigated the RZ-related gradation effects based on different experiments. A general finding from the study was that fine-graded (ARZ and TRZ) mixtures usually provided better performance than BRZ gradation mixtures, and in technical terms, adequate HMA performance could always be

obtained with gradations ranging from ARZ to BRZ, indicating no significant relationship between the Superpave RZ and HMA rutting or fatigue performance.

Sebaaly et al. (2004) analyzed results gathered from field test sections and the laboratory performance data. The test sections were designed using a series of mixtures for a range of traffic and environmental conditions typically encountered in Nevada. The field performance was monitored for up to five years after construction. Their findings concerning the Superpave RZ requirement showed that TRZ mixtures performed better than coarse-graded mixtures (BRZ mixes). They also found that TRZ mixtures had greater stiffness than BRZ mixtures made of the same materials.

Kandhal and Cooley Jr. (2002) compared coarse-graded Superpave mixtures (BRZ) with fine-graded Superpave mixtures (ARZ) in terms of resistance to rutting. To determine whether restrictions on gradation type (either coarse- or fine-graded mixtures) are necessary, three laboratory performance tests (APA, simple shear tester (SST), and repeated load confined creep (RLCC)) were performed. The test results indicated no significant difference in performance among the mixes analyzed.

Chowdhury et al. (2001a, 2001b) performed a comprehensive investigation of the RZ effect on HMA rutting-based performance. They accounted for the effect of RZ with respect to aggregate types (crushed granite, crushed limestone, crushed river gravel, and a mixture of crushed river gravel as coarse aggregate with natural fines) and gradations (ARZ, TRZ, and BRZ). The research concluded that there is no relationship between the RZ and permanent deformation when crushed aggregates are used in the mixture design. They also concluded that Superpave BRZ mixtures were generally the most susceptible to permanent deformation, whereas ARZ mixtures were the least susceptible to permanent

deformation. Recommendations include elimination of the RZ from HMA design specifications.

2.7. Pavement Distresses

There are several factors and mechanisms that cause failure of asphalt concrete structures. Figure 2.16 shows a section of pavement in the west Lincoln, Nebraska, with severe damage.

Figure 2.16 - Distresses of a low traffic pavement in Lincoln, NE

Among the documented distresses in asphalt concrete layers, the main ones are:

Alligator or fatigue cracking: It occurs due to an inadequate structural support for the given loading, which can be caused by: the decrease in pavement-load-supporting characteristics due to loss of base, subbase, or subgrade support resulting from poor

drainage or stripping at the bottom of the HMA layer; the level of load that exceeds the level anticipated by the design; inadequate structural design (very thin layers); and poor construction procedures such as inadequate compaction. Brown et al. (2001) suggested that for thin pavements, fatigue cracking starts at the bottom of the HMA due to high tensile strains and migrates upward toward the surface. Whereas for thick pavements, cracks start on the HMA surface due to tensile strains at the surface and migrate downward. If not repaired on time, this distress allows moisture to infiltrate and lead to problems arising from moisture damage. Figure 2.17 illustrates a fatigue failure of a pavement section in Lincoln, Nebraska. The potholes (shown in Figure 2.18), which are physically separated pieces of HMA dislodged from the pavement by the action of traffic, are also a consequence of the fatigue-related alligator cracking.

Figure 2.17 - Fatigue damaged pavement in Lincoln, NE

Figure 2.18 - Pothole created as a result of severe fatigue in Lincoln, NE

Rutting (see Figure 2.19): It represents the surface depressions. Possible causes of rutting are: insufficient compaction effort during construction, which results in increasing densification of the mix under traffic loads; inadequate pavement structure, which causes subgrade rutting; improper mix design (many rounded aggregates, excessive asphalt content, or very less air voids). Kandhal and Mallick (2001) also suggested that stiffer binder courses with larger aggregates generally have less rutting potential compared with more flexible wearing courses with finer aggregates and higher asphalt contents.

Figure 2.19 - Permanent deformation (rutting)

Transverse cracking (see Figure 2.20): Cracks are typically perpendicular to the pavement centerline. There are two types of transverse cracks: 1) reflective - occurs in a regular pattern and are due to cracks beneath the surface HMA layer; 2) thermal - occurs when the stresses caused by the shrinkage of the HMA surface under low temperatures exceed the HMA stress-relaxation ability. If those cracks are not repaired, moisture can infiltrate and can cause problems to the pavement structure.

Figure 2.20 - Thermal cracking

2.8. Material Viscoelastic Properties and Performance Tests

Tangella et al. (1990) reviewed the main factors affecting the fatigue performance of dense-graded HMA mixtures. They also reviewed various available fatigue test methods and addressed the advantages and disadvantages of these methods and ranked them in order of preference. The test methods evaluated were: simple flexural test, supported flexure test, direct axial test, indirect tensile test (IDT), fracture mechanics test, and wheel-tracking test. The flexural test was ranked as the best. Even though it results in a complex biaxial stress state and underestimates fatigue life, the IDT test was ranked second because it is simple and uses the same equipment as that for other tests.

Brown et al. (2001) evaluated available information on permanent deformation, fatigue cracking, low-temperature cracking, moisture susceptibility, and friction

properties, and recommended performance tests that could be immediately adopted to ensure improved performance. The authors focused more on the permanent-deformation testing procedures. On the basis of equipment availability, cost, testing time, quality control-quality assurance (QC-QA) aspects, and easiness to use, the researchers ranked the following permanent-deformation tests in the order of priority for recommended use: APA, Hamburg wheel-tracking device (HWTD), and French rutting tester (FRT).

Wen and Kim (2002) characterized viscoelastic properties of asphalt concretes in IDT testing mode and developed a simple performance test for fatigue cracking. The authors used the theory of viscoelasticity to develop analytical solutions for creep compliance and center strain from displacements measured on the specimen surface. Those solutions were verified by a 3-D finite element viscoelastic analysis. The tests conducted on the specimens were creep and tensile strength, both in the IDT mode. From their study, the researchers concluded that the creep compliance (a measurement of the stiffness and the time dependence of the material) at a given testing time does not contain enough information to predict resistance of the mixture to fatigue cracking. They also could not find any relationship between the *m*-value (constant slope of the secondary-flow region) and the amount of fatigue cracking in the HMA. Finally, they found an excellent correlation between fracture energy (defined as the area under the stress-strain curve in the loading portion of the test, which represents the sum of the strain energy with the dissipated energy due to structural changes, such as microcracking) at 20℃ and mixture resistance to fatigue cracking of both laboratory-made and field specimens.

Witczak et al. (2002) conducted a study on the different available testing procedures for characterization of HMA performance related to rutting, fatigue cracking,

and low-temperature cracking. The final product of their study consisted of five test methods named as simple performance tests (SPTs) as follows:

- Test method for dynamic modulus of asphalt concrete mixtures for permanent deformation;
- Test method for repeated load testing of asphalt-concrete mixtures in uniaxial compression;
- Test method for static creep - flow time of asphalt-concrete mixtures in compression;
- Test method for dynamic modulus of asphalt concrete mixtures for fatigue cracking;
- Test method for indirect tensile creep testing of asphalt mixtures for thermal cracking.

Kim et al. (2004) suggested that dynamic modulus is the most important HMA property to be characterized. The dynamic modulus represents the temperature- and frequency-dependent (and thus time-dependent) stiffness characteristics of the material. Contrary to the SHRP SPT uniaxial testing procedure for the characterization of the dynamic modulus, the authors claimed the IDT mode to be the most appropriate. This is due to the limitation in size of the in-situ cored samples. The uniaxial mode requires a long specimen for testing. This is not practically easy considering the few centimeters of the typical asphalt layer thickness.

2.8.1. Dynamic Modulus

Kim et al. (2004) proposed an analytical solution for testing the dynamic modulus of HMA sample in the IDT mode, considering the biaxial state of stresses and strains created and the theory of linear viscoelasticity. From their derivations, the final expression used to predict the dynamic modulus ($|E^*|$) and Poisson's ratio (υ) were as follows:

$$|E^*| = 2\frac{P_0}{\pi a d}\frac{\beta_1\gamma_2 - \beta_2\gamma_1}{\gamma_2 V_0 - \beta_2 U_0} \tag{2.54}$$

$$\upsilon = \frac{\beta_1 U_0 - \gamma_1 V_0}{-\beta_2 U_0 + \gamma_2 V_0} \tag{2.55}$$

where P_0 = amplitude of the sinusoidal load applied;

a = loading strip width;

d = specimen thickness;

U_0 = constant amplitude of horizontal displacements;

V_0 = constant amplitude of vertical displacements;

$\beta_1, \beta_2, \gamma_1, \gamma_2$ = coefficients related to the specimen diameter and gauge lengths used.

The calculated values for several combinations of specimen diameter and gauge lengths are given in Table 2.3. The authors validated the accuracy of their solution with experimental data from both uniaxial and IDT tests.

Table 2.3 - Coefficients for Poisson's ratio and dynamic modulus determination from IDT testing mode (Kim et al., 2004)

Specimen Diameter (mm)	Gauge Length (mm)	β_1	β_2	γ_1	γ_2
101.6	25.4	-0.0098	-0.0031	0.0029	0.0091
101.6	38.1	-0.0153	-0.0047	0.0040	0.0128
101.6	50.8	-0.0215	-0.0062	0.0047	0.0157
152.4	25.4	-0.0065	-0.0021	0.0020	0.0062
152.4	38.1	-0.0099	-0.0032	0.0029	0.0091
152.4	50.8	-0.0134	-0.0042	0.0037	0.0116

2.8.2. Creep Compliance

Wen and Kim (2002) derived linear viscoelastic solutions for Poisson's ratio and creep compliance for IDT creep tests and specimen center strain (ε_x=0) for IDT strength tests. Those are given as follows:

$$\nu = -\frac{\alpha_1 U(t) + V(t)}{\alpha_2 U(t) + \alpha_3 V(t)} \tag{2.56}$$

$$D(t) = -\frac{d}{P}\left[\beta_1 U(t) + \beta_2 V(t)\right] \tag{2.57}$$

$$\varepsilon_{x=0} = U(t)\frac{\gamma_1 + \gamma_2 \nu}{\gamma_3 + \gamma_4 \nu} \tag{2.58}$$

where $U(t)$ = horizontal displacement, m;

$V(t)$ = vertical displacement, m;

d = specimen thickness, m;

P = applied load, N;

$\alpha_1, \alpha_2, \alpha_{3,} \beta_1, \beta_2, \gamma_1, \gamma_2, \ \gamma_3, \ \gamma_4$ = coefficients related to the specimen diameter and gauge lengths used.

The calculated values of those coefficients for several combinations of specimen diameter and gauge lengths are given in Table 2.4.

Table 2.4 - Coefficients for Poisson's ratio, creep compliance, and center strain determination from IDT testing mode (Wen and Kim, 2002)

Specimen Diameter (mm)	*Gauge Length (mm)*	α_1	α_2	α_3	β_1	β_2	γ_1	γ_2	γ_3	γ_4
100	25.4	3.385	1.081	3.122	0.7874	2.2783	12.40	37.7	0.291	0.908
	50.8	4.580	1.316	3.341	0.4032	1.0240	12.40	37.7	0.471	1.570
150	25.4	3.172	1.039	3.060	1.1990	3.5330	8.48	25.6	0.207	0.634
	50.8	3.673	1.154	3.192	0.6110	1.6850	8.48	25.6	0.373	1.180
	76.2	4.559	1.330	3.311	0.4150	1.0340	8.48	25.6	0.478	1.590

CHAPTER 3

METHODOLOGY

3.1. Material Selection

3.1.1. Binder

Two binders were used in this study, a PG 64-22 from Koch Materials and a SBS-polymer-modified PG 64-28 from Jebro Inc. The PG 64-22 was used in this study to evaluate the effects of aggregate gradation and angularities on the rutting performance of HMA mixtures and the effects of mineral fillers on the stiffness of mastics.

The PG 64-28 binder was used for the fabrication of SP-4 Special mixtures, which are used to produce HMA mixtures for low-traffic-volume roadways (0.3 to 1.0 million ESALs) and have been used by the NDOR over the past four years as a replacement for SP-2 mixtures. For the compaction process of the mixture, the number of gyrations necessary for the SP-4 Special mixtures is the same as that for the SP-2 mixtures, but the consensus aggregate properties follow recommendations for SP-4 Special. According to Koves (2006), SP-4 Special mixtures require more crushed materials than do SP-2, which produces more rut-resistant materials. He said that this does not make those mixtures expensive (actually they are the cheapest one currently used by the NDOR) because of the high amount of recycled asphalt pavement (RAP) allowed. This PG 64-28 binder was

also used to obtain $|G^*|$ for mastics and to study the effect of hydrated lime in the mastic on the viscoelastic properties and performance of HMA mixtures.

3.1.2. Aggregates

The aggregates used in this research were: 1/4" Limestone (LS), 5/8" LS, screenings, 2A, and 3ACR. Beason (2006), 1/" LS, 5/8" LS, and screenings are angular materials obtained from the explosion of natural rocks in rock quarries (Weeping Water, Nebraska). The aggregate 3ACR, which represents three aggregates crushed and combined together, is an angular crushed gravel obtained from the Platte river in Nebraska.

According to Kettler (2007) and Baumgarten (2007), 3ACR can be classified as granitic gravel primarily composed of quartz and feldspar. They also mentioned that 3ACR has a neutral pH close to 7.3 and was also characterized as a hard material with hardness of approximately 7 in the Mohs hardness scale, varying from 0 to 10 (smallest to highest hardness). Kettler (2007) and Baumgarten (2007) also mentioned that screenings have a basic pH of approximately 12 and its hardness is approximately half of 3ACR. This information will be useful for the data analysis in the section related to the effect of fillers on the mastic stiffness. The aggregate, 2A, is an uncrushed (less angular) gravel, which is also taken from the boundaries of the Platte river. Those materials were chosen because of their wide use in Nebraska.

The HMA specimens produced throughout this research used the 1/4" LS, 5/8" LS, and 2A as coarse aggregates, and 3ACR and screenings for fine fractions and fillers.

3ACR and screenings were also used in this study to analyze the effect of fillers on the viscoelastic property ($|G^*|$) of mastics.

3.1.3. Hydrated Lime

Hydrated lime was obtained from Mississippi Lime Company. Although this additive has been used by NDOR as an antistripping agent to reduce the damage caused by moisture, this research uses it differently as a filler.

All mixtures fabricated for the evaluation of the viscoelastic property contain hydrated lime as one of their constituents. The effect of hydrated lime on the fatigue performance of HMA was also evaluated.

3.2. Material Characterization

3.2.1. Binder

Properties of the PG 64-22 and PG 64-28 were provided by NDOR. Table 3.1 and Table 3.2 present properties of the PG 64-22 and the PG 64-28, respectively. The mixing and compaction temperatures provided by NDOR were 152-157ºC (306-315ºF) and 139-144ºC (283-292ºF) for the PG 64-22 and 146-157ºC (295-315ºF), and 135-143ºC (275-290ºF) for the PG 64-28, respectively.

Table 3.1 - Mechanical properties of the PG 64-22 binder

Test	Temperature (°C)	Test Result	Required Value
Unaged DSR, G*/sinδ (kPa)	64	1.480	Min. 1.000
RTFO - Aged DSR, G*/sinδ (kPa)	64	3.499	Min. 2.200
PAV - Aged DSR, G*sinδ (kPa)	25	4,576	Max. 5,000
PAV - Aged BBR, Stiffness(MPa)	-12	203.970	Max. 300.000
PAV - Aged BBR, m-value	-12	0.312	Min. 0.300

Table 3.2 - Mechanical properties of the PG 64-28 binder

Test	Temperature (°C)	Test Result	Required Value
Unaged DSR, G*/sinδ (kPa)	64	1.205	Min. 1.000
RTFO - Aged DSR, G*/sinδ (kPa)	64	3.011	Min. 2.200
PAV - Aged DSR, G*sinδ (kPa)	19	2,112	Max. 5,000
PAV - Aged BBR, Stiffness(MPa)	-18	181	Max. 300
PAV - Aged BBR, m-value	-18	0.319	Min. 0.300

3.2.2. Aggregates

The aggregates were characterized by the standard methods discussed earlier. Table 3.3 summarizes the results.

Table 3.3 - Aggregate properties

Fine Aggregate							*Coarse Aggregate*
Aggregate	**$*G_{sb}$**	**Absorption Capacity (%)**	**FAA (%)**	**$*G_{sb}$**	**Absorption Capacity (%)**	**CAA (%)**	**Sand Equivalency (%)**
2A	2.580	0.76	37.6	2.589	0.68	28	100
1/4" LS	N/A	N/A	N/A	2.607	1.54	100	N/A
Screenings	2.478	3.66	46.7	N/A	N/A	N/A	26
5/8" LS	N/A	N/A	N/A	2.624	1.25	100	N/A
3ACR	2.556	1.13	43.7	2.588	0.75	70	84
47B	2.605	0.49	37.3	2.594	0.65	35	98

** Specific gravity of the aggregates.*

3.2.3. Hydrated Lime

Properties of the hydrated lime provided by the supplier are summarized in Table 3.4.

Table 3.4 - Physical and chemical properties of hydrated lime

Physical Properties	
Specific Gravity	2..343
Dry Brightness, G.E.	92
Median Particle Size - Sedigraph	2 micron
pH	12.4
BET Surface Area	22 m^2/g
-100 Mesh (150 µm)	100%
-200 Mesh (75 µm)	99%
-325 Mesh (45 µm)	94%
Apparent Dry Bulk Density - Loose	22lbs./ft^3
Apparent Dry Bulk Density - Packed	35lbs./ft^3
Chemical Properties (%)	
$Ca(OH)_2$ - Total	98.0000
$Ca(OH)_2$ - Available	96.8000
CO_2	0.5000
H_2O	0.7000
$CaSO_4$	0.1000
Sulfur - Equivalent	0.0240
Crystalline Silica	<0.1000
SiO_2	0.5000
Al_2O_3	0.2000
Fe_2O_3	0.0600
MgO	0.4000
P_2O_5	0.0100
MnO	0.0025

3.3. Fabrication of Mastics

Mastics are asphalt mixtures composed of binder and aggregates smaller than 75 microns (passing through No. 200 sieve). The mastics used in this research were blended in such a way that the filler/asphalt (F/A) ratio was always 0.3 in volume. This represents approximately 0.75 F/A in mass, which is within the NDOR limits: 0.7-1.7. The constituents are given in Table 3.5.

Table 3.5 - Recipes of mastics

Mastic	F/A		Mass of materials (g)			
	by mass	by volume	Binder	3ACR	Screenings	HL
3ACR	0.77	0.301	600.0	462.0	-	-
Screenings	0.77	0.302	600.0	-	460.0	-
3ACR + HL	0.75	0.300	600.0	337.5	-	112.5
Screenings + HL	0.75	0.300	600.0	-	337.5	112.5
HL	0.70	0.299	600.0	-	-	420.0

As shown in Table 3.5, the fabrication of mastics required 600 g of binder. Figure 3.1a shows the mixing process for producing the mastics, and Figure 3.1b shows the asphalt sample being poured into the DSR testing mold.

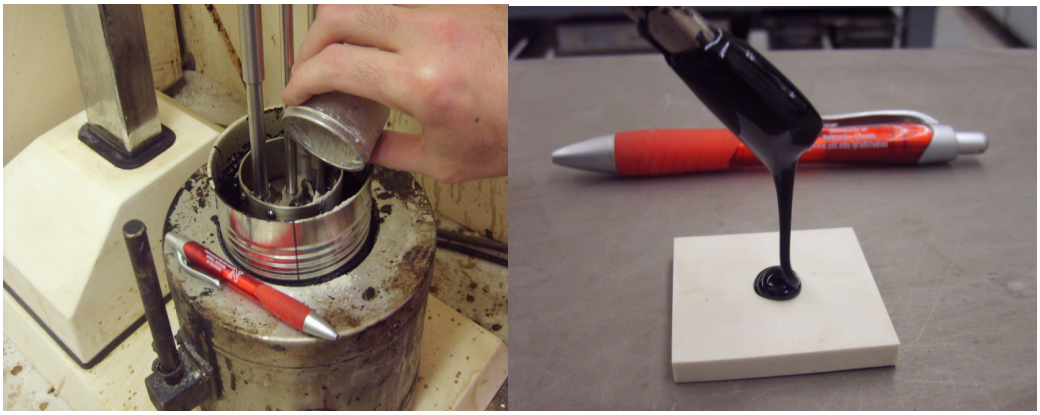

(a) **(b)**

Figure 3.1 - Mastic fabrication and the sample used for DSR testing

For both PG 64-22 and PG 64-28 binders, the specific gravities were assumed to be 1.0. The specific gravities of each filler (screenings, 3ACR, and hydrated lime) were measured and they are 2.552, 2.561, and 2.343, respectively.

For the fabrication of mastic, the 600 g of binder was placed in a metallic can and heated up to 150ºC. Then, the can with the binder was transported from the oven to a mechanical blender, which also has a heating system. Filler was then added slowly into the can and mixed to provide well-dispersed homogeneous mastics. After the mixing process, small amounts of DSR samples were prepared.

3.4. Viscoelastic Characterization of the Mastics

3.4.1. DSR

The DSR as shown in Figure 3.2 was used to characterize viscoelastic properties of the mastics. The first task for the characterization was to determine the level of strains over which the mastics showed a linear viscoelastic behavior. Strain sweep tests were conducted, and the $|G^*|$ was monitored. As presented by Kim et al. (2003), if the $|G^*|$ is 90% or above of the initial value, the level of strains corresponded to linear viscoelastic behavior of the binder or mastic.

Figure 3.2 - Dynamic Shear Rheometer (DSR)

Once the level of strains representing the linear viscoelastic behavior was determined, frequency sweep tests were conducted using an arbitrary value of strain within the linear viscoelastic region at different temperatures (20ºC, 30ºC, and 40ºC in this study).

From the frequency sweep test results, master curves for $|G^*|$ vs. loading frequency were constructed (Figure 3.3) by using the time (or frequency)-temperature superposition principle. This was done by applying a shifting factor (a_T) that produces the best match as shown in Figure 3.3(b). Once the master curves were constructed for a certain temperature (so-called reference temperature), material property (in this case $|G^*|$) can be predicted for any arbitrary temperature by using the shift factor. A graph relating log (a_T) with temperature can be developed as shown in Figure 3.4. Figure 3.5 shows the horizontal shifting used to produce a master curve at 24ºC from the master curve for reference temperature of 20ºC shown in Figure 3.3.

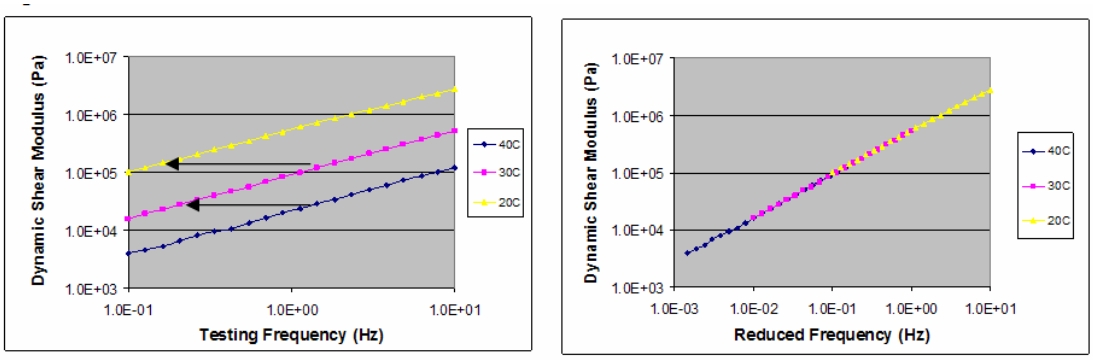

(a) **(b)**

Figure 3.3 - Master curve for 20 ℃

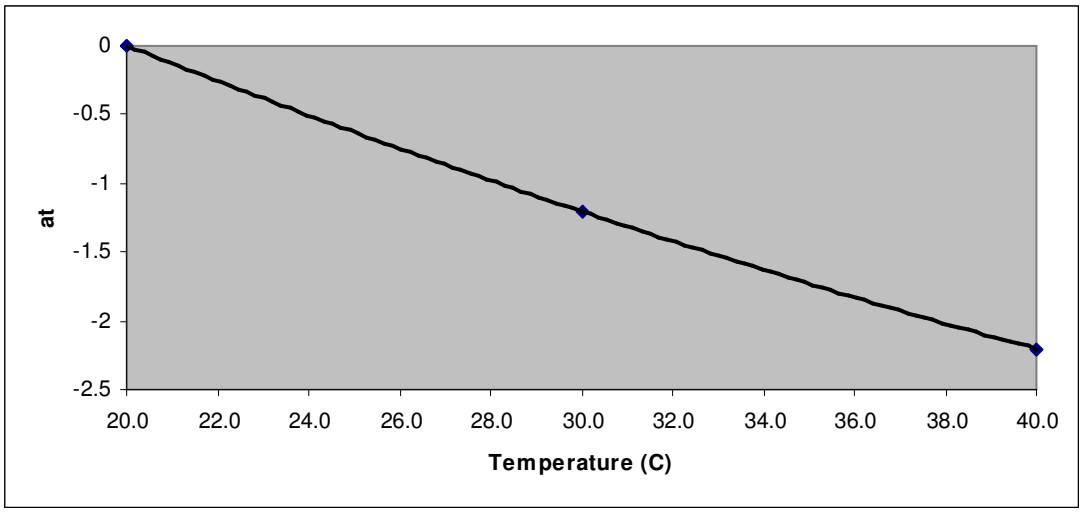

Figure 3.4 - Shifting factor vs. temperature

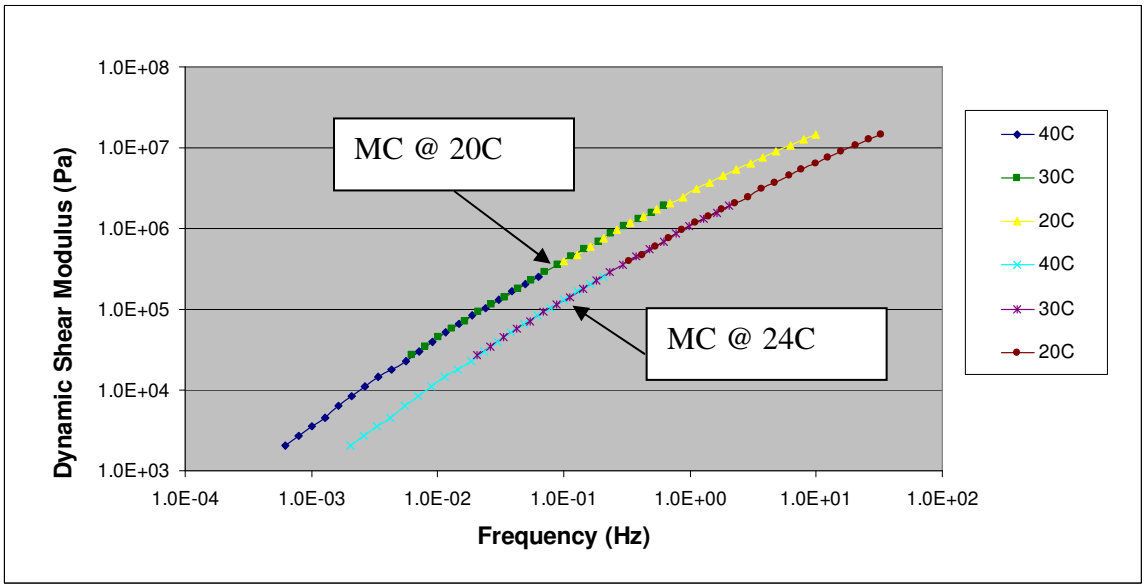

Figure 3.5 - Determining a master curve for any desired temperature

The same procedure can be applied to construct master curves in terms of G' (storage modulus), instead of $|G^*|$. From the master curves represented for the G', Prony series coefficients of the Wiechert's model can be found. As mentioned eariler, this can be accomplished by using a relationship between G(t) and the G' (see Equation 2.53).

3.5. HMA Mix Design

The HMA mixtures were designed following Superpave procedures and NDOR specifications. First, each aggregate was sieved, and the screenings were washed to remove additional dust adhering to fine particles. The aggregates were then proportioned for the fabrication of trial blends. Aggregate proportioning was performed with the aid of an Excel spreadsheet developed for monitoring overall properties of combined aggregate blends such as CAA, FAA, and specific gravities.

Once the gradation was determined, CAA and FAA were measured following ASTM 5821 and AASHTO T304-96, respectively. F&E and SE were not measured directly in this study, but they were measured and provided from NDOR.

The next step was to determine the optimum binder content that would create 3-5% air voids in the mixture as suggested by the NDOR specification. To determine the optimum binder content, trial HMA specimens were mixed and compacted using the Superpave gyratory compactor (SGC). Figure 3.6 is a schematic view of the SGC.

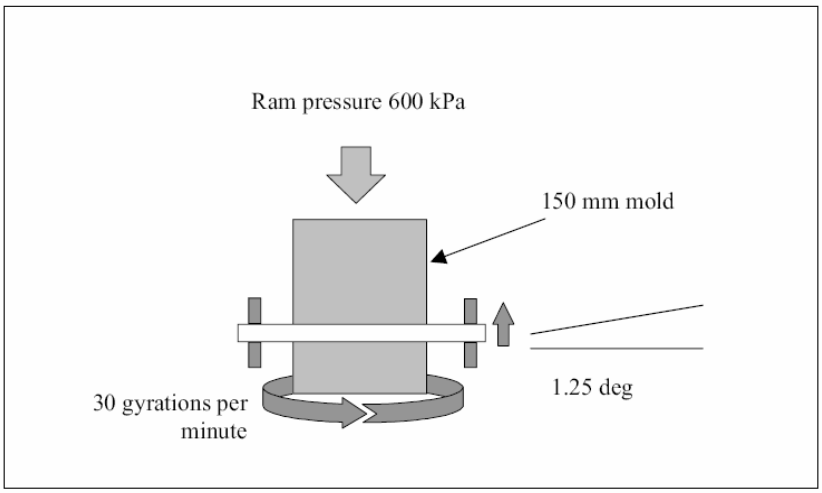

Figure 3.6 - Superpave Gyratory compactor (SGC)

For the mix design, the number of gyrations was controlled with 117 gyrations for both *SP-2* and *SP-4 Special* mixtures based on the NDOR HMA specification. The compaction effort (117 gyrations) was estimated based on the average value of high air temperature of 36.67ºC (98ºF) in Omaha, Nebraska. The diameter of the HMA sample was 150 mm. Figure 3.7 through Figure 3.9 summarize the steps involved in sample fabrication.

Figure 3.7 - Binder, aggregates, and sieves

Figure 3.8 - Mixing process

(a) **(b)**

Figure 3.9 - Loose mixtures into the SGC mold and compacted HMA sample

After the compaction, the theoretical maximum specific gravity (G_{MM}) and the bulk specific gravity (G_{MB}) of the HMA mixture were obtained. Using these two measurements, the air voids ($\%VA$), the voids in mineral aggregate ($\%VMA$), and the voids filled with asphalt ($\%VFA$) were calculated as follows:

$$\%VA = 100 * \frac{G_{MM} - G_{MB}}{G_{MM}} \tag{3.1}$$

$$\%VMA = 100 - \frac{G_{MB} @ N_{design}}{G_{SB}} * P_S \tag{3.2}$$

$$\%VFA = 100 * \frac{\%VA - \%VMA}{\%VA} \tag{3.3}$$

where $P_S = \%$ stone or is equal to 1 - %binder (by total mix);

Finally, the dust/binder (D/B) ratio was calculated. It should be noted that the D/B ratio used in this study follows NDOR definition, which is not same as the one proposed by National Superpave Program. The D/B ratio for this study was calculated by:

$$D/B = \frac{P_{200}}{P_b'} \tag{3.4}$$

where $P_{200} = \%$filler in the mixture;

$P_b' = \%$binder in mass by total mix.

Table 3.6 shows the requirements specified by NDOR for compaction efforts, aggregate properties, and volumetric parameters of *SP-2* and *SP-4 Special* mixtures.

Table 3.6 - Requirements proposed by NDOR for SP2 and SP4 special mixtures

	NDOR Mix Type	
	SP2	**SP4 special**
Compaction Effort (#of gyrations)		
@Nini	7	
@Ndes	76	
@Nmax	117	
Aggregate Properties		
%CAA (min)	65	85/80
%FAA (min)	43	45
%SE (min)	40	45
%F&E (max)	10	
Volumetric Parameters		
%VA	3 to 5	
%VMA (min)	14	
%VFA	65 to 78	65 to 75
%Pb	-	
D/B	0.7 to 1.7	

3.6. Characterization of Rutting by APA

To investigate the effects of RZ, CAA, and FAA of aggregates on HMA rutting performance, HMA samples of 150 mm diameter and 75 mm thickness with 4.0 ± 0.5% air voids were produced to conduct the APA testing. Figure 3.10 shows APA testing machine. The testing temperature was 64ºC as recommended by Kandhal and Cooley Jr. (2003). Before testing, samples were preheated for 6 - 24 hours in the APA chamber. The equipment could hold up to three pairs of samples at one time and repetitive linear loads through the pressurized hoses over wheels were applied. The hose pressure and wheel load were 690 kPa and 445 N (100 psi and 100 lb), respectively. The APA tests were conducted under dry conditions. The samples were tested up to a rut depth of 12 mm or were tested when 8,000 cycles were completed, whichever was attained first. If the sample reached 12 mm rut depths before the completion of 8,000 cycles, the test was manually stopped and the strokes (cycles of loading) corresponding to 12 mm rut depths were recorded.

Figure 3.10 - APA testing machine (NDOR)

3.7. Viscoelastic Properties of HMA Mixtures

The characterization of the viscoelastic property $|E^*|$ of HMA mixtures was conducted using a mechanical testing equipment named UTM-25kN. Figure 3.11 shows the UTM-25kN.

Viscoelastic properties of HMA mixtures were characterized in IDT mode. The procedure described herein is similar to the one proposed by Kim et al. (2002). SGC samples of 150 mm diameter and approximately 115 mm height were cored to finally produce a sample of approximately 100 mm diameter. Figure 3.12 shows the coring machine used and a cored sample from the SGC-compacted HMA mixture.

Figure 3.11 - UTM-25kN testing equipment

Figure 3.12 - Coring the SGC compacted HMA mixture

Each cored specimen was then cut to finally produce two IDT specimens (100 mm diameter and 38 mm high). Figure 3.13 shows the cutting process, and Figure 3.14 shows IDT specimens with gauge points attached. This coring and cutting process was employed to reduce the variation in the distribution of air voids in the sample and to obtain smooth surfaces that provide better bonding of the gauge points on the specimen.

Figure 3.13 - Cutting the cored HMA sample

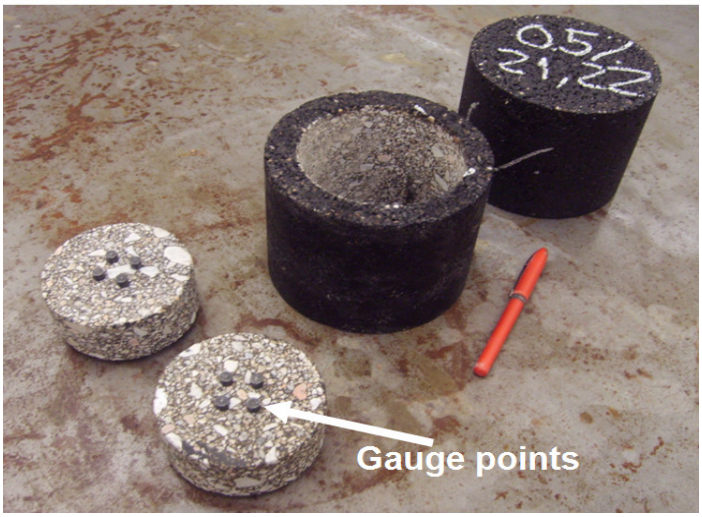

Figure 3.14 - IDT specimens from the coring-cutting process

The gauge points were placed as close as possible to the center of the specimen to alleviate positioning errors. A gauge-point mounting device as shown in Figure 3.15 was

developed. Lateral metallic bars were also used to avoid rotation and translation of the top and bottom plates while gluing the gauge points.

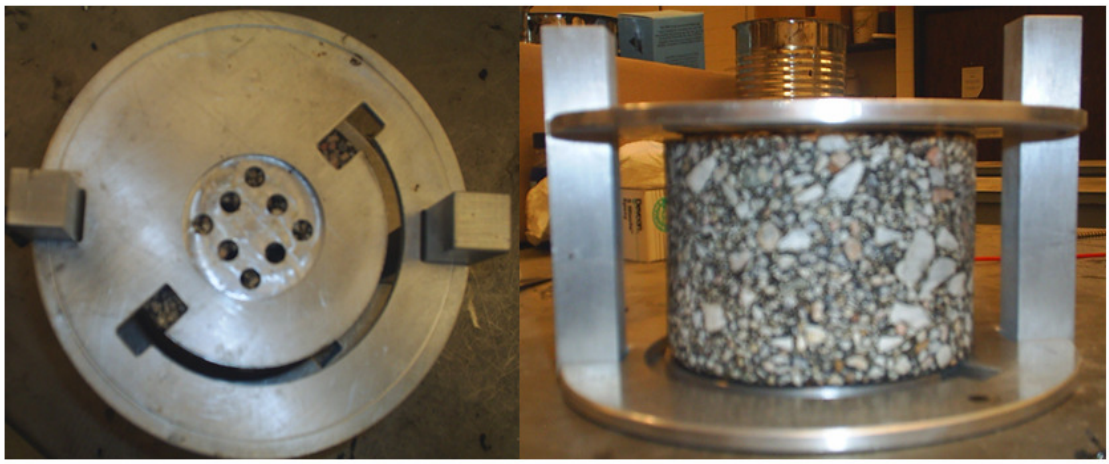

Figure 3.15 - Gauge points gluing device

The gauge length used to mount the extensometers for measuring deformations was 25.4mm. After gluing the gauge points and attaching the extensometers in both sides of the specimen, the specimen was placed between loading strips held together by two cylindrical bars. The specimens were then placed into the environmental chamber of the UTM-25kN for temperature conditioning, required for each test. A range of temperature that can be controlled by the environmental chamber is between -15°C and 60°C. Figure 3.16 shows the testing set-up with the specimen installed.

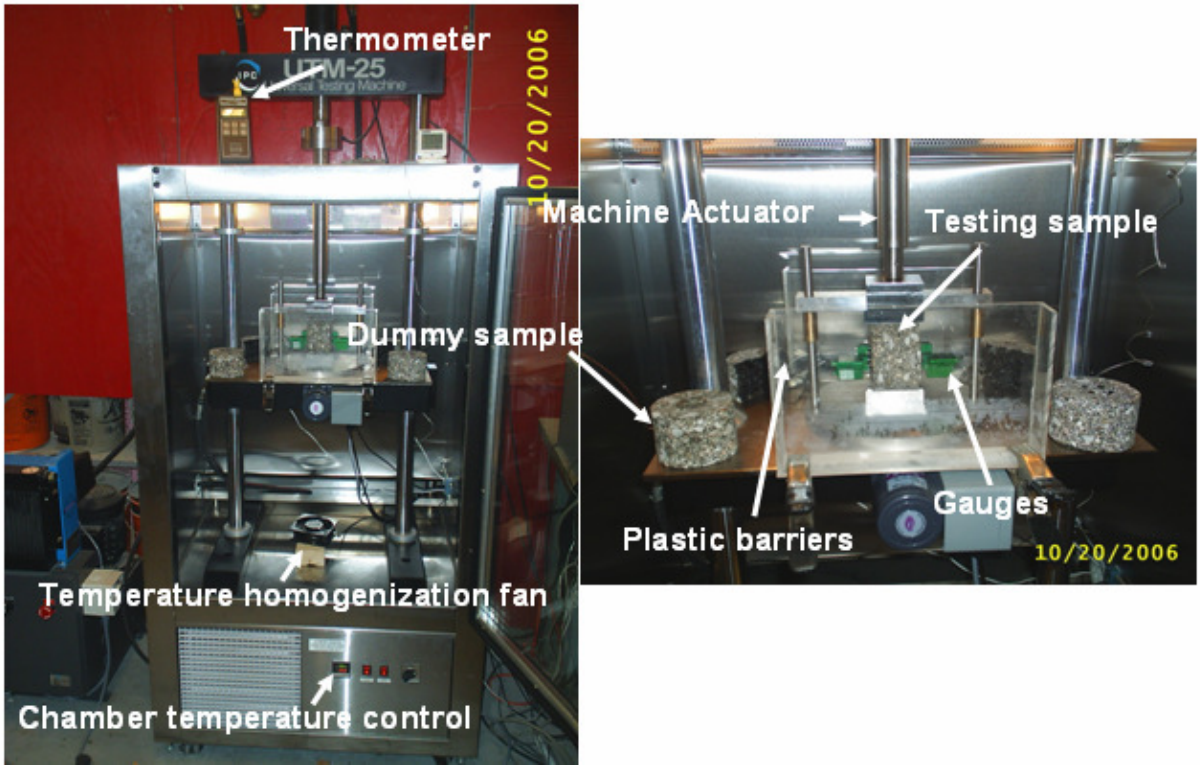

Figure 3.16 - Testing apparatus

In the IDT testing, a biaxial distribution of stresses and strains is created as shown in Figure 3.17. Kim et al. (2004) suggested that considering this biaxial stress-strain state, care must be taken when deriving the material properties. The modulus of the material cannot be obtained by simply dividing the horizontal stress by the horizontal strain. Instead, the modulus is associated with the ratio between the biaxial stress and the horizontal strain as given in Equation 3.5.

$$E = \frac{(\sigma_t - \upsilon\sigma_c)}{\varepsilon_x} \tag{3.5}$$

where $E =$ Young's modulus;

$\sigma_t =$ tensile stress along the horizontal direction (perpendicular to the direction of the applied load);

σ_c = compressive stress along the vertical direction (parallel to the direction of the applied load);

ε_t = strain along the horizontal direction;

υ = Poisson's ratio.

For viscoelastic materials subjected to sinusoidal load, Equation 3.5 becomes:

$$E^* = \frac{(\sigma_t - \upsilon\sigma_c)}{\varepsilon_x} \tag{3.6}$$

where E^* = complex modulus.

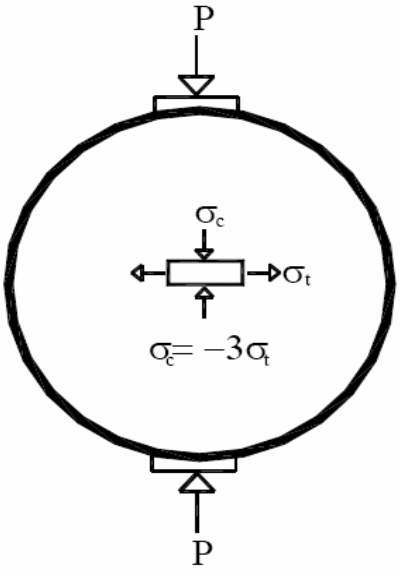

Figure 3.17 - Biaxial state of stresses at the center of an IDT sample

3.7.1. Dynamic Modulus Test

Appendix D of NCHRP report 465 (2002) and AASHTO TP62 (2003) recommend using uniaxial tests to determine the dynamic modulus of HMA mixtures. In the NCHRP protocol, a single effective temperature between 4ºC and 20ºC and a single design frequency between 5 Hz and 20 Hz are required to be chosen for testing. The linearity is controlled by applying a haversine load that will produce axial strains over the range of 50-150 microstrain. This loading level is higher at colder temperatures. Preconditioning of the specimen with 200 cycles at 25 Hz should be done before the actual test. Calculations of dynamic moduli and phase angles are made using the results of the last six loading cycles. The number of specimens required is related to the number of LVDTs used AASHTO TP62 (2003) recommends the following set of temperatures and frequencies: -10ºC, 4.4ºC, 21.1ºC, 37.8ºC, and 54.4ºC and 0.1 Hz, 0.5 Hz, 1 Hz, 5 Hz, 10 Hz, and 25 Hz. The number of cycles required for each of the frequencies is 15, 15, 20, 100, 200, and 200, respectively. The tests should be conducted from the lowest to the highest temperature and from the highest to the lowest frequency. The linearity is also controlled by applying a haversine load that will produce axial strains between 50 and 150 microstrain. The number of specimens required for a certain accuracy level depends on the number of LVDTs used. Calculations of dynamic moduli and phase angles are made based on the data of the last five cycles.

This research used procedures suggested by Kim et al. (2004). They derived an analytical solution for the dynamic modulus, considering linear viscoelasticity and the biaxial stress-strain state developed in an IDT testing mode. The authors suggested that

the reduction of the number of temperatures required by NCHRP 1-37A (2004) and/or the AASHTO TP62 (2003) could be compensated by adding two more testing frequencies based on the time-temperature superposition principle. This action can reduce the required testing time to obtain a master curve from 11 or 12 hours to less than 8 hours. The temperatures suggested for testing were 10ºC, 10ºC, and 35ºC, and the frequencies were 0.01 Hz, 0.05 Hz, 0.1 Hz, 0.5 Hz, 1 Hz, 5 Hz, 10 Hz, and 25 Hz. A comparison plot between master curves with the five temperatures and those with the three temperatures was made by the authors, and no major differences were observed. A good agreement between master curves obtained by IDT testing mode and the uniaxial testing mode also validate their recommendations to the IDT testing for characterizing the dynamic modulus of HMA mixtures. Table 3.7 summarizes loading frequencies and the number of loading cycles applied to each loading frequency used in this study.

Table 3.7 - Frequencies and number of cycles of IDT dynamic modulus tests

Frequency (Hz)	Cycles
25	200
10	200
5	100
1	20
0.5	15
0.1	15
0.05	15
0.01	15

From the testing results, the dynamic moduli for each frequency were calculated using Equation 2.54, and the data are shown in Table 2.3 for the specimen of 100 mm diameter and 38.1 mm height. The phase angles were also calculated by simply measuring the time delay between stress and strain for last five cycles. From $|E^*|$ and ϕ,

the storage moduli were calculated using Equation 2.13. Using Equation 2.45 and the collocation method, Prony series coefficients ρ_i and E_i were determined for identifying the relaxation modulus function E(t).

3.8. Indirect Tension (IDT) Fatigue Performance Test

The characterization of fatigue performance was conducted by applying haversine loads at 10 Hz to IDT specimens designed with two different amounts of hydrated lime (0.5% and 2.0% by total weight of aggregates) in the HMA mixture. The number of loading cycles at the beginning of the tertiary flow from the horizontal gauges was used for measuring the fatigue life of the specimen. Figure 3.18 illustrates the shape of the applied load, and Figure 3.19 shows the fatigue-failure criterion adopted in this study. Finally, *S-N* (applied stress - the number of loading cycles to failure) curves of each mixture were drawn and compared to characterize the material-specific fatigue behavior due to the addition of hydrated lime.

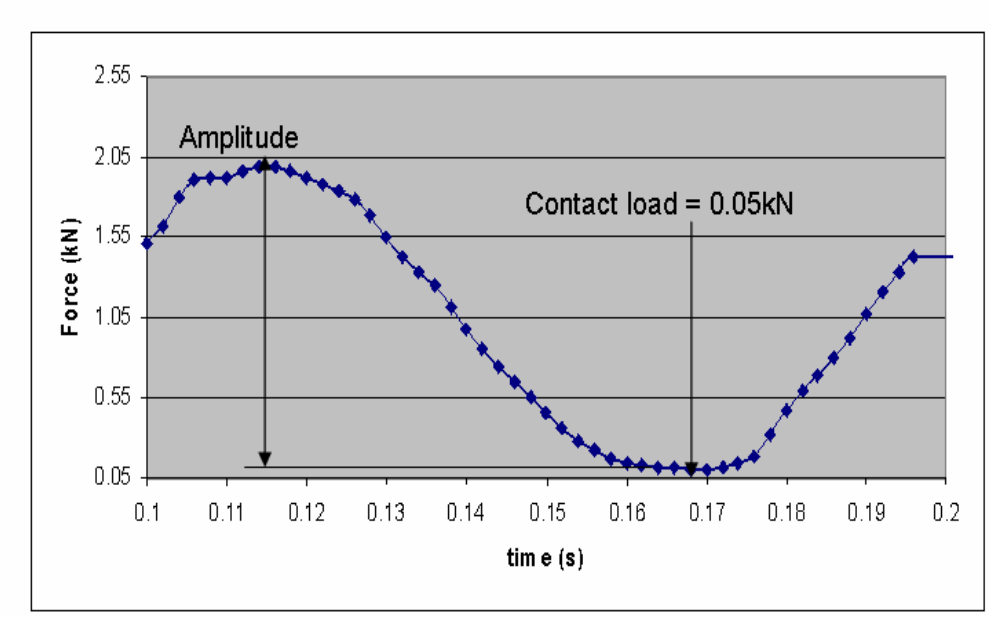

Figure 3.18 - Sinusoidal load applied for the fatigue test

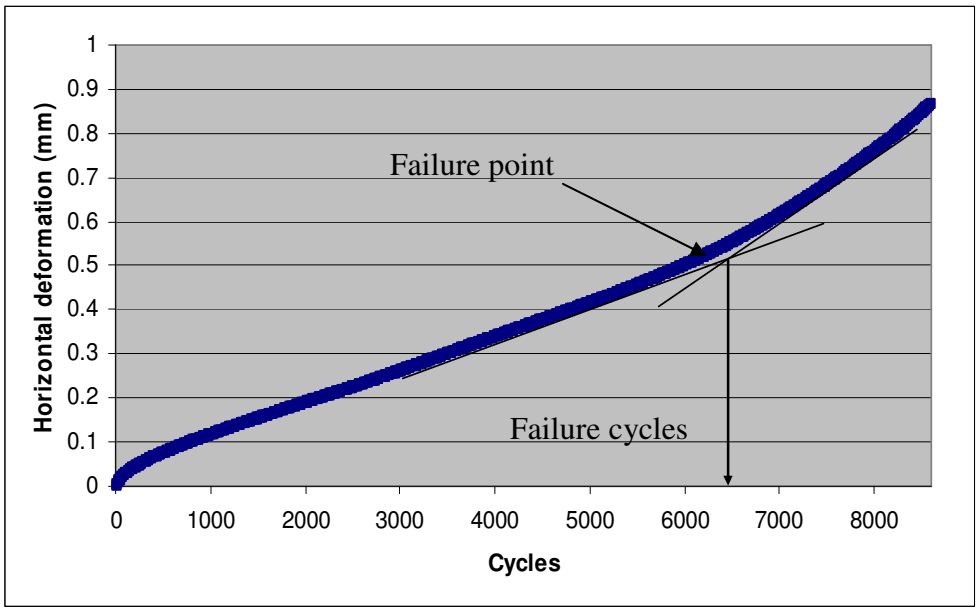

Figure 3.19 - Fatigue failure criterion

3.9. Permanent Deformation Potential

The creep and recovery tests were performed at 35ºC, and the permanent deformation region (Region 6 in Figure 2.5) of each mixture was compared to characterize the effect of hydrated lime on rutting-related HMA behavior.

In addition to the creep and recovery test at 35ºC, the temperature was increased to 60ºC to simulate the behavior of the mixtures under high-temperature conditions. Similar to the fatigue test, the beginning of the tertiary flow in the deformation-loading time curve was captured to define sample failure due to permanent deformation.

CHAPTER 4

RESULTS AND DISCUSSION

4.1. Analyses of RZ, CAA, and FAA

The rutting performance from the APA testing was qualitatively analyzed for five different mixture gradations. Two of those gradations violate the Superpave RZ concept by passing through the restricted zone (TRZ1 and TRZ2), and two gradations are located below the restricted zone (BRZ1 and BRZ2), and one above the restricted zone (ARZ) was also considered. Table 4.1 and Figure 4.1 show the gradations used in this study.

Table 4.1 - Gradations of each mixture

Sieve size		% accumulated passing						
		ARZ	TRZ 1	BRZ 1	TRZ 2	BRZ 2	RZ limits	
19.0 mm	3/4"	100.0	100.0	100.0	100.0	100.0	-	-
12.5 mm	1/2"	95.0	95.0	95.0	95.0	95.0	-	-
9.5 mm	3/8"	89.0	89.0	89.0	89.0	89.0	-	-
4.75 mm	#4	72.0	72.0	72.0	72.0	72.0	-	-
2.36 mm	# 8	57.0	55.0	36.0	55.0	32.0	39.1	39.1
1.18 mm	# 16	42.0	24.0	21.0	35.0	19.0	25.6	31.6
0.60 mm	# 30	30.0	15.0	14.0	19.0	13.0	19.1	23.1
0.30 mm	# 50	19.0	11.0	10.0	11.0	9.0	15.5	15.5
0.15 mm	# 100	7.0	7.0	7.0	7.0	7.0	-	-
0.075 mm	# 200	1.5	3.5	3.5	3.0	3.5	-	-

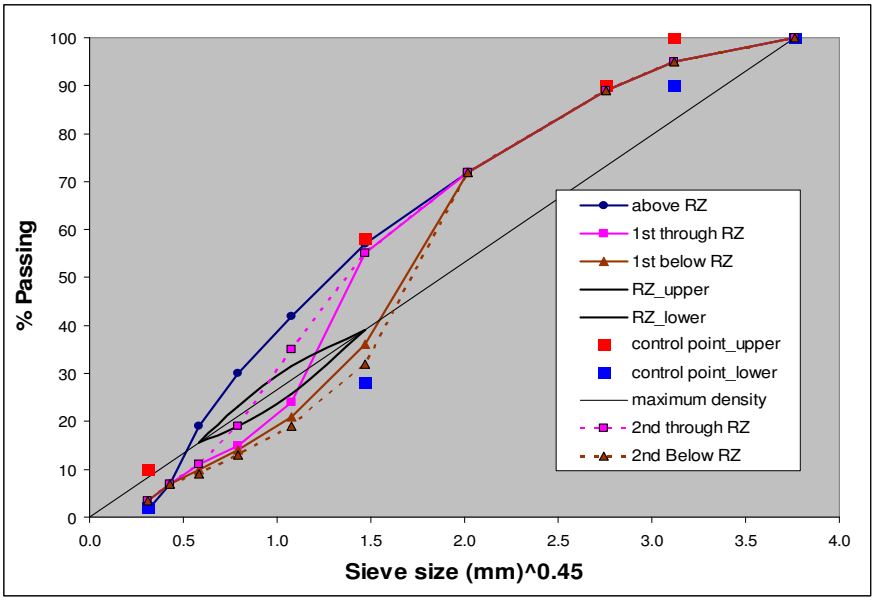

Figure 4.1 - Gradations of each mixture on 0.45-power chart

All mixtures were designed to support a traffic level of 0.3 to 1.0 million ESALs. NDOR classifies it as the SP-2 mixture. The specified limits for the NDOR SP-2 mixture are given in Table 4.2.

Table 4.2 - NDOR limits for SP2 mixtures

Parameter	NDOR Specification (SP-2 Mix)
Compaction Effort	
N_{ini}: the number of gyration at initial	7
N_{des}: the number of gyration at design	76
N_{max}: the number of gyration at maximum	117
Aggregate Properties	
CAA (%): Coarse Aggregate Angularity	> 65
FAA (%): Fine Aggregate Angularity	> 43
SE (%): Sand Equivalency	> 40
F&E (%): Flat and Elongated aggregates	< 10
Volumetric Parameters	
%VA: Air Voids	4 ± 1
%VMA: Voids in Mineral Aggregates	> 14
%VFA: Voids Filled with Asphalt	65 - 78
$\%P_b$: Asphalt Content	-
D/B (ratio): Dust-Binder ratio	0.7 - 1.7

All five mixes designed in asphalt/concrete laboratory at the University of Nebraska-Lincoln (UNL) were submitted to NDOR asphalt/aggregate laboratories for validation of material properties and volumetric mix-design parameters. UNL design values and NDOR validations are presented and compared in Table 4.3.

Table 4.3 - The results of mix design results from UNL and NDOR validation

Parameter	*NDOR LIMITS*	*ARZ*		*TRZ 1*		*TRZ 2*		*BRZ 1*		*BRZ 2*	
		UNL	**NDOR**	**UNL**	**NDOR**	**UNL**	**NDOR**	**UNL**	**NDOR**	**UNL**	**NDOR**
G_{mm}	-	2.447	2.456	2.421	2.437	2.443	2.447	2.429	2.44	2.418	2.42
G_{sb}	-	2.583	2.583	2.582	2.582	2.582	2.582	2.575	2.58	2.581	2.58
G_{mb}	-	2.336	2.338	2.312	2.336	2.339	2.348	2.331	2.34	2.311	2.31
CAA	> 65	84.6	91	84.6	90	84.6	84	84.6	90	84.6	82
FAA	> 43	42.9	43.8	42.95	42.7	42.89	42.6	42.93	43.8	40.87	41.7
SE	> 40	-	73	-	73	-	73	-	81	-	81
F&E	< 10	-	1	-	0	-	0	-	0	-	0
$\%V_a$	4 ± 1	4.6	4.8	4.5	4.14	4.2	4.05	4	4.1	4.4	4.58
VMA	> 14	14.4	14.26	15.5	14.7	14.2	14.04	14.3	14.3	15.5	15.5
VFA	65 - 78	68.4	66.32	71	71.78	70.2	71.18	71.7	71.3	71.5	70.4
$\%P_b$	-	5.36	5.28	5.65	5.7	5.29	5.47	5.27	5.55	5.6	5.65
D/B	0.7 - 1.7	1.56	0.77	1.19	1.16	1.46	1.14	1.31	1.32	1.3	1.14
Sieve		**Gradation (% Passing)**									
3/4"	-	100	100	100	100	100	100	100	100	100	100
1/2"	-	97.4	96.2	93.6	94.3	95.1	95.5	95.5	94.2	96.9	93.5
3/8"	-	91.8	91.1	87	89.4	89.2	89.4	90.6	88.2	87.6	87.9
# 4	-	79	73.9	71.8	72.4	71.8	75.2	72.8	70.6	72.1	71.3
# 8	-	62.7	57.9	53.9	54.7	54.5	56.5	36.8	35	34.3	32.1
# 16	-	46.4	43.2	26	26.1	36.3	36.6	22.4	21.8	21.1	19.8
# 30	-	34	31	17.1	16.8	21.2	20.7	15.6	15.4	14.8	14.1
# 50	-	23.3	20	12.7	12.8	13.3	12.6	11.5	11.4	11	10.4
# 100	-	11.4	8.1	8.8	8.5	9.4	8.4	8.5	5.7	9	8.3
# 200	-	6.8	3.2	5.8	5.4	6.4	5	5.9	5.9	6.4	5.5

As can be seen in Table 4.3, volumetric properties of the mix and the characteristics of aggregates obtained from UNL laboratory matched well with NDOR measurements and met NDOR *SP-2* mix specifications. On the basis of the NDOR validation, it can be inferred that UNL mix designs have been conducted successfully. However, it can be noted from the table that CAA estimated from UNL is somewhat different from NDOR measurements. All *SP-2* mixes were designed with a target value of CAA of approximately 85; however, CAA values measured from each batch delivered to NDOR were approximately 80-90. This is not so surprising since the CAA testing protocol in the Superpave specification is not quite repeatable in nature because CAA value is substantially influenced by aggregate sampling. Furthermore, CAA test results are generally dependent on the individual who performs the testing many times. Some researchers have recommended new testing methods such as the one based on image analysis for better characterizing aggregate angularity in a more appropriate way. In fact, as shown in Table 4.3, NDOR CAA results demonstrated variation in the test results: 82 for the BRZ2 mixture vs. 91 for the ARZ mixture, even though exactly same types and amounts of aggregate were blended for all the five mixtures. Except for the difference in CAA, no significant discrepancy in design parameters was observed between UNL and NDOR.

Following the procedures described in Chapter 3, APA samples were fabricated and tested under dry condition. The APA test results are summarized in Table 4.4. “Front” and “back” in the table refers to the positioning of the sample (for each pair) in the APA machine.

Table 4.4 - Results of rutting performance of APA

HMA mixes	Sample position	G_{mm}	G_{mb}	$\%V_a$	Strokes	Rut depths (mm)	Pass or Fail (12mm @ 8,000 cycles)
ARZ	Front1	2.439	2.341	4.0	8000	5.14	Pass
	Back1	2.448	2.350	4.0	8000	4.84	
	Front2	2.442	2.341	4.1	8000	6.12	Pass
	Back2	2.441	2.344	4.0	8000	5.12	
TRZ 1	Front1	2.432	2.328	4.3	8000	8.13	Pass
	Back1	2.441	2.330	4.5	8000	6.85	
	Front2	2.423	2.332	3.7	5300	12.01	Fail
	Back2	2.428	2.333	3.9	5300	6.15	
TRZ 2	Front1	2.443	2.345	4.1	8000	4.60	Pass
	Back1	2.443	2.343	3.9	8000	3.88	
	Front2	2.444	2.343	4.2	8000	6.34	Pass
	Back2	2.442	2.344	4.0	8000	6.92	
BRZ 1	Front1	2.434	2.336	3.9	4000	6.70	Fail
	Back1	2.434	2.343	3.9	4000	12.60	
	Front2	2.436	2.333	4.2	6000	7.97	Fail
	Back2	2.434	2.337	4.0	6000	12.80	
	Front3	2.429	2.337	3.8	8000	8.85	Pass
	Back3	2.432	2.332	4.1	8000	6.28	
BRZ 1 (CAA 75)**	Front4*	2.441	2.344	4.0	6390	11.71	Fail
	Back4*	2.441	2.345	3.9	6390	12.01	
	Front*	2.431	2.343	3.6	5975	11.19	Fail
	Back*	2.431	2.344	3.6	5975	12.92	
	Front*	2.442	2.344	4.0	5805	13.18	Fail
	Back*	2.442	2.349	3.8	5805	10.91	
BRZ 2	Front1	2.424	2.328	4.0	5480	6.00	Fail
	Back1	2.426	2.337	3.7	5480	12.00	
	Front2	2.421	2.327	3.9	6324	11.44	Fail
	Back2	2.426	2.334	3.8	6324	12.30	

* For these mixtures, each sample was fabricated by splitting 10,000 g batch in 2.

** For these mixtures, the manual stop was performed when the average rutting was approximately 12 mm.

4.1.1. Effects of Restricted Zone

Figure 4.2 summarizes APA test results to investigate the effect of restricted zone. From the figure, one can observe that ARZ and TRZ mixtures generally showed a good performance, and BRZ mixtures showed more susceptible characteristics to rutting than the ARZ and TRZ mixtures. Another fact to be noted from the figure is that TRZ2 mixture, which is closer to ARZ mixture gradation (inferring finer graded mixture), was more rut-resistant than the TRZ1 mixture, which is closer to BRZ gradation (inferring coarser graded mixture). Figure 4.2 indicates that HMA aggregate gradations passing through the restricted zone showed performance similar to or better than mixtures with gradations entirely outside the restricted zone, as long as the aggregate and mixture satisfied other Superpave requirements.

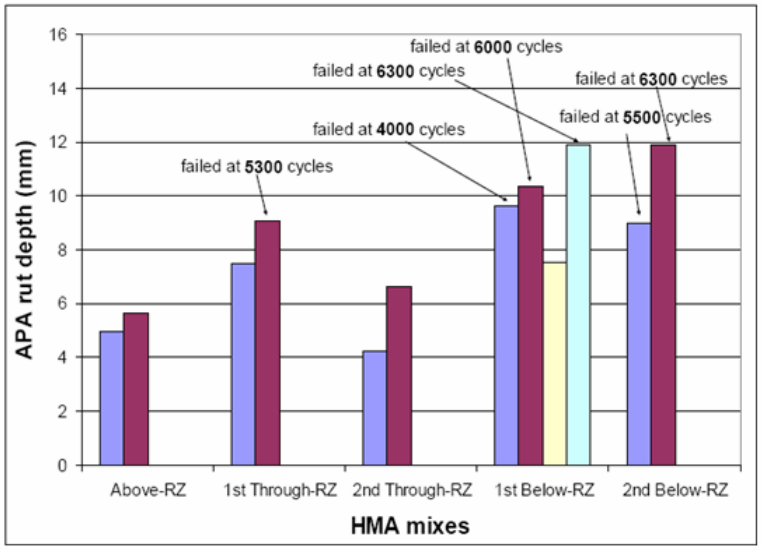

Figure 4.2 - Rut depths of the APA samples

4.1.2. Effects of CAA

To investigate the effect of CAA on rutting performance of HMA, samples of BRZ1 gradation with a CAA of 75 were additionally fabricated and tested using the APA machine. As presented in

Table 4.4, three of four pairs of the BRZ1 mixtures with a CAA of 90 failed before 8,000 cycles and both pairs of BRZ1 mixtures with a lower CAA (i.e., 75) failed at relatively less number of cycles than the BRZ1 mixtures with a CAA of 90. On the basis of this observation, one can infer that the lower CAA might be a potential factor that can cause more severe HMA rut-damage. However, this is not conclusive and needs more comprehensive investigations to ensure the effects of CAA.

4.1.3. Effects of FAA

As shown in Table 4.3, the BRZ2 mixture was designed with a lower FAA (approximately 41) than the other mixtures (approximately 43). Since BRZ1 and BRZ2 are all subject to very similar gradations, their rutting performances can be compared to observe the effect of FAA. As noticed earlier, three out of four pairs of BRZ1 mixture failed, whereas all pairs of BRZ2 mixture failed. Simply considering the number of strokes at failure between the BRZ1 and BRZ2, no significant relationship between FAA values and APA rut-depth was observed from test data currently obtained. However,

APA test results infer that the lower fine angularity is a factor that might cause more rut damage based onthe fact that the BRZ2 mixture is similar to or slightly more susceptible to rutting compared with the BRZ1 mixture. This may be due to reduced aggregate interlocking in the mixture. Further comprehensive investigations need to be performed to draw a more generalized finding.

4.3. Effects of Fillers on Mastics

The strain sweep tests were conducted on different mastics at two different temperatures (20ºC and 40ºC), which are the extreme temperatures used for the frequency sweep tests. The test results that were obtained by varying the dynamic shear modulus and increasing the strains indicated that an arbitrary strain less than 0.6% can be used to perform the frequency sweep tests because the strain level less than 0.6% is low enough that it does not cause any nonlinear viscoelastic behavior of the binders and mastics.

The frequency sweep tests were then performed at 20ºC, and test results are given in Figure 4.3 and Figure 4.4, representing mastics with the binder PG 64-22 and binder PG 64-28, respectively. As expected, hydrated lime produced a higher stiffening effect than other fillers. This is probably due to certain reactions that occur between hydrated lime and the binder. For both binders, the mastics with 3ACR fillers provided better stiffening than the mastics with screening fillers. Interestingly, the mastics mixed with 3ACR and hydrated lime together were less stiff than the mastics with 3ACR only, which is not always true for the cases with screenings fillers. On the basis of this observation, it

can be inferred that hydrated lime does not function as an ordinary volume-filling agent, but acts as a chemically active material producing material-specific characteristics.

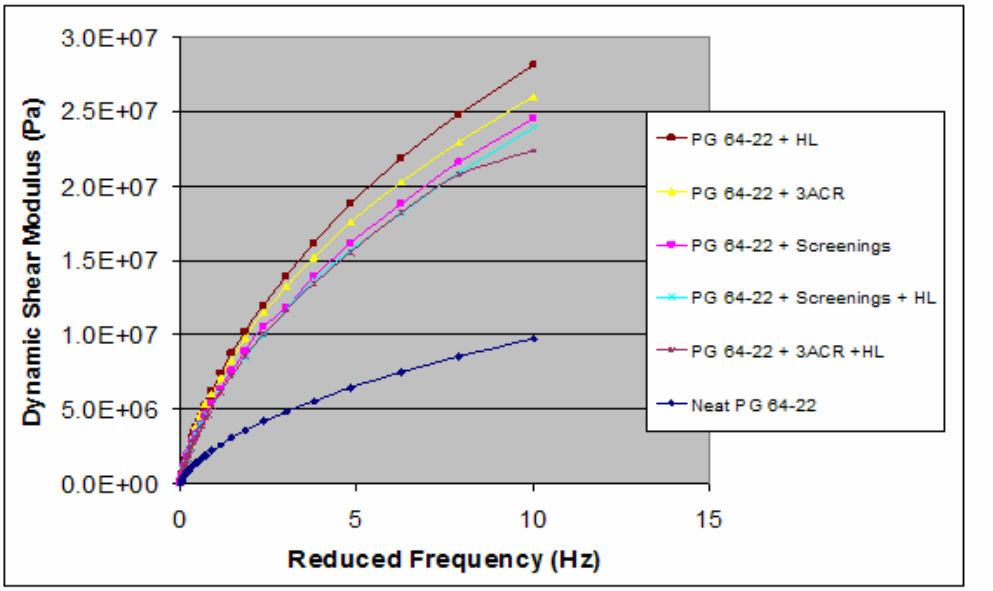

Figure 4.3 - Stiffness of mastics with PG 64-22 binder

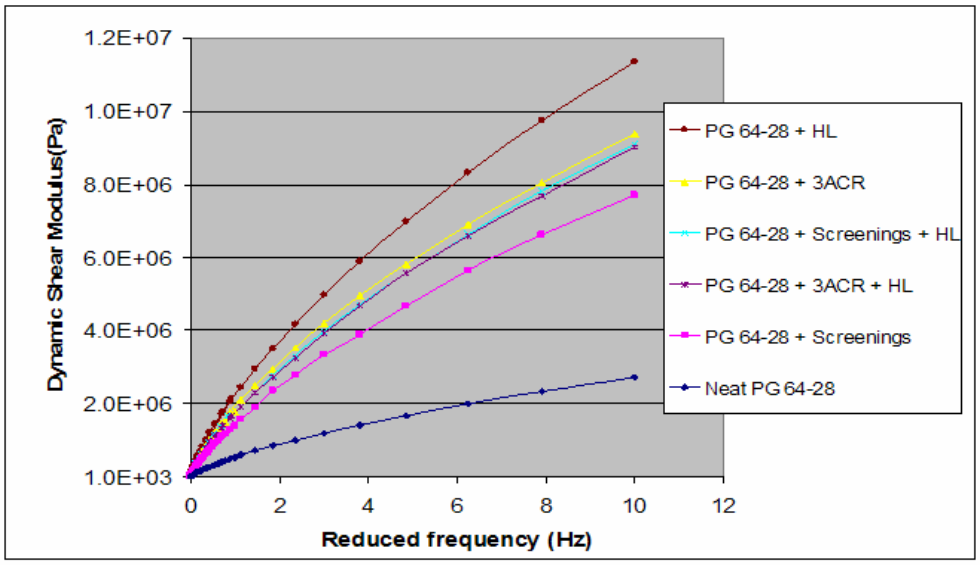

Figure 4.4 - Stiffness of mastics with PG 64-28 binder

4.4. Effects of Hydrated Lime on HMA Performance

The gradation chosen for this investigation was the same as that for the BRZ1-mixture gradation as redrawn in Figure 4.5. Two different mixtures with an addition of different volumes of hydrated lime (0.5 and 2.0% by weight of total aggregates) were designed and tested under IDT mode to characterize their stiffness, fatigue behavior, and rutting performance depending on the amount of hydrated lime added to the mixture.

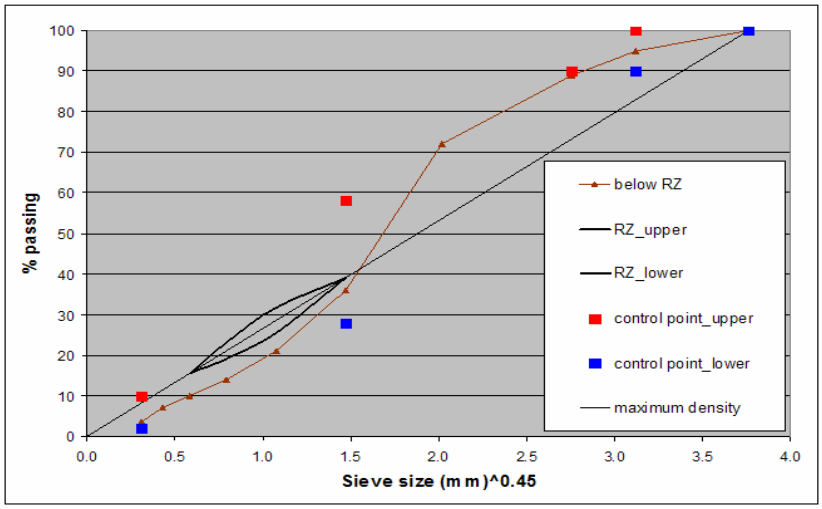

Figure 4.5 - Gradation of HMA mixture

All mixtures designed at the UNL were submitted to NDOR laboratories for validation of material properties and volumetric mix-design parameters. The UNL design values and NDOR validations are presented and compared in Table 4.5.

Table 4.5 - Results of mix design (UNL vs. NDOR)

Parameter	NDOR Limits	0.5% HL		2.0% HL	
		UNL	NDOR	UNL	NDOR
G_{mm}	-	2.428	2.421	2.431	2.438
G_{sb}	-	2.577	2.577	2.577	2.577
G_{mb}	-	2.328	2.334	2.334	2.347
$\%V_a$	4 ± 1	4.1	3.6	4.0	3.8
VMA	> 14	15.1	14.9	14.2	13.7
VFA	65 - 78	72.9	75.9	71.9	72.6
$\%P_b$	-	5.91	5.99	5.08	5.17
D/B	0.7 - 1.7	0.93	0.95	1.48	1.45
Sieve		**Gradation (% Passing)**			
3/4"	-	100.0	100.0	100.0	100.0
1/2"	-	95.6	93.7	93.4	94.1
3/8"	-	89.6	87.1	86.8	87.6
# 4	-	72.4	69.6	70.2	70.6
# 8	-	36.8	35.2	37.8	37.1
# 16	-	22.3	22.4	23.6	23.4
# 30	-	15.5	15.7	16.5	16.7
# 50	-	11.5	11.1	12.6	12.5
# 100	-	8.6	8.5	9.6	9.8
# 200	-	5.5	5.7	7.8	7.5

To evaluate the stiffening effect provided by the addition of hydrated lime, dynamic moduli at three different temperatures were obtained based on the analytical solution for the IDT testing mode described by Kim et al. (2004). The loading levels were carefully adjusted until the sample deformations were between 50 and 75 microstrain.

The resulting dynamic moduli calculated using Equation 2.54 were then used to construct master curves as shown in Figure 4.6. Frequency-domain dynamic modulus master curves in Figure 4.6 were transferred into the time-domain master curves represented for the relaxation moduli. The relaxation modulus plots of each mixture that were finally obtained are shown in Figure 4.7.

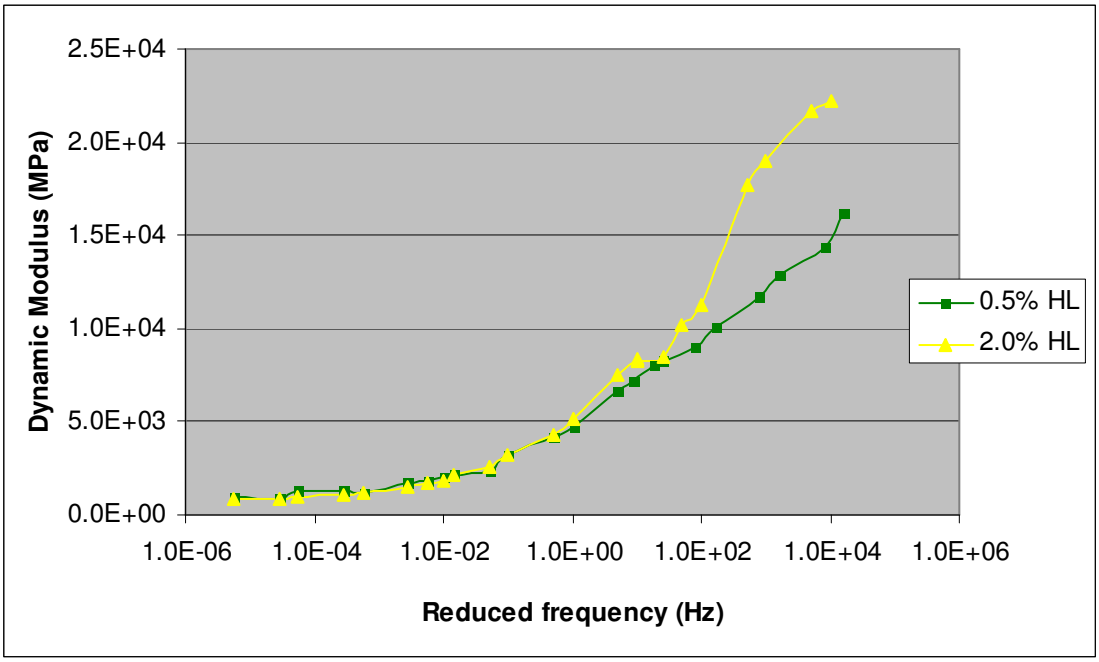

Figure 4.6 - Results of dynamic modulus

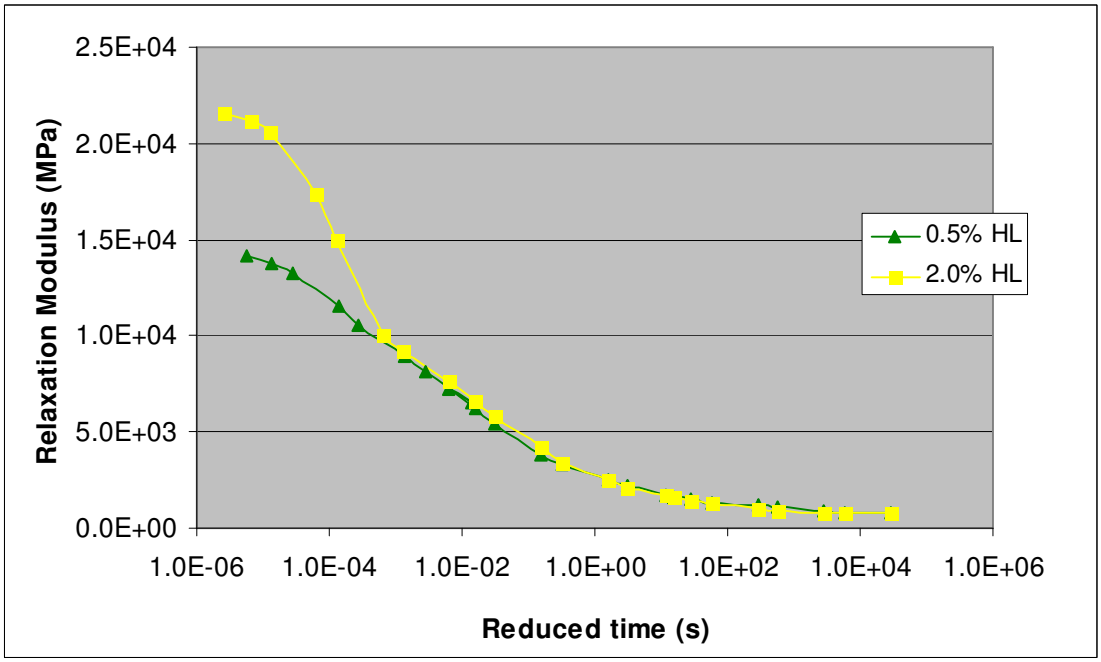

Figure 4.7 - Results of relaxation modulus results

As can be seen, the 2.0% hydrated lime did not improve the stiffness of the mixture at low loading frequencies (or long loading times). However, beginning at approximately 1 Hz, there is a clear trend of gain in stiffness due to the 2.0% lime addition compared with the mixture that included 0.5% hydrated lime.

For fatigue testing, the IDT specimens were subjected to cyclic loads at 20ºC and at a frequency of 10 Hz. Table 4.6 summarizes the loads applied and the resulting number of cycles to failure (i.e., fatigue lives) of each mixture. Figure 4.8 shows the IDT specimen before and after the fatigue test. The figure clearly shows the crack path that developed in the sample after the test.

Table 4.6 - Fatigue testing loads and fatigue lives

0.5% HL addition		2.0% HL addition	
Force (kN)	**Cycles**	**Force (kN)**	**Cycles**
2	5,500	2.5	4,900
2	6,500	2.5	5,100
1.5	24,000	2	19,000
1.5	20,000	2	25,000
1	93,000	1.5	92,000
1	-	1.5	112,000

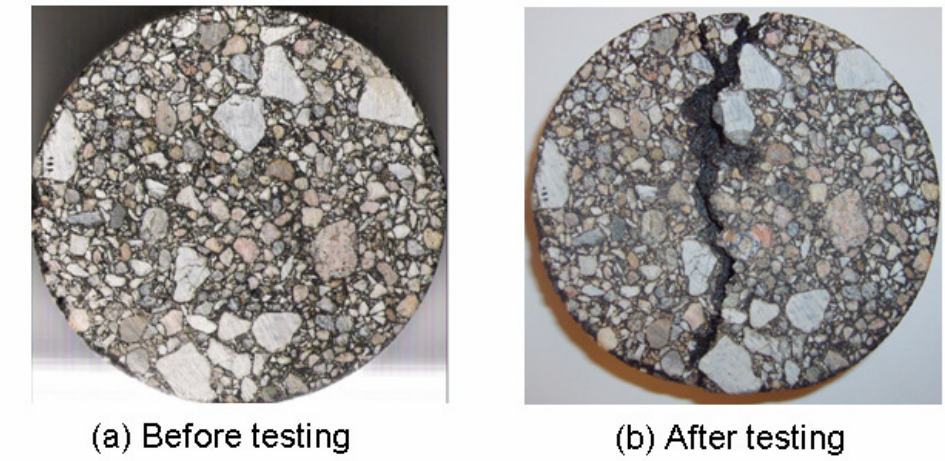

Figure 4.8 - IDT sample before and after fatigue test

The data in Table 4.6 can then be used to draw S-N curves representing the fatigue behavior of the mixtures, as shown in Figure 4.9. Hydrated lime improved the resistance of mixtures against the damage resulting from fatigue, which is the expected phenomena since the addition of hydrated lime resulted in the stiffening of the binder and mixture as shown in Figures 4.3, 4.4, and 4.10. Stiffer mixtures typically last longer under the load-controlled fatigue-testing mode, which is not true any more in case of displacement-controlled fatigue testing. For better insights into the effects of hydrated lime on fatigue performance of HMA, the displacement-controlled fatigue tests need to be performed as well.

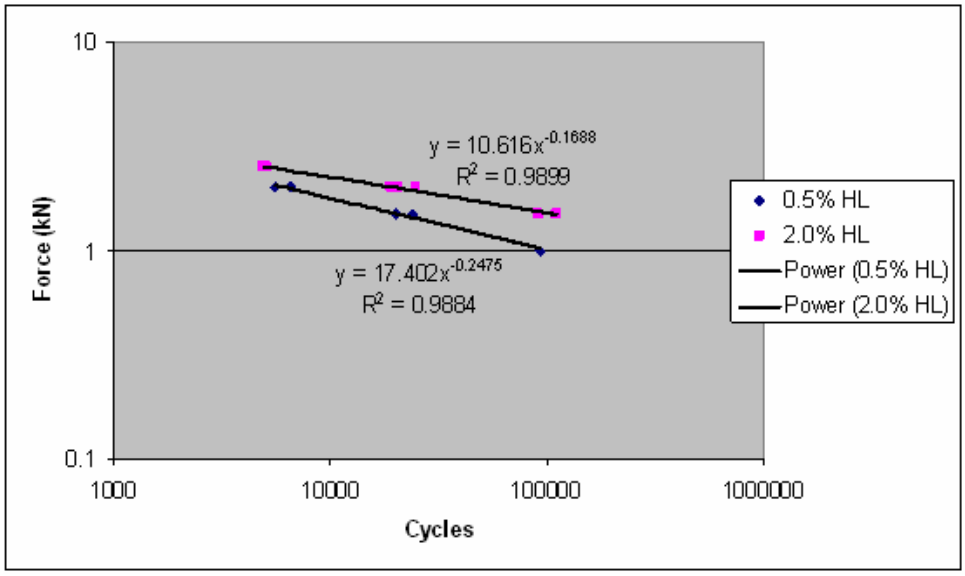

Figure 4.9 - S-N curves for controlled-force testing mode

For the analysis of rutting potential affected by the addition of hydrated lime, the creep and recovery tests were performed, and the slope (represented by *R* in Figure 4.10) of the creep behavior and permanent deformation after recovery were recorded for

comparisons between mixtures with 0.50% hydrated lime and mixtures with 2.0% lime. The tests were conducted at 35ºC, and the applied load was 0.11 kN.

The mixture with 2.0% additional hydrated lime exhibited a lower permanent-deformation potential. After 1,000 seconds of loading, the vertical deformation on the mixture with 0.5% hydrated lime was 0.016 mm, which is 32% higher than the vertical deformation experienced by the mixture with 2.0% hydrated lime (0.0072 mm).

Also, the rate of increase of the deformations (*R*) for the 2.0% hydrated lime was approximately 58% of *R* value for the 0.5% case (0.0000125 mm/s vs. 0.00000528 mm/s). The figure clearly shows that hydrated lime improved resistance to the permanent deformation of the mixtures.

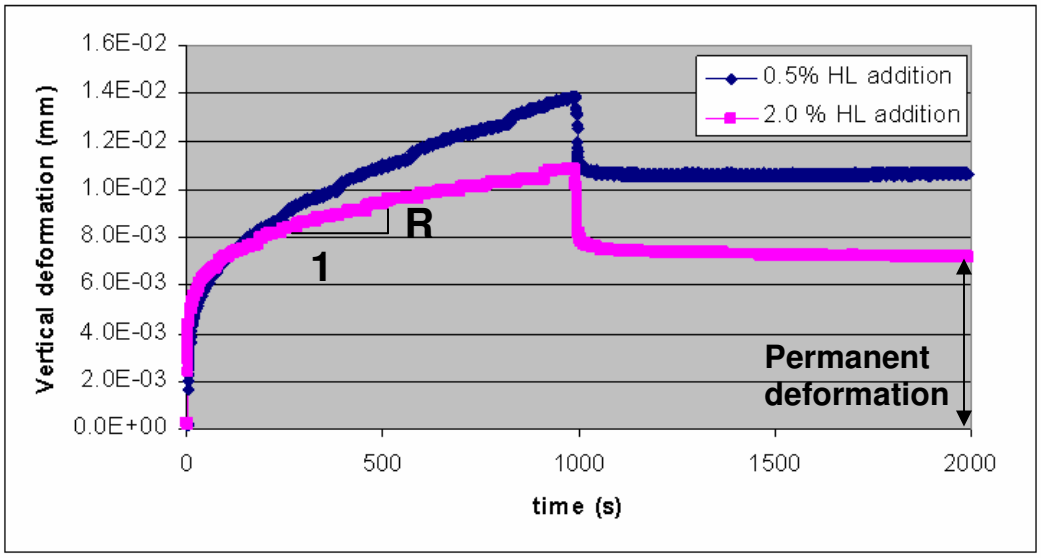

Figure 4.10 - Creep & recovery test vertical deformations

Furthermore, to simulate the rut-associated behavior at a temperature close to the maximum pavement temperature, a constant load of 0.27 kN was applied to the samples at 60ºC, and the actuator deformations were recorded. The beginning of the tertiary flow

in the deformation-loading time curve was monitored as the failure criterion. The corresponding loading times at failure of each mixture are given in Figure 4.11.

The higher amount of hydrated lime amazingly improved the resistance of the mixtures to permanent deformations. For the case of 0.5% hydrated lime, mixtures failed before 300 seconds. For the 2.0% case, this number increased to 12,000 seconds on average.

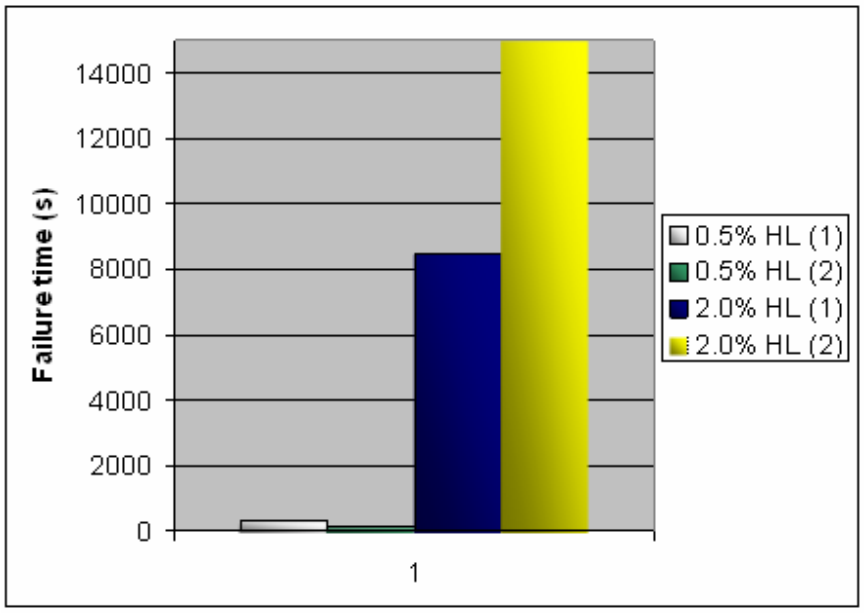

Figure 4.11 - Permanent deformation failure times

CHAPTER 5

CONCLUSIONS AND RECOMMENDATIONS

This research presented a study of different aspects of the effects of aggregates on the properties and performance of mastics and Superpave HMA asphalt mixtures. The variables considered herein were gradations, angularities (shape), and type and amount of fillers.

The effect of gradations on the resistance of HMA mixtures to permanent deformations was evaluated. For this purpose, five different gradations of Superpave restricted zone (RZ) were considered. The restricted zone was not a significant factor that controls rut performance of HMA. In some cases, mixtures violating the RZ showed better performance than others in compliance with the restricted zone. A typical trend observed is that coarser graded mixtures such as the below-RZ mixtures are generally more susceptible to rutting than fine-graded mixtures such as above-RZ mixtures.

Next, a brief investigation on the permanent-deformation performance of mixtures with different aggregate angularities showed that mixtures with lower CAA and/or FAA showed slightly worse performance than mixtures with higher CAA and/or FAA. However, a more comprehensive study needs to be conducted for better conclusions.

This study also investigated the effects of mineral fillers and hydrated lime on material properties and characteristics of HMA performance. Hydrated lime produced a higher stiffening effect than other fillers, which might be due to some physico-chemical

reactions between hydrated lime and the binder; however, it has not been considered in this study. Hydrated lime also showed somewhat material-specific characteristics, which is not typically observed in case of commonly used mineral fillers.

The effects of hydrated lime have been further investigated by performing several mixture tests for two different lime additions (0.5% and 2.0%). Hydrated lime improved the stiffness, fatigue resistance, and rut resistance of the HMA mixtures. However, the contribution of hydrated lime to fatigue behavior of the mixture needs to be investigated with more care, since better resistance to fatigue damage observed from the mixtures containing more amount of hydrated lime may not be true in case of displacement-controlled fatigue testing. This study has only investigated fatigue behavior of mixtures under the force-controlled mode.

BIBLIOGRAPHY

1. AASHTO - American Association of State Highway and Transportation Officials, 2000, T304 "Uncompacted Void Content of Fine Aggregate."

2. AASHTO - American Association of State Highway and Transportation Officials, 2002, T315 "Determining the Rheological Properties of Asphalt Binder Using a Dynamic Shear Rheometer (DSR)."

3. AASHTO - American Association of State Highway and Transportation Officials, 2003, T322 "Determining the Creep Compliance and Strength of Hot-Mix Asphalt (HMA) Using the Indirect Tensile Test Device."

4. AASHTO - American Association of State Highway and Transportation Officials, 2003, TP62 "Determining Dynamic Modulus of Hot-Mix Asphalt Concrete Mixtures."

5. ASTM - American Society for Testing and Materials, 2006, D1073 "Standard Specification for Fine Aggregate for Bituminous Paving Mixtures."

6. ASTM - American Society for Testing and Materials, 2004, D242 "Standard Specification for Mineral Filler for Bituminous Paving Mixtures."

7. ASTM - American Society for Testing and Materials, 2000, D692 "Standard Specification for Coarse Aggregate for Bituminous Paving Mixtures."

8. ASTM - American Society for Testing and Materials, 2001, D5821 "Standard Test Method for Determining the Percentage of Fractured Particles in Coarse Aggregate."

9. Anderson, D. A, Christensen, D. W., Bahia, H. U., Dongre, R., Sharma, M. G., Antle , C. E., & Button, J. (1994). Binder Characterization and Evaluation - Volume 3:

Physical Characterization. *Report SHRP-A-369, Strategic Highway Research Program*, National Research Council, Washington, D.C.

10. Bari, J., & Witczak, M. W. (2005). Evaluation of the Effect of Lime Modification on the Dynamic Modulus Stiffness of Hot-Mix Asphalt. *In Transportation Research Record*, *TRB,* 1929, 10-19. National Research Council, Washington, D.C.

11. Baumgarten, K., 2007, *Personal Contact*, Department of Geosciences - UNL.

12. Beason, J., 2006, *Personal Contact*, NDOR aggregates lab.

13. Bettenhausen, R., 2006, *Personal Contact*, IT Business Systems Analyst - NDOR Project Scheduling & Program Management.

14. Brown, E. R., Mallick, R. B., Haddock, J. E., & Bukowski, J. (1997) Performance of Stone matrix Asphalt (SMA) Mixtures in the United States. *Report 97-1, National Center for Asphalt Technology (NCAT),* Auburn.

15. Brown, E. R., Kandhal, P. S., & Zhang, J. (2001) Performance Testing for Hot Mix Asphalt (Executive Summary). *Report 01-05A, National Center for Asphalt Technology (NCAT)*, Auburn.

16. Buchanan, M. S. (2000) Evaluation of the Effect of Flat and Elongated Particles on the Performance of Hot Mix Asphalt Mixtures. *Report 00-03, National Center for Asphalt Technology (NCAT),* Auburn.

17. Castelo Branco, V. T. F. (2004). Caracterização de Misturas Asfálticas Com o Uso de Escória de Aciaria como Agregado. (Characterization of Hot Asphalt Mixes using Steel Slag as Aggregate). *Master Thesis approved by the Universidade Federal do Rio de Janeiro (Federal University of Rio de Janeiro*). Rio de Janeiro, Brazil.

18. Chehab, G.R., & Kim, Y. R. (2007) Inter-Relationships among Asphalt Concrete Stiffnesses. In-Press, Chapter 9, ASCE Book, Modeling of Asphalt Concrete, McGraw Hill.

19. Choubane, B., Page, G. C., & Musselman, J. A. (2000) Suitability of Asphalt Pavement Analyzer for Predicting Pavement Rutting. *In Transportation Research Record,* TRB, 1723, 107-115*,* National Research Council, Washington, D.C.

20. Chowdhury, A. T., Grau, J. D. C., Button, J. W., & Little, D. N. (2001) Effect of Gradation on Permanent Deformation of Superpave Hot-Mix Asphalt. Presented at 80th *Annual Meeting of the Transportation Research Board*, Washington, D.C.

21. Chowdhury, A. T., Button, J. W., & Grau, J. D. C. (2001). Effects of Superpave Restricted Zone on Permanent Deformation. Project Title: Evaluation of Superpave Aggregate Specifications. *Report No. 201-2, Texas A&M University*.

22. Cooley Jr., L. A., Zhang, J., Kandhal,P. S., Hand, A. J., & Martin, A. E. (2002) Significance of Restricted Zone in Superpave Aggregate Gradation Specification. Transportation *Research Circular number E-C043 in Transportation Research Record*, TRB, Washington D.C.

23. Daniel, J. S., & Kim, Y. R. (1998). Relationships Among Rate-Dependent Stiffnesses of Asphalt Concrete Using Laboratory and Field Test Methods. *In Transportation Research Record 1630*, 3-9. TRB, National Research Council, Washington, D.C.

24. Dougan, C. E., Mahoney, J., Hansem, G. (2003). E* - Dynamic Modulus. Test protocol - Problems and Solutions. *Report number CT-SPR-0003084-F-03-3 for the*

Connecticut Department of Transportation in Cooperation with the U.S. Department of Transportation. University of Connecticut.

25. Druta, C. (2006). A Micromechanical Approach for Predicting the Complex Shear Modulus and Accumulated Shear Strain of Asphalt Mixtures from Binder and Mastics. *Doctoral Dissertation approved by the Louisiana State University and Agricultural and Mechanical College*. Louisiana.

26. Elseifi, M. A., Al-Qadi I. L., & Yoo, P. J. (2006). Viscoelastic Modeling and Field Validation of Flexible Pavements. *In Journal of Engineering Mechanics (ASCE),* 172-178.

27. Federal Highway Administration (FHWA). Connecticut division. http://www.fhwa.dot.gov/ctdiv/whatsnew.htm.

28. Federal Highway Administration (FHWA). Highway Statistics Series/Highway Statistics Publications/Highway Statistics 2005/Public Road Length in the United States, classified by type of surface and ownership/functional system (national summary). http://www.fhwa.dot.gov/policy/ohim/hs05/pdf/hm12.pdf.

29. Findley, W. N., Lai, J.S., & Onaran, K. (1976). *Creep and Relaxation of Nonlinear Viscoelastic Materials with an Introduction to Linear Viscoelasticity*. Dover Publications, New York.

30. Gittus, J. (1975). *Creep, Viscoelasticity and Creep Fracture in Solids*. Applied Science Publishers LTD, London, England.

31. Haifang, W. (2001) Fatigue Performance Evaluation of Westrack Asphalt Mixtures Based on Viscoelastic Analysis of Indirect Tensile Test. *PhD dissertation*

approved by the Department of Civil Engineering of North Carolina State University, North Carolina.

32. Hand, A. J., Epps, A. L. (2001). Impact of Gradation Relative to Superpave Restricted Zone on Hot-Mix Asphalt Performance. *In Transportation Research Record*, TRB, 1767, 158-166. National Research Council, Washington, D.C.

33. Hand, A. J., Stiady, J. L., White, T. D., Noureldin, A. S., & Galal, K. (2001). Gradation Effects on Hot-Mix Asphalt Perfomance. *In Transportation Research Record x TRB*, TRB, 152-157. National Research Council, Washington, D.C.

34. Huang, Y. H. (2004). *Pavement Analysis and Design*. Pearson Prentice Hall, Second Edition, New Jersey.

35. Jones, D. R., & Kennedy, T. W. (1991). The Asphalt Model: Results of the SHRP Asphalt Research Program. *In Transportation Research Record, TRB*, National Research Council, Washington, D.C.

36. Kandhal, P. S., & Cooley Jr., L. A. (2001). The Restricted Zone in the Superpave Aggregate Gradation Specification. *NCHRP Report No. 464*, Transportation Research Board - National Research Council

37. Kandhal, P. S., & Cooley Jr., L. A. (2002) Coarse- versus Fine-Graded Superpave Mixtures - Comparative Evaluation of Resistance to Rutting. *In Transportation Research Record, TRB*, 1789, 216-224. National Research Council, Washington, D.C.

38. Kandhal, P. S., & Cooley Jr., L. A. (2003). Accelerated Laboratory Rutting Tests: Evaluation of the Asphalt Pavement Analyzer. *NCHRP Report No. 508*, Transportation Research Board - National Research Council.

39. Kandhal, P. S., & Mallick, R. B. (2001) Effect of Mix Gradation on Rutting Potential of Dense-Graded Asphalt Mixtures. *In Transportation Research Record*, TRB, 1767, 146-151. National Research Council, Washington, D.C.

40. Kandhal, P. S., & Mallick, R. B. (1998). Open-Graded Asphalt Friction Course: State of the Practice. *Report 98-07 for the National Center for Asphalt Technology (NCAT)*. Auburn.

41. Kandhal, P. S., Lynn, C. Y., & Parker Jr., F. (1998). Characterization Tests for Mineral Fillers Related to Performance of Asphalt Paving Mixtures. *Report 98-2 for the National Center for Asphalt Technology (NCAT).* Auburn.

42. Kettler, D., 2007, *Personal Contact*, Department of Geosciences - UNL.

43. Kim, Y. R., Little, D. N., & Song, I. (2003) Effect of Mineral Fillers on Fatigue Resistance and Fundamental Material Characteristics: Mechanistic Evaluation. *In Transportation Research Record*, *TRB*, 1832, 1-8. National Research Council, Washington, D.C.

44. Kim, Y. R., Aragao, F. T. S., & Lutif, J. E. S. (2006). Restricted - Zone Requirements for Superpave Mixes Made with Local Aggregate Sources. *Report for the Nebraska Department of Roads (NDOR)*. Nebraska.

45. Kim, Y. R., Seo, Y., King, M., & Momen, M. (2004). Dynamic Modulus Testing of Asphalt Concrete in Indirect Tension Mode. *In Transportation Research Record, TRB,* 1891, 163-173. National Research Council, Washington, D.C.

46. Kim, Y. R., Daniel,, J. S., & Wen, H. (2002). Fatigue Performance Evaluation of WesTrack Asphalt Mixtures Using Viscoelastic Continuum Damage Approach. *Final Report FHWA/NC/2002-004 for the North Carolina Department of Transportation*.

47. Kohsla, N. P., Sadasivam, S., & Malpass, G. (2001). Performance Evaluation of fine graded Superpave Mixtures for Surface Courses. *Final Report FHWA/NC/2002-005 in Cooperation with North Carolina Department of Transportation*.

48. Koves, L., 2006, *Personal Contact*, NDOR asphalt pavement lab.

49. Krishnan, J. M., & Rajagopal, K. R. (2003). Review of the Uses and Modeling of Bitumen from Ancient to Modern Times. *Applied Mechanics Reviews*, vol. 56, issue 2, 149-214.

50. Labout, J. W. A. (1950). Constitution of Asphaltic Bitumen. *In The Properties of Asphaltic Bitumen*, J. P. Pfeiffer, ed. Elsevier, New York, pp. 13-48.

51. Lee, H. J., & Kim, Y. R. (1998). Viscoelastic Constitutive Model for Asphalt Concrete under Cyclic Loading. *American Society of Civil Engineers (ASCE) - Journal of Engineering Mechanics*, 32-40.

52. Little, D. N., & Petersen, J. C. (2005). Unique Effects of Hydrated Lime Filler on the Performance-Related Properties of Asphalt Cements: Physical and Chemical Interactions Revisited. *American Society of Civil Engineers (ASCE) - Journal of Materials in Civil Engineering, 207*-218.

53. Little, D. N., Epps, J. A., & Sebaaly, P. E. (2006). The Benefits of Hydrated Lime in Hot Mix Asphalt. *Report for the National Lime* Association (updated version*)*.

54. Lundström, R., & Isacsson, U. (2004). Linear Viscoelastic and Fatigue Characteristics of Styrene-Butadiene-Styrene Modified Asphalt Mixtures. *American Society of Civil Engineers (ASCE) - Journal of Materials in Civil Engineering*, 629-638.

55. Mack, C. J. (1932). Colloidal Chemistry of Asphalts. *Phys. Chem*., vol. 36, pp. 2901-2194.

56. Mallick, R. B., Kandhal, P. S., Cooley Jr., L. A., & Watson, D. E. (2000). Design, Construction, and Performance of New-Graded Friction Courses. *Report 2000-01 for the National Center for Asphalt Technology (NCAT).* Auburn.

57. Marasteanu, M. O., & Anderson, D. A. (2000). Establishing Linear Viscoelastic Conditions for Asphalt Binders. *In Transportation Research Record*, *TRB*, 1728, 1-6. National Research Council, Washington, D.C.

58. Miller, J., 2006, *Personal Contact*, Highway Contracts Supervisor - NDOR's Construction Division.

59. National Lime Association. (2006). Hydrated Lime - A Solution for High Performance Hot Mix Asphalt. http://www.lime.org/Aasphalt.pdf.

60. NCHRP 1-37A (2004). Guide for Mechanistic - Empirical Design of New and Rehabilitated Pavement Structures. *Final Report. NCHRP, ARA Inc., and ERES Consultants Division*, Washington, D. C.

61. Nebraska Department of Roads. Annual Report, 2003. http://www.dor.state.ne.us/docs/ar2003.pdf.

62. Nebraska Department of Roads. Annual Report, 2005. http://www.nlc.state.ne.us/epubs/R6000/A005-2005.pdf.

63. Nellensteyn, F. J. (1924). The Constitution of Asphalt. *Inst. Petrol. Technol.*, vol. 10, pp. 311-325.

64. Nukunya, B., Roque, R., Tia, M., & Metha, Y. A. (2002). Effect of Aggregate Structure on Rutting Potential of Dense-Graded Asphalt Mixtures. *In Transportation Research Record, TRB*, 1789, 136-145. National Research Council, Washington, D.C.

65. Pan, T., Tutumluer, E., & Carpenter, S. H. (2006). Effect of Coarse Aggregate Morphology on Permanent Deformation Behavior of Hot Mix Asphalt. *American Society of Civil Engineers (ASCE) - Journal of Transportation Engineering*, 580-589.

66. Park, D., & Epps, M. A. (2003). Use of the Asphalt Pavement Analyzer and Repeated Simple Shear Test at Constant Height to Augment Superpave Volumetric Mix Design. *Journal of Transportation Engineering*, 129(5), 522-530.

67. Petersen, J. C., Robertson, R. E., Branthaver, J. F., Harnsberger, P. M., Duvall, J. J., Kim, S. S., Anderson, D. A., Christiansen, D. W., & Bahia, H. U. (1994). Binder Characterization and Evaluation - Volume 1. *Report SHRP-A-367, Strategic Highway Research Program*. National Research Council. Washington, D.C.

68. Prowell, B. D., Zhang, J., & Brown, E. R. (2005). Aggregate Properties and the Performance of Superpave-Designed Hot Mix Asphalt. *Report NCHRP-539, National Cooperative Highway Research Program*. National Research Council, Washington, D.C.

69. Roberts, F. L., Kandhal, P. S., Brown, E. R., Lee, D. Y., & Kennedy, T. W. (1996). *Hot Mix Asphalt Materials, Mixture Design, and Construction*. National Center for Asphalt Technology (NCAT), Auburn University, 2nd edition.

70. Sebaaly, P. E., Hand, A. J.T., McNamara, W. M., Weitzel, D., & Epps, J. A. (2004). Field and Laboratory Performance of Superpave Mixtures in Nevada. *In Transportation Research Record, TRB*, 1891, 76-84. National Research Council, Washington, D.C.

71. Sebaaly P. E., Hitti, E., & Weitzel, D. (2003). Effectiveness of Lime in Hot-Mix Asphalt Pavements. *In Transportation Research Record, TRB*, 1832, 34-41. National Research Council, Washington, D.C.

72. Smith, B. A. (2004). Cellular Biomechanics Investigated by Atomic Force Microscopy. *Doctoral Dissertation approved by the Department of Physics of McGill University*. Montreal, Canada.

73. Tangella, S. C. S., Craus, J, Deacon, J. A., & Monismith, C. L. (1990) Summary report on Fatigue Response of Asphalt Mixtures. *Report SHRP-A-312, Strategic Highway Research Program.* National Research Council, Washington, D.C.,

74. WSDOT - Washington State Department of Roads, 2006, http://training.ce.washington.edu/WSDOT/Modules/03_materials/03-3_body.htm#chemical_properties.

75. Webster's Basic English Dictionary, (1995). Merriam-Webster, Springfield, IL.

76. Wen, H., & Kim, Y. R. (2002). Simple Performance Test for Fatigue Cracking and Validation with WesTrack mixtures. *In Transportation Research Record, TRB,* 1789, 66-72. National Research Council, Washington, D.C.

77. White, T. D., Haddock, J. E., & Rismantojo, E. (2006). Aggregate Tests for Hot-Mix Asphalt Mixtures Used in Pavements. *Report NCHRP-557, National Cooperative Highway Research Program*. National Research Council, Washington, D.C.

78. Wikipedia, the free Encyclopedia (http://en.wikipedia.org/wiki/Mastic_asphalt).

79. Wikipedia, the free Encyclopedia (http://en.wikipedia.org/wiki/Stone_mastic_asphalt).

80. Witczak, M. W., Kaloush, K., Pellinen, T., Basyouny, M. E., & Quintus, H. V. (2002). Simple Performance Test for Superpave Mix Design. *Report NCHRP-465*, *National Cooperative Highway Research Program*. National Research Council, Washington, D.C.

81. Wu, Y., Parker, F., & Kandhal, K. (1998). Aggregate Toughness/Abrasion Resistance and Durability/Soundness Tests Related to Asphalt Concrete Performance in Pavements. *Report 98-04 for the National Center for Asphalt Technology (NCAT)*, Auburn.

82. Zhang, J., Cooley Jr., L. A., Hurley, G., & Parker, F. (2004). "Effect of Superpave Defined Restricted Zone on Hot-Mix Asphalt Performance. *In Transportation*, *TRB,* 1891, 103-111. National Research Council, Washington, D.C.,